Integrated microwave biosensors on SiGe BiCMOS technology: A "More Than Moore" approach

Vorgelegt von

Master of Science

Subhajit Guha

geb. in Kolkata, India

Von der Fakultät IV

Elektrotechnik und Informatik

der Technischen Universität Berlin

zur Erlangung des akademischen Grades

Doktor der Ingenieurwissenschaften

(Dr.-Ing)

genehmigte Dissertation

Promotionsausschuss

Vorsitzender: Prof. Dr. Klaus Petermann

Berichter: Prof. Dr. Roland Thewes

Berichter: Dr. rer nat. habil Christian Wenger

Berichter: Prof. Dr. Hermann Schumacher

Tag der wissenschaftlichen Aussprache: 18.01.2017

Berlin 2017

I lovingly dedicate this thesis to my parents and my sister, who have always been a great support through-out the journey

Abstract

There has been an ever increasing demand for the establishment of Point-of-Care testing systems for rapid detection and diagnosis of diseases and as well for monitoring vital health parameters. The development in the area of microfluidic systems as well as microsystem technology as a whole gave birth to new avenue of research called the Lab-on-a-chip devices, which are an essential part of point-of-care testing systems. Such devices are expected to perform biochemical analysis with sensitivity and accuracy of the order of the state of the art bioanalytical laboratories and at the same time use extremely small volume of the samples. This led to the development of biosensors with extremely high sensitivity and accuracy especially based on optical techniques. However, optical techniques although produced extremely sensitive sensor systems, suffered from serious drawbacks like requirement of labeling compounds, bulky test-benches for measurement and many more. Therefore, the real goal of establishing miniaturized point-of-care diagnostic system for rapid measurements was very difficult to achieve.

The obvious choice as an alternative to optical platform was to establish electrical sensing schemes to avoid the requirement of using labeling compounds and markers. The electrical approaches explored at the initial phase although circumvented the problems of optical techniques, had other issues which still continued a bulky overall measurement setup (for e.g. use of reference electrodes).

In this thesis, "all-electrical" sensor systems operating at the GHz frequency range of the electromagnetic spectrum, and fabricated on standard CMOS/BiCMOS process have been explored and demonstrated. The focus of the thesis is to demonstrate the capability of integrating biological sensing on the standard CMOS/BiCMOS process. This approach takes a step ahead of the established electrical biosensors with a hybrid approach where the front end electronics for data acquisition and processing is integrated in a hybrid fashion with the biosensor system. The approach explored in this thesis has the biosensor on the same technology platform where the front end electronics for read out, data acquisition and processing are fabricated. This kind of an approach stems out from the "More than Moore" technique of semiconductor technology roadmap and offers extremely high sensitivity due to close proximity of the sensor to the front end electronics. The high-frequency approach on the other hand offers other advantages like nullifying low-frequency dispersion mechanisms and evading unwanted electrochemical effects at the sensor and electrolyte interface (avoiding the use of reference electrodes). Sensors operating at high frequency have dimensions of the order of the biomaterials (cells) that are probed. Therefore, the high-frequency CMOS compatible sensor approach explored in this thesis takes a step forward towards establishing simple, low cost, miniaturized point-of-care systems.

Several relevant sensor applications are explored in this thesis in order to demonstrate the feasibility of the established approach. An immunosensor operating at 6 GHz has been established and the functionality has been demonstrated with the detection of concentration of creatinine

molecules. The sensor system demonstrates the capability of detection of the concentration of creatinine molecules in the clinically relevant range and with the sensitivity equivalent to the established optical techniques. Applications like sensing of glucose concentration in a suspension and cytometric applications like detection of concentration of particles in a solution has been shown. Finally, a novel approach to make the overall sensor system flexible and with extremely rapid measurement capability has been demonstrated. In such a system, the sensor output is a DC signal, therefore, making the sensor system function with DC inputs and DC outputs, thus setting the platform for ideal miniaturized point-of-care diagnostic systems.

Zusammenfassung

Die Nachfrage nach „Point-of-Care-Testing“ Systemen zur schnellen Erkennung und Diagnose von Krankheiten und auch für die Überwachung von lebenswichtigen Gesundheitsparametern steigt an. Neue Entwicklungen im Bereich der Mikrofluidik-Systeme sowie der Mikrosystemtechnik als Ganzes ermöglichte einen neuen Forschungszweig für sogenannten Lab-on-a-Chip Bauelemente, die ein wesentlicher Bestandteil der „Point-of-Care-Testing“ Systeme sind. Von diesen Bauelementen wird erwartet, dass sie die biochemische Analyse mit der Empfindlichkeit und Genauigkeit von modernen bioanalytischen Laboren mittels der Verwendung von extrem kleinen Probenvolumen durchführen können. Das führte, basierend auf optischen Technologien, zu der Entwicklung von Biosensoren mit extrem hoher Empfindlichkeit und Genauigkeit. Obwohl durch die Nutzung von optischen Techniken extrem empfindliche Sensoren hergestellt werden können, existieren schwerwiegenden Nachteilen wie das Markieren von Molekülen und die Größe der Messaufbauten. Damit war das Ziel der Miniaturisierung von Point-of-Care-Diagnosesystemen für schnelle Messungen schwer zu erreichen.

Eine Alternative zu optischen Testsystemen war es, elektrische Sensorsysteme zu etablieren, um das Markieren von Molekülen zu vermeiden. Die elektrischen Ansätze, die in der Anfangsphase untersucht wurden, umgingen die Probleme der optischen Techniken, besaßen immer noch einen ziemlich sperrigen Gesamtmessaufbau (z.B. durch die Verwendung von Referenzelektroden). Daher ist das Ziel, hochempfindliche Sensorsysteme für miniaturisierte Point-of-Care Diagnostiksysteme herzustellen, bei weitem noch nicht erreicht. In diesem Zusammenhang ist ein neuer Ansatz erforderlich, der hochempfindliche Biosensoren sowie die Miniaturisierung des gesamten Sensorsystems ermöglicht.

In dieser Arbeit werden "all-electrical" Sensorsysteme, die im GHz-Frequenzbereich des elektromagnetischen Spektrums arbeiten und mittels eines Standard-CMOS / BiCMOS-Prozesses hergestellt wurden, entwickelt und untersucht. Der Schwerpunkt dieser Arbeit ist, die Integration von biologischen Sensoren mittels eines Standard-CMOS / BiCMOS-Prozesses zu demonstrieren. Dieser Ansatz geht einen Schritt weiter als in bereits etablierte elektrischen Biosensoren, denn mittels des hybriden Ansatzes wird die Front-End-Elektronik für die Datenerfassung und -verarbeitung in einem Hybrid-Ansatz in das Biosensor-System integriert. Der Ansatz in dieser Arbeit ist, den Biosensor in die gleiche Technologie-Plattform zu integrieren, in der auch die Front-End-Elektronik zum Auslesen, Datenerfassung und Verarbeitung hergestellt wird. Diese Art des Ansatzes stammt aus der "More than Moore" Philosophie der Halbleiter-Technologie und bietet eine, aufgrund der Nähe des Sensors zur „Frontend“ Elektronik, extrem hohe Empfindlichkeit. Der Hochfrequenz-Ansatz auf der anderen Seite bietet weitere Vorteile das Ausblenden der niederfrequenten Dispersionsmechanismen und das Verhindern von unerwünschten elektrochemischen Effekten an der Sensor und Elektrolyt-Grenzfläche, denn es sind keine Referenzelektroden erforderlich. Sensoren, die bei diesen hohen Frequenzen arbeiten, haben Abmessungen in der Größenordnung der zu untersuchenden Biomaterialien (Zellen). Daher

liefert der in dieser Arbeit untersuchte Hochfrequenz CMOS-kompatible Sensoransatz einen wichtigen Schritt nach vorne, auf dem Weg zu einfachen, kostengünstigen, miniaturisierten Point-of-Care-Systemen.

In dieser Arbeit wurden mehrere relevante Sensoranwendungen untersucht, um die Fähigkeit dieses Ansatzes zu demonstrieren. Ein Immuno-Sensor, der bei 6 GHz arbeitet, wurde entwickelt und dessen Funktionalität wurde durch die Detektion der Konzentration von Kreatinin-Molekülen nachgewiesen. Das Sensorsystem demonstriert die Fähigkeit der Konzentrationsmessung von Kreatinin Molekülen im klinisch relevanten Bereich mit einer Empfindlichkeit der entsprechend etablierten optischen Techniken. Weitere Anwendungen wie die Bestimmung der Glukosekonzentration in einer Suspension und zytometrische Anwendungen wie die Konzentrationsbestimmung von gelösten Partikeln, wurden gezeigt. Ein neuartiger Ansatz, der das gesamte Sensorsystem flexibler und extrem schnellen Messzyklen ermöglicht, wurde nachgewiesen. In einem solchen System besteht das Sensorausgangssignal aus einem DC-Signal und ermöglicht deshalb, das Sensorsystem mit DC-Eingänge und DC-Ausgänge zu nutzen und bietet somit die ideale Plattform für miniaturisierte „Point-of-care“-Diagnosesysteme.

.

Acknowledgement

This thesis would not have been possible without the help and support from a lot of people in my professional and personal life. A PhD thesis is one of the very few cherished documents in one's life. I would like to take this opportunity to thank all the people who have supported me in this segment of my life while pursuing my doctoral studies in IHP Microelectronics.

First and foremost I would like to thank my parents Mrs. Sankari Guha and Mr. Abhijit Guha and my sister Ms. Rumpa Guha who have been the pillars of support in my life. I deeply acknowledge their belief in me and the blessings and wishes that they have bestowed on me. The support they have extended to me to come to Germany and pursue my career aspirations and continue my doctoral studies is immense. I thank them from the bottom of my heart for all that they have done for me.

Dr. rer nat. habil. Christian Wenger, the supervisor of my doctoral studies in IHP, has been in a true sense an excellent support, a wonderful guide and a very good friend during my stay in IHP. As a supervisor, he has given me complete freedom to carry out my research activities and supported me in all my research ventures. As a guide he has given me valuable suggestions to enhance my research standards and establish my research work in an international platform. As a friend he has been very supportive in my ups and downs during my stay at IHP and has given me valuable advices in taking very important steps both in my personal and my professional life. I deeply and sincerely acknowledge the presence of him during my doctoral studies. I would also like to acknowledge Prof. Dr. Roland Thewes, chair of Sensors and Actuators department, TU Berlin. The technical suggestions and advices given by him have increased the technical significance of the thesis by many folds. I would also like to thank him for taking his time out from his very busy schedule and agreeing to be the supervising professor of my PhD work. I would also like to extend my acknowledgement to Prof. Dr. Hermann Schumacher, University of Ulm, for agreeing to co-supervise the PhD thesis. The valuable suggestions given by him aided in improving the quality of the thesis.

There have been many people in IHP who have been a valuable help from the technical aspect of the thesis. I would like to thank all of them for their support. Firstly, I would like to thank Dr. Klaus Schmalz of the dept. of circuit design, IHP. He has been a great support to me while I was designing the high-frequency sensors. I had some valuable conversations and suggestions from him. Dr. Chafik Meliani, guided the work with respect to plaque characterization and imaging. I would like to acknowledge his guidance in the technical aspects. Dr. Frank Herzel, dept. circuit design, IHP, was involved in designing the sensor system, which is used for single particle sensing. I would like to thank him for all the valuable technical insights he provided during the design of the sensor system. Dr. Axel Warsinke, dept. of biotechnology, University of Potsdam, was involved in the immobilization of protein molecules for the establishment of immunosensors. My

heartfelt thanks to him for the support. Mr. Alexander Wolf, dept. of material research, IHP was a hiwi student and supported me while I was designing the microfluidic system for integration with the sensors. Mr. Farabi Ibne Jamal, also working in the same area of high frequency biosensors, dept. circuit design, IHP, has been a constant support and a wonderful colleague. We have designed a lot of circuits together and he was always my support during the critical biological measurements. I would like to thank him for all the work that we have done together.

My acknowledgement would be incomplete if I don't mention the name of Prof. Dr. Thomas Schröder and Prof. Dr. Giovanni Cappellini. Dr. Schröder, head of the department of material research, IHP, has indeed made my stay here quite wonderful. Although he was not a part of the PhD work, he has given me innumerable suggestions about paper writing skills, selecting conferences, writing future proposals and many more. I have thoroughly enjoyed my discussions with him and acknowledge him for all the valuable suggestions. With Dr. Capellini, I have worked on designing of Ge LASERs on CMOS technology which was not a part of my PhD work. The working spirit that I have learnt from him is noteworthy. I deeply acknowledge him for that.

Ms. Ankita Arora, although she was not actively involved during my doctoral thesis, she made a special place for herself while I was finishing the writing of the dissertation. I would like to express my heartfelt gratitude to Ankita for being extremely supportive and above all for being an extremely special person making my life ever so beautiful.

During this thesis work there were a lot of friends who were a personal support. Firstly, Karthik, my closest friend for a long time now, has been a wonderful support all through-out. He has seen my ups and downs very closely and has always stood by me. I cannot thank him in words for all that he has done for me. Payel, a very close friend was a strong support for me always. The long and deep conversations with her kept me going at all stages of my research life, starting way back in my IISC days in India. Mudita who is my sister and a dear friend, made my staying in Germany so easy. Her contribution towards my getting settled in Germany and leading an easy life is immense. I heartily acknowledge her for that. Iria and Pedro, two of my very good friends in IHP, indeed made my living in Frankfurt (Oder) very interesting and lively. Living in the same city and working in the same organization, they really knew the professional and the personal aspects of me and have been very supportive all through-out. I sincerely thank them for that. I would like to thank all my IHP colleagues and friends whose names I could not mention here for making my stay in IHP beautiful. Friends in Germany, like Kiran, Aishcharya, Pragya, were a great company right from the time I started my master studies in Hamburg and continued during my doctoral studies in IHP as well

Above all, I would thank almighty God for giving me the strength to pursue my career aspirations.

Table of Contents

INTRODUCTION

1.1 Motivation

There is an ever-increasing demand for establishment of point-of-care (POC) testing approaches in the field of medical applications and health care. The advancement in the POC technology ensures a positive impact on health, wellness and quality-of-life in both developed and developing world [1]. One of the primary aims of establishing POC devices is to bring down the overall time required to produce the diagnostic test results [2, 3, 4] along with easy handling of medical test devices. Developing sensitive and fast biomedical analysis systems is the foundation for such POC systems. At the same time, keeping the cost of POC systems low is also of prime significance [3] in order to address a mass-market. The design of cheap POC systems with extremely sensitive bio-analysis unit calls for the convergence of various research domains ranging from life science, chemistry, sensor design, circuit design, microfabrication, system design and more.

Presently specialized personnel in laboratories, utilizing off-the-shelf components and instrumentations, carry out most clinical analyses, assuring extreme precision and accuracy of the obtained results. Typical steps for present day medical diagnostics and clinical analysis is shown in Fig. 1.1

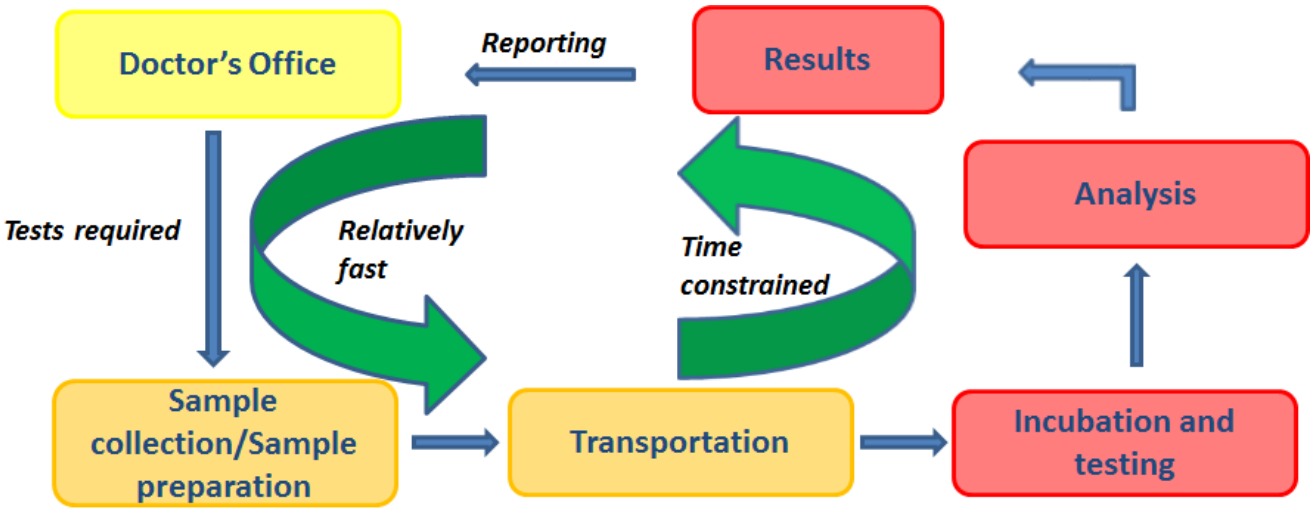

Figure 1.1 Steps for typical clinical diagnostics.

The tests conducted in clinical laboratories require high incubation and analysis time. Therefore, although extremely precise, the present clinical diagnostic approaches require a substantial amount of time to produce the results.

POC systems aim to reduce this time required for the overall clinical diagnostic, for fast detection of disease and easy treatment of them. Fig. 1.2 shows the steps for a typical POC testing. Due to limited number of steps involved in POC systems, the total time between the decision of clinical diagnosis and reporting of final clinical analysis is considerably small. Alongside fast analysis time scale, in order to be an effective system comparable to the clinical laboratories, extremely sensitive sensors (biosensors) are to be used for the clinical analysis in POC systems.

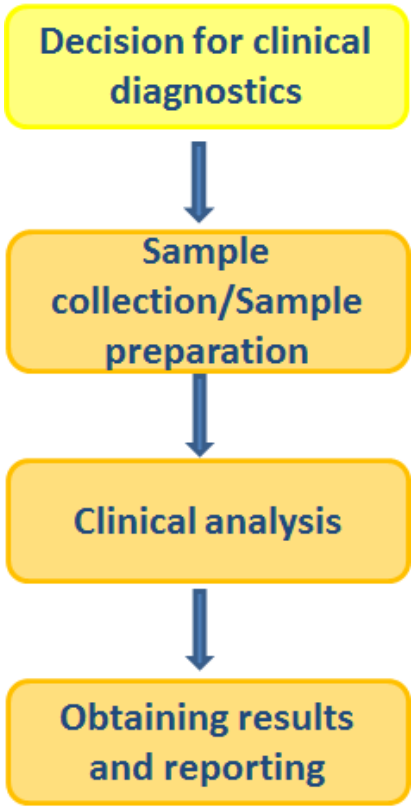

Figure 1.2 Steps for point of care diagnostics. The time constraints are considerably reduced when compared to the standard clinical diagnostic approaches.

This multi-disciplinary design approach of the POC systems as mentioned above has given rise to lab-on-chip (LOC) devices, which are the fundamental bio-analysis blocks of POC systems. LOC devices aim at developing miniaturized sensor platforms, which integrate several laboratory functions on a single chip or a single system. Considerable amount of research work has been dedicated to establish such high sensitive sensors also called biosensors or chem-bio sensors. A biosensor is a device that is used to detect or/and quantify biomolecules based on a biochemical reaction [5]. The biomolecule can be a specific protein or DNA, biomarkers, pathogenic organisms, hormones or other medically relevant analytes [6]. To comply with the standard used in the clinical laboratories, development of innovative analytical devices with enhanced sensitivity, specificity, precision, speed, usability and miniaturization is needed. State-of-the-art

biosensor platforms are mainly based on optical detection schemes. The optical sensors are taken as gold-standard in the field of biomedical diagnostics and they have made their way to commercially available non-invasive POC diagnostic devices. One such example is the pulse oximeter based on optical absorption principles [7] measuring proportion of oxygenated hemoglobin in blood. Commercially available pulse oximeters are hand held devices showing a classical example of POC diagnostic system. The success of such clinical diagnostic devices led to the research of optical biosensors in the area of biomarker detection like immunosensors [8], cytometric applications [6], proteomic analysis [9], infectious disease diagnostics [10], etc. On the other hand, electrochemical sensors have also been another cornerstone technique for POC diagnostic systems. The evolution of the electrochemical glucose sensor into a viable cheap commercial product ever since its inception in 1960's is an example of the success of electrochemical techniques. Therefore, electrochemical techniques for biosensors applied now to biomolecule detection or cytometric applications are also being researched for application in POC systems [11,12,13]. Hence, it is worthwhile to review some of these optical and electrochemical techniques and compare them with the microwave (high-frequency) sensing technique for biological applications, like immunosensors, cytometry, etc., that has been explored in this thesis.

1.2 Optical biosensors

As mentioned above, the success of commercially available optical POC diagnostic systems has prompted the research of optical biosensors for disease detection, viral detection and more. Optical biosensors are based on detection schemes like fluorescence based, [14-28], chemiluminescence [29-40], surface plasmon resonance schemes, [41-47], absorbance based [48, 49] for DNA detection, protein analysis, immunosensing applications etc.

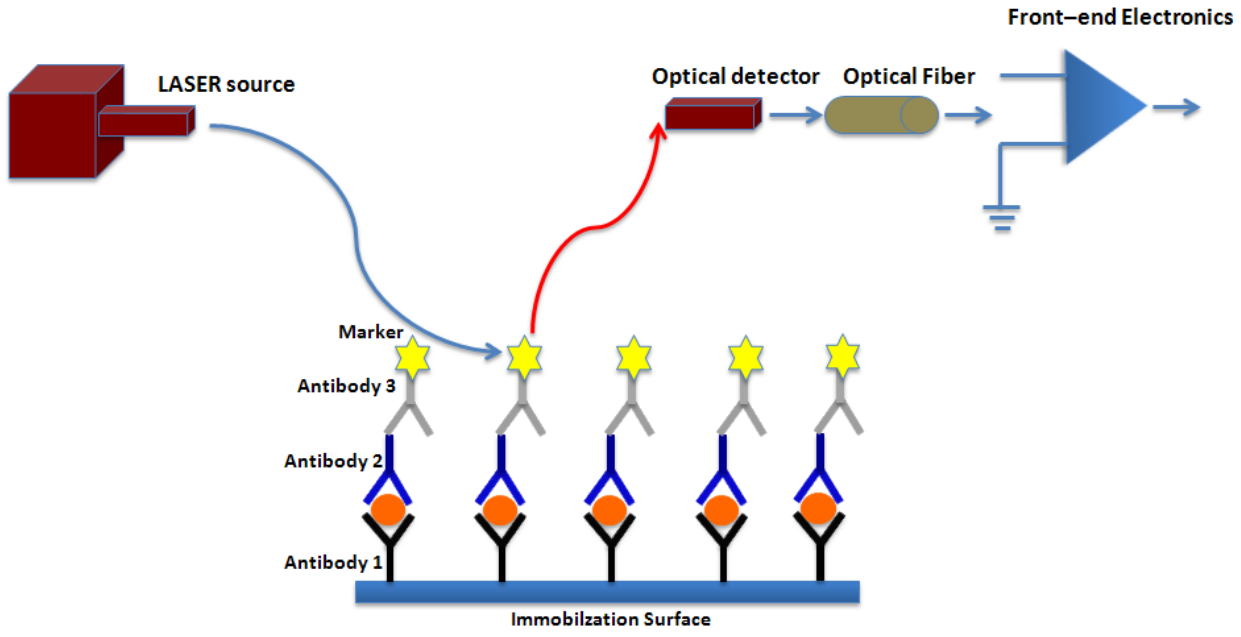

Figure 1.3 Schematic of optical immunosensors based on fluorescence detection.

For example, optical immunosensors have already become the gold-standard approach for clinical diagnostics for determining various biomarkers. Immunosensors provide highly repeatable measurements for a wide range of biomarkers relating the immunoassay event into an optical signal. Fig. 1.3 shows the schematic of a typical optical immunosensor based on fluorescence detection. This is the most common method of detection using an immunoassay. Antibodies are immobilized on an electrode surface. Specific antigens bind to the immobilized antibodies forming an antigen-antibody pair. A second antibody is then bound to the antigen in a sandwich configuration, where the antigen is between two antibodies [50, 51]. An additional antibody with a fluorophore label is bound to the top antibody. Optical signal emitted from a LASER source impinges upon the antigen-antibody pair; fluorescence emission from the fluorophore labels or markers is detected by a photo-detector, for example a photo-multiplier or a CCD camera [7]. The fluorescence gives a direct understanding of the concentration of captured biomarkers in the sandwich approach and therefore, allows for quantitative determination of captured biomarker concentration. A further extension with optical fiber cables is needed to bring the optical signal to the front-end electronics. The fluorescence marker based sensing scheme shows excellent sensitivity and high specificity; such a technique is also suitable for a large variety of biomolecules. The sandwich scheme of antigen-antibody binding and using specific markers for an antigen-antibody couple increases the specificity of the system.

Labeling a biomolecule can often lead to change of the properties of the biomolecule which in turn can lead to falsified output from the sensor. The above mentioned sandwich approach overcomes the issue by not directly labeling the target molecule but using an intermediate step. The established ELISA (Enzyme linked immunosorbent assay) is a classic example of this technique. However, the development cost is increased due to the sandwich approach. Also the use of labeling compounds makes the overall cost of the sensor high. Also additional antibody molecules are needed for the sandwich approach and further for the binding of the fluorophore markers [5]. The translation of the optical sensor signal to electrical signal can lead to signal degradation and also degradation of signal to noise ratio. Although, commercial products like the pulse oximeters mentioned above have achieved excellent integration scheme and translation of optical signal to electrical signal, for biomarker detection and single particle analysis this can be a limiting factor, because of low concentration of test molecules.

Label free optical techniques are developed using approaches like surface plasmon resonance (SPR). This utilizes the coupling of the optical signal to a thin metallic surface as shown in Fig. 1.4. The antigen-antibody pair is immobilized on the surface of the thin metal surface. The optical method in this technique detects the localized refractive index variation around the vicinity of the metal structures. Binding of specific antigen to the antibody changes the refractive index around the vicinity of the metal structure, resulting in the shift of the resonance peak of the reflected light. Being label free, this approach reduces the complexity and cost involved in fluorophore marker based sensors.

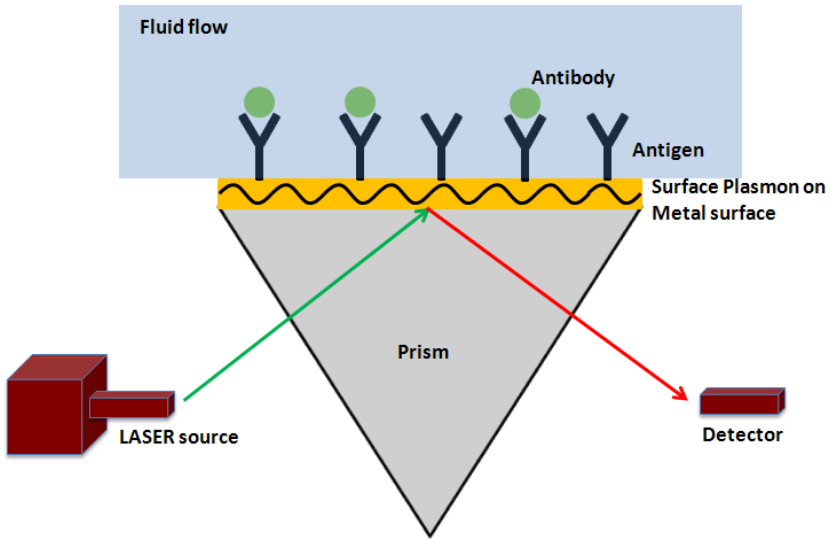

Figure 1.4 Schematic of optical immunosensors based on surface plasmon resonance.

This technique is limited in the detection of smaller concentration of biomolecules [44], because of localized refractive index change. The amount of target molecules required to create a detectable change is high. In other cases, a complex circuit is needed to amplify or detect a minute change of refractive index, which has to additionally overcome the issues of signal degradation while translating optical signal into electrical signal. Other methods of increasing the detection limit of SPR is using nanoparticles or nanostructures which also require stringent fabrication technique. Also in SPR based biosensors, false signal is a problem in complex solution like blood or urine [43]. Hand-held POC diagnostic devices have been demonstrated [45], which could overcome the shortcomings of limited detection or selectivity using the techniques mentioned above.

1.3 Electrochemical biosensors

Electrochemical sensors are based on interaction of chemical species with electrodes resulting in electrical signals primarily current (amperometric sensors) [52-60], potential (potentiometric sensors) [61-65] or impedance (impedimetric sensors) [66-70]. Integration of electrochemical sensors with the front-end electronic circuits for signal read-out is considerably easier when compared to optical sensors, due to inherent electrical signal output from the sensor. Therefore,

at the integration level, which involves packaging and assembling, electrochemical sensors are less complex when compared to their optical counterparts. This has led to inexpensive, easy to use POC diagnostic systems, like the commercially available blood-glucose monitoring devices.

On the same lines, there has been considerable effort to extend the research of electrochemical sensors towards detection of concentration of biomarkers, viral detection and more. Electrochemical sensors are known for being label free, thus nullifying the issues related to labeling compounds. However, for applications like immunosensor, labeling is still required. Fig. 1.5 shows a typical electrochemical (amperometric) immunosensor approach using labeling technique. Amperometric techniques use a three electrode measurement setup, with a working electrode, counter electrode and a reference electrode. The immunosensors operate by the detection of current on the working electrode. The current is generated due to the redox reaction at the surface of the electrode. It should be noted the same sandwich approach for antibody-antigen pairing as was seen in optical sensor is used in most of the electrochemical immunosensors as well. In case of electrochemical sensors, redox markers are used instead of fluorophore markers in optical sensors. The redox markers initiate a cyclic oxidation-reduction process at the working electrode and produce a current due to the exchange of electrons [59].

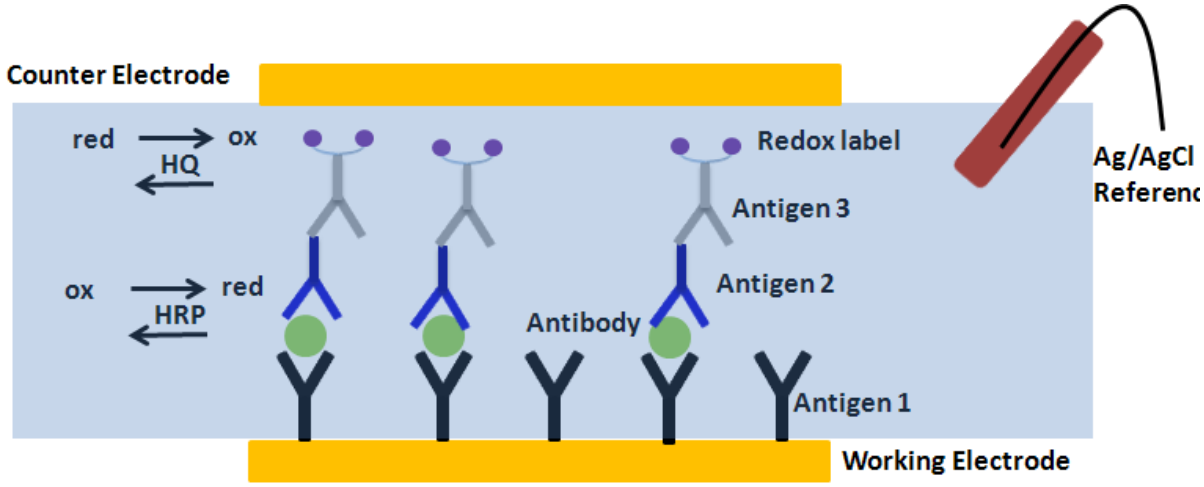

Figure 1.5 Schematic of optical immunosensors based on amperometric detection technique.

Labeled electrochemical amperometric techniques also offer high specificity due to labeling technique with fairly less complex front-end integration when compared to optical immunosensors. However, the limitations caused by labeling compounds still persist in this kind of electrochemical immunosensors. Therefore, the cost of the sensor system is still considerably higher due to the use of labeling compounds. In single molecule detection, label free electrochemical sensors are used [71]. Such sensors no longer suffer from the problems of labeling compounds.

Electrochemical sensors based on impedance measurements and have been demonstrated by various research groups like, Goh and Ram [72], Krommenhoek *et al.* [73], Faenza *et al.* [74]. Commercial products based on electrochemical impedance spectroscopy have been demonstrated by Micronit microtechnologies [75], Gamry Instruments [76] and more. Usually impedance measurements are performed at frequency range of 100 KHz to a few MHz as described by Krommenhoek *et al.* [73]. In this frequency range ("low-frequency"), biological suspensions especially of suspended cells show dielectric dispersions based on their properties, for example, potential across the cell membrane and cell walls [77]. Therefore, designing the sensors in this frequency range is competent for detection cellular properties governed by low-frequency dispersion mechanisms (for e.g., in case of cells, membrane capacitance). Electrochemical sensors based on impedance measurements also require reference electrode for precise measurements.

It is seen that an important component of any form of electrochemical sensor is the reference electrode. The use of reference electrode is needed to keep the sample solution at a thermodynamic equilibrium. The additional reference electrode can often make the overall integration scheme cumbersome [59]. However, considerable effort has been put into miniaturization of reference electrodes, but it is still an irreplaceable component of electrochemical sensor, therefore, increasing the overall development cost and design complexity of the sensor. Commercial products like i-STAT (Abbott Point of Care, U.S.A) [70] for blood analysis, have overcome the miniaturization issue with respect to reference electrodes with additional effort in the overall design. However, the penetration of electrochemical based immunosensors, pathogen concentration detector products is still very slow even after 10 years of research activities. The biggest challenge for electrochemical sensor is the establishment of automated array platform with fast electrical response and signal processing.

All in all, it is seen the technique of sensing applied for biological purposes is application specific and is therefore, difficult to establish a universal biosensing technique for POC diagnostic device. While optical sensing technique is feasible for a vast number of applications (pulse oximeter, ELISA technique as examples), electrochemical sensing is suited for other applications like blood glucose monitoring systems. Low-frequency impedance sensors are suited for determining cellular parameters like cell membrane properties. However, in detection of concentration of biomarkers, pathogens, high-frequency (GHz range) dielectric sensing is becoming an extremely attractive option. Concentration of molecules in a medium influences the permittivity of the medium which can be detected with a capacitive sensor. The use of high frequency aids in miniaturization of the overall system. Compared to labeled optical sensors used for the same applications, the high-frequency dielectric sensors require no labeling compounds. It is an all-electrical sensing technique. Sensitivity of the order of single particle detection can be demonstrated by the established high-frequency capacitive sensors. Therefore, extremely low concentrations of analyte can be detected with better signal to noise ratio as compared to label free optical sensors. When compared to electrochemical techniques high-frequency capacitive

sensors for dielectric detection require no additional reference electrodes for the system. Therefore, the complexity with regard to the overall development of the sensor system is reduced. In detection of concentration of analytes in a suspension high-frequency dielectric detection avoids the low-frequency dispersion mechanisms, therefore, eliminating the chances of false data. Integration of these high-frequency sensors with CMOS/BiCMOS technology opens up the possibility of a new market for POC diagnostics involving detection of concentration of biomarkers, viruses, analytes and more. Such a market if established, the CMOS integrated high-frequency biosensors can usher in cheap POC diagnostic products utilizing batch fabrication of the standard CMOS process. In this thesis, high-frequency capacitive sensors operating at microwave frequencies and fabricated in standard CMOS process, have been explored for applications like immunosensor, analyte concentration detection, cytometry.

1.4 CMOS/BiCMOS microwave biosensor platform

The growth of semiconductor industry can be tracked back to the famous paper published by the INTEL co-founder Gordon Moore in 1965, where he stated, that, "the number of components that could be incorporated per integrated circuit would increase exponentially with time" [78] This trend that has been observed since 1970, of number of transistors in an integrated circuit doubling every eighteen months is called the Moore's law. As a consequence of this trend, miniaturization of circuits by scaling down of transistors has been the driving force for technology advancements. At the same time there has been considerable advancement in microfabrication technology leading to fabrication of structures of the order of few nano-meters possible.

The trend of miniaturization with increasing performance is often traded off with power consumption. This leads to the direction of new transistor concepts, new materials, and is referred to as "More Moore" [79]. Then there is a second trend, which is characterized by diversification of functionalities on semiconductor based devices. This trend is referred to as "More Than Moore". The additional functionalities incorporated on the semiconductor based devices also aid in miniaturization and scaling, although not at the same rate as the transistor scaling. Functional diversification includes interaction with the outside world through sensors and transducers, and can be implemented with the incorporation of passive components, micro-electro-mechanical systems (MEMS), surface acoustic wave filters and actuators, microfluidic integration etc. Thus, More Than Moore is a heterogeneous integration technology of digital and non-digital applications on the same semiconductor process platform leading to wide variety of application fields. Establishment of biochips or biosensors is one such field and is depicted in the technology roadmap in Fig. 1.6.

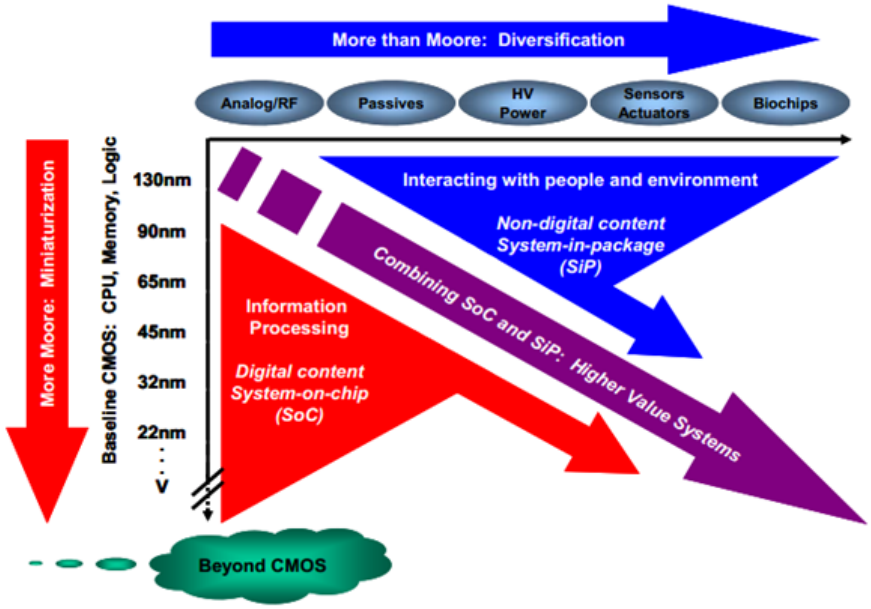

Figure 1.6 Technology road-map showing More Than Moore concept [72].

The primary advantages of monolithically integrated biochips on a CMOS platform are:

- Signal processing capabilities in close proximity to the sensor
- Batch fabrication for large number of device manufacturing
- Miniaturization of the overall system
- "All-electrical" sensor systems requiring no labeling

Additionally, as mentioned above, if the monolithic CMOS POC diagnostic devices become a reality for commercial products, low cost can be achieved due to batch fabrication technique.

The concept of CMOS based biochips is shown in Fig. 1.7. The first and second generation biosensors used functionalized bio-receptor coupled to a transducer. Further microelectronic circuits were then integrated with the transducer to extract the signal output. The new approach of complete CMOS biosensor chip involves the elimination of bioreceptors and capability of using the metal layers of the CMOS process for immobilization or detection of biomolecules. This is shown in Fig. 1.7 where the biomolecules are shown to be captured on the passivation layer of the back-end-of-line (BEOL) stack of the CMOS process or the exposed metal layer of the CMOS process. Complete CMOS biosensors or biochips have then been explored by researchers for various applications like DNA characterization [80-82], detection of biomarkers [83], cytometric application [84-86]. DNA sensor developed by Stagni *et al.* [81] shows an additional post-processing step of depositing gold electrodes on top of the CMOS chip for DNA immobilization.

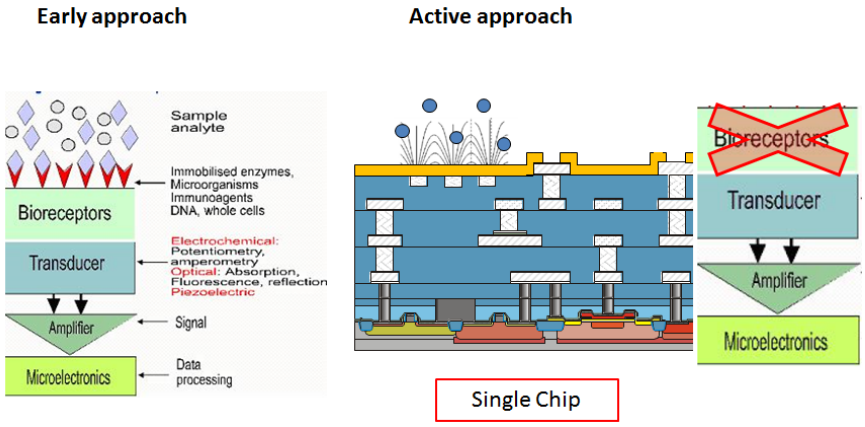

Figure 1.7 CMOS single chip biosensor approach.

On the other hand, CMOS image sensors developed by Hassibi *et al.* [83] shows the use of exposed top metal layer of a five metal CMOS process for the capture of biomolecules. The sensing scheme in the mentioned CMOS sensor is primarily based on the interface capacitance of the electrodes and the fluid containing the biomolecules.

The advances in RF engineering have further led research groups to explore high frequency characterization of biological suspensions and biomaterials. As early as 1998, Stuchly *et al.* [87] demonstrated biosensors based on waveguide structures. Since then considerable amount of research work have been devoted to the establishment of microwave based biosensors. Sensors based on whispering-gallery mode resonator [88], coaxial resonator [89], coplanar lines [90,91], capacitors [92] have been demonstrated for the distinction of cells and proteins, DNAs, biomarkers for tumors and cancer etc. Ferrier *et al.* [93] have also shown interferometric microwave sensors for detection of single cells.

Fig. 1.8 shows one such approach used by Grenier *et al.* [91,92]. Coplanar multi-fingered capacitor is used as a passive sensor structure in order to detect different concentration of cells.

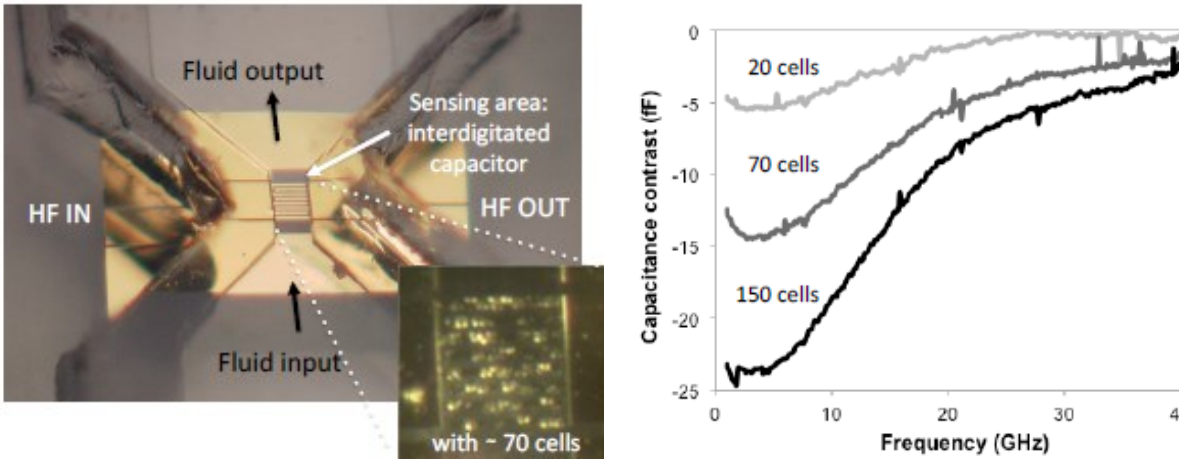

Figure 1.8 Passive microwave sensors for detection of concentration of cells [91].

The capacitive sensor is fabricated on a microwave substrate and a fluidic system is integrated on top of the sensor. The advantages of microwave sensing towards miniaturization can be understood from the sensor setup. The dimension of the sensor in the order of micrometers matches the dimensions of the cells being investigated. Therefore, along with the miniaturization, the sensitivity is also improved due to the physical dimension. The measurement setup in such a sensor system involves measuring of the scattering parameters of the passive capacitor. As mentioned above, the ionic background and the electrode electrolyte interface do not play any role in microwave sensing. The high frequency of the electrical signal penetrates through the interface or double layer capacitance, nullifying its influence.

Another often used configuration for microwave detection technique is based on interferometry. Sensitivity of the order of single cells has been demonstrated by Yang *et al.* [94]. Such a configuration of the sensor is shown in Fig. 1.9.

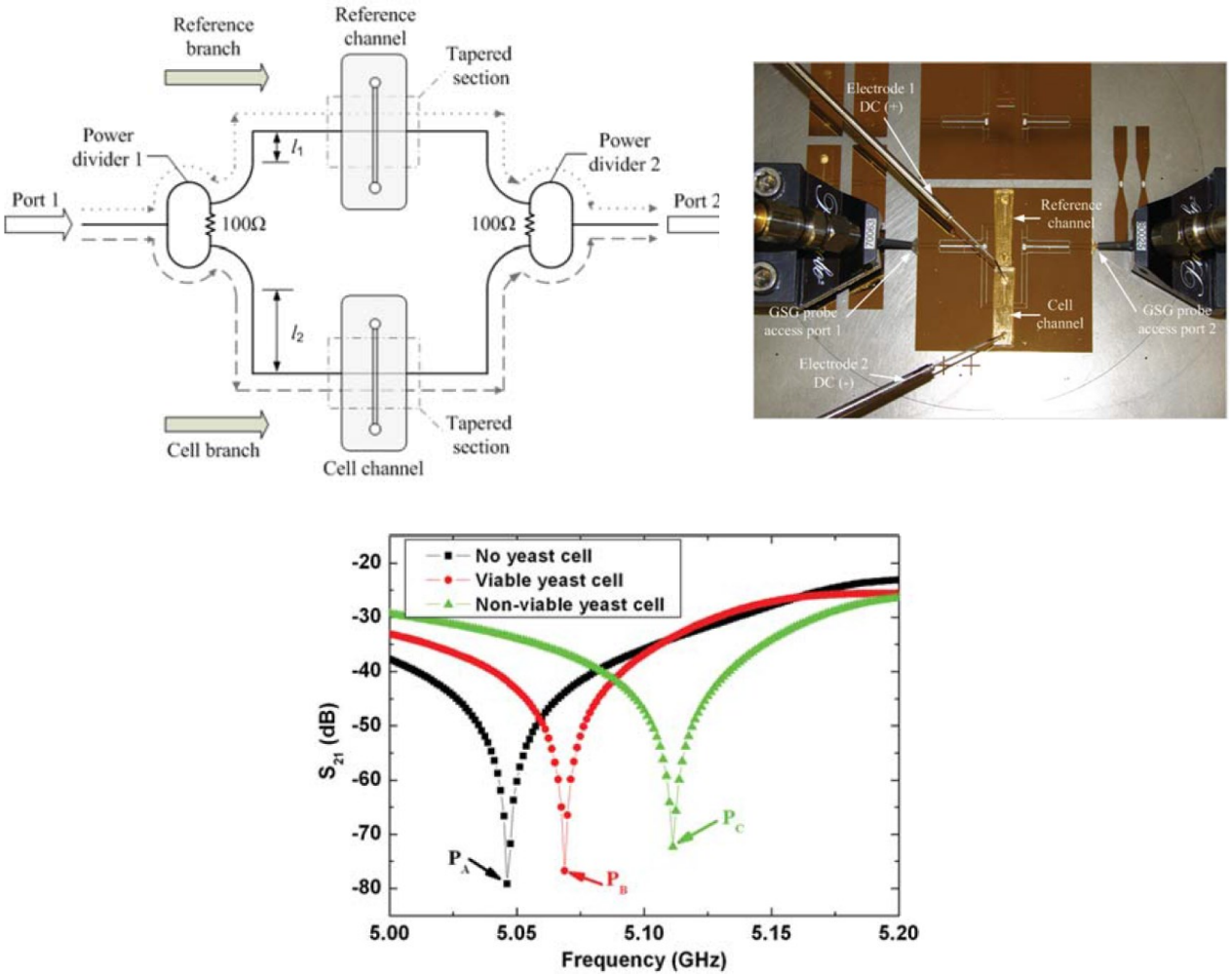

Figure 1.9 Interferometric approach based on passive structures for biosensors [88].

The interferometric approach offers very high sensitivity due to a differential measurement technique. The sensor architecture which involves coplanar transmission lines are fabricated on a microwave substrate and similar scattering parameter measurement is employed as discussed in case of the capacitive sensor. This is shown in Fig. 1.9. However, all the microwave sensor configurations are passive structures.

Therefore, the next step is the monolithic integration of microwave sensor architecture on CMOS/BiCMOS platform. In this thesis work, sensor concepts based on CMOS integrated microwave sensors are presented. Efforts are being made by few contemporary research groups around the world to establish CMOS microwave sensors but majorly focused on cytometric applications like counting of cells [95], or particles based on magnetic makers [96]. This work is focused on establishing a unique platform for significant biosensor applications like immunosensors, analyte concentration detection and cytometric applications as well.

A sensing scheme is introduced in the thesis work which is applied to all the sensing applications explored in this work. The sensing principle is based on the variation of capacitance (here an interdigitated capacitor) embedded in a CMOS oscillator, causing a shift in the resonant frequency of the oscillator. The change of capacitance is caused by the variation of fringing electric fields of the interdigitated capacitor (IDC), due to the change of permittivity on top of it. The sensor capacitor is fabricated on one of the two top metal layers in a BiCMOS process with seven metal layers or five metal layers. The sensor topology is shown Fig. 1.10.

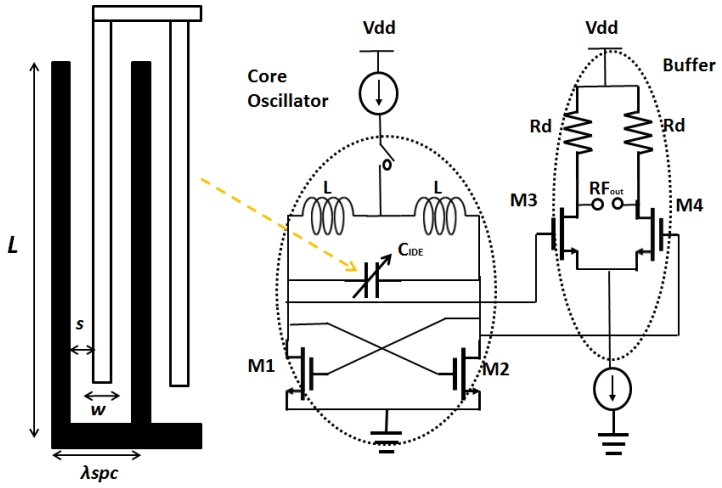

Figure 1.10 Sensor architecture used in this thesis. Capacitive sensor is embedded in a CMOS oscillator circuit.

For the application of immunosensor detection of creatinine molecule is demonstrated. For the proposed dielectric immunosensor the permittivity variation is brought about by the different amounts of anti-creatinine antibodies binding to the creatinine molecules immobilized on the

IDC. In this work, a method to immobilize creatinine molecules on the surface of silicon nitride (Si_3N_4) layers has been demonstrated. Si_3N_4 is the standard passivation layer for CMOS technologies; therefore, the capability of immobilizing creatinine molecules on its surface helps to evade any additional post processing steps for future label free sensors used in creatinine detection.

For the cytometric applications, microfluidic system was integrated with the sensor system for accurate handling of the probe solution. Polymer based microfluidic system has been used in this work. A chemical mechanical polishing step is conducted on the fabricated to chip to adhere to the planarity issues for integration of microfluidic system with the silicon chip. On chip signal processing capabilities for improved sensitivity and POC system applications is shown in this work.

1.5 Need for microfluidic integration

Advancement in the field of microfluidic technology has played a key role in the development of LOC devices. The first advancement of microfluidics towards LOC applications was demonstrated by Manz *et al.* [97]. Since then considerable improvement has been made in the microfluidic technology for precise handling of biological suspensions. Microfluidic platforms provide a well-defined volume of fluid samples and provide easy handling of fluid samples. Fluid sample of extremely small volumes can be handled using present microfluidic systems. The active geometry of the microfluidic systems also matches closely the dimensions of biological samples (cells, bio-molecules etc.). The main limitation of integration of microfluidic system with electrical sensors is the overall size of the sensor system, which is often defined by the size of the microfluidic system.

In this aspect two approaches are being often explored. The first approach is based on silicon microfluidics. Silicon microfluidics is gaining interest because of easier integration with the CMOS process technology. Kaynak *et al.* [98, 99] have explored the integration of a microfluidic platform on BiCMOS platform with the backside etching of the silicon wafer after the fabrication of the BiCMOS sensor circuit. Such a technique is extremely advantageous for building monolithic sensor system and also standard microfluidic components such as microfluidic switches, valves, mixers, micro-pumps can be implemented on the silicon substrate using standard CMOS or BiCMOS process steps. However, thinning or polishing of the backside of the wafer in order to have microfluidic channels of desired dimension is a major challenge in such systems. Standard 8'' Silicon wafers have a thickness of 750 µm. Microfluidic channels have thicknesses of the order 50 µm to 200 µm depending upon the applications. Therefore, in order to fabricate microfluidic channels of that order based on backside etching of silicon wafer, the wafer has to be polished or thinned to the order of few 100 µm. This requires complex process steps. The mechanical stability of the silicon wafer during and after the polishing step is also of

primary concern, as the thin wafer is prone to bowing and breaking. Therefore, often a less complex microfluidic integration based on polymer is used for faster system design and sensor prototype establishment.

The concept of polymer based microfluidic technique was established and shown by Whiteside *et al.* [100, 101], for integration of microfluidic systems with sensors based on glass substrate. In this thesis, polymer based microfluidic technique is used to handle liquid samples and analytes. In order to integrate the polymer microfluidic systems on BiCMOS silicon chip additional polishing step of the chip is conducted in order to obtain the topographical planarity required for the integration process. Polydimethysiloxane (PDMS) is used as the polymer in such microfluidic approaches and there is a strong affinity between PDMS and glass, resulting in strong bonding between the glass substrate and PDMS microfluidic system. Therefore, in order to establish comparable bonding strength between the silicon BiCMOS chip and PDMS microfluidic system, the process recipe for preparation of the PDMS microfluidic system and the bonding steps are determined based on the material properties of PDMS and the passivation layer of the BiCMOS process.

Organization of thesis

The thesis is organized in the following manner. The second chapter deals with the theoretical aspect of integration of biosensors on a BiCMOS platform. The challenges from the design aspect and the possible solutions are discussed in this chapter. The choice of the sensor topology and its functioning is shown.

The subsequent three chapters deal with significant applications of the established biosensor technology. The first among them is the immunosensor application discussed in chapter 3. Immunosensors is one of the main applications discussed in the thesis. In this chapter the application of the sensor operating at 6 GHz as immunosensor for detection of creatinine concentration is shown. The operation of the sensor system is further compared with the established optical sensing techniques in terms of sensitivity and dynamic range.

Chapter 4 deals with the sensors operating in the frequency range of 6 GHz to 12 GHz for primarily detection of concentration of a solute in a suspension. In this aspect glucose sensors are discussed. Further cytometric application like detection of concentration of particles in a fluid system has been addressed. A major focus in this chapter is the integration of microfluidic system with the BiCMOS sensor chip. Possible techniques based on polymer based microfluidic systems or based on non-conducting wall around the sensor have been explored.

Chapter 5 shows the establishment of a total sensor system, which is capable of particle counting in a flow-based fluidic system. The main focus of this chapter is the establishment of extremely sensitive sensor system in order to detect single particles. The other aspect of the sensor system

is to have DC read-out and the same has been investigated. Further theoretical investigations are done for the elimination of noise form such biosensors.

Conclusion of the thesis based on the application of the sensors in various biological avenues is presented in chapter 6. Each application has been concluded depicting the ability of the sensor architecture to replace the established complex biosensors. An outlook of the work showing the future perspectives of the thesis is presented in the end.

DESIGN and INTEGRATION

2.1 Introduction

In line with the "More Than Moore" diversification of semiconductor technology, integration of the biosensors on standard CMOS technology platform has the potential to bring in a new market for POC diagnostic applications [79]. This has been discussed in chapter 1. Bringing together "biology" and CMOS technology on a single chip is a significant step in terms of integration of technologies. The integration of biosensors on CMOS technology ensures high yield and reliability of the overall system; primarily due to the robustness of the established CMOS process technology [102]. However, it should be emphasized here that the integration of "biology" and the process steps required for the integration of the biosensor system should not cause any degradation of the performance of the CMOS active circuit components [103]. CMOS technology platforms are primarily optimized with the goal of increasing the performance and yield of the CMOS devices like transistors. However, interaction of biology with the CMOS active devices can play a significant role affecting their performance [103]. For example, one such situation is the issue of integration of microfluidic platform with the CMOS/BiCMOS sensor chip. The fluid in the microfluidic channel influences the passive components and the active devices in the circuit. Therefore, the design of the sensor chip and the integration of microfluidics have to be such that the fluid channel has minimum or no interaction with the other circuit components other than the sensor structure. This consideration has been demonstrated in this chapter in designing the sensor layout, pad-frame of the chip and the footprint for the polymer microfluidic system used for sensing of the analytes.

CMOS sensors operating in the frequency range of 5 GHz to 15 GHz are explored in this thesis. Therefore, influence of "biological" integration on the high-frequency performance of the circuit components has to be taken into account. One such example is the influence of dielectric loss due to the sensing material on the overall sensor and the circuit performance. The design of the sensor circuit has to carefully take into account the dielectric losses that can be incurred during the sensor operation. This design consideration has been taken into account and demonstrated in this chapter.

The sensor architecture employed in this thesis is based on a capacitive sensor embedded in a CMOS oscillator. The oscillator design involves use of inductors as an integral part of the sensor system. The inductors coupled with the sensor capacitor constitute a resonator, and the oscillation of the resonator is driven by a pair of transistors. A change in permittivity is detected by the sensor capacitor which translates into the change in oscillation frequency of the resonator. The change in permittivity can also influence the inductors by changing its parasitic capacitance.

Therefore, the apparent inductance can change or in other words there can be a detuning of the inductor. The design of the sensor chip layout and the positioning of the "biological" integration should take into account of this influence.

The sensor used in this thesis is an interdigitated capacitor (IDC). The sensing mechanism is based on the effect of dielectric materials on the fringing electric fields between the fingers of the IDC. The analysis and design of the IDC is based on the coplanar transmission line and is addressed in this chapter.

It is also significant to understand the technology platforms used for the designing of the overall biosensors. In this aspect it is necessary to understand the back-end-of line (BEOL) metal stack of the BiCMOS process used. Therefore, this chapter deals with the technology platforms followed by the design and integration challenges of the biosensor.

2.2 Technology and integration

2.2.1 Technology

The sensors are fabricated in standard BiCMOS technology of IHP namely SG25H1 (0.25 µm BiCMOS process) and SG13S (0.13 µm BiCMOS process). The technology platforms offer high performance heterojunction bipolar transistors capable of operating up to 300 GHz. Therefore, the technology platform is highly suitable for designing high-frequency circuits. Integrated biosensors on the BiCMOS technology platform bring diversification of the BiCMOS platforms, which are primarily used for radio-frequency (RF) to microwave communication systems [104]. The performance parameters of the two technologies are given in Table 2.1 and Table 2.2.

Table 2.1: performance parameters of SG25H1

Parameter	High performance
HBT fmax	220 GHz
HBT ft	180 GHz
Maximum HBT breakdown voltage (BV_CBO)	4.8 V
MIM Capaitor	1.15 ff/µm^2
Varactor (Cmax/Cmin)	3

Table 2.2: performance parameter of SG13S

Parameter	High performance
HBT fmax	300 GHz
HBT ft	250 GHz
Maximum HBT breakdown voltage(BV_CBO)	6V
MIM Capaitor	1.65 ff/μm^2
Varactor (Cmax/Cmin)	3

The transistors constitute the front-end-of-line (FEOL) of the silicon process, with the passive structures and interconnect fabricated with the metallization layers on the BEOL. Fig. 2.1 shows the cross-sectional schematic of the BEOL stack of the SG13S and SG25H1 process of IHP.

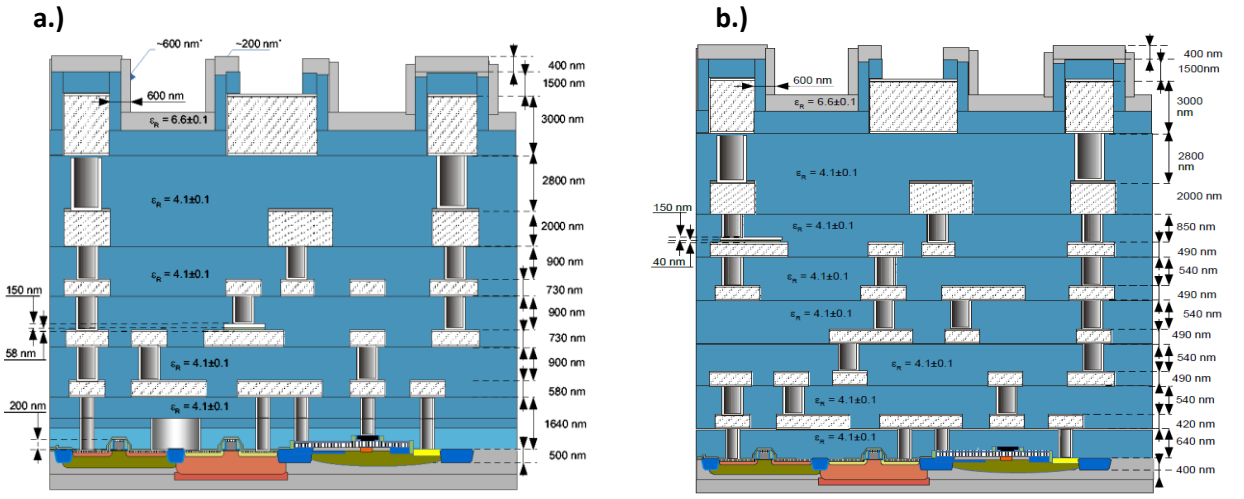

Figure 2.1 Cross section schematic of BiCMOS Back-end-of-line stacks of IHP. a) SG25H1 BiCMOS process with five metal layers. b) SG13S BiCMOS process with seven metal layers.

There are five metallization layers in the BEOL stack for SG25H1 process, while the SG13S process has seven metallization layers. The top two metallization layers (TM1 and TM2) of both the processes have higher thickness compared to the other metallization layers. These metal layers are used to fabricate high quality factor RF passive components like inductors, transmission lines, etc. The lower metal layers are used for interconnects within the circuits. As mentioned above, integrated biosensors on such standard BiCMOS/CMOS platform is considered as major technology advancement and the sensors are termed as the next generation biosensors. The schematic shown in Fig. 2.2, shows the approach in which the biological integration is performed on top of the BEOL stack of the CMOS/BiCMOS process. The

biological integration includes immobilization of proteins or other biomolecules on top of the passivation layer of the BiCMOS stack or bonding of microfluidic systems carrying biological suspensions on top of the BiCMOS stack.

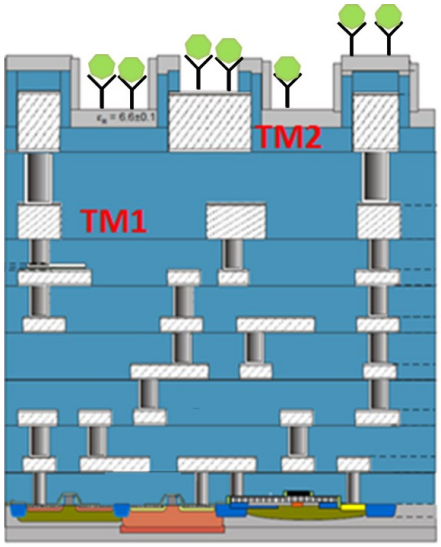

Figure 2.2 New sensor approach: Integrated CMOS sensor scheme.

One of the metallization layers in BEOL stack is used as the sensor/transducer and the electronic circuitry for sensor read-out, data acquisition and signal processing is constituted with the BiCMOS active devices (transistors) and passive components (MIM capacitors, resistors) integrated in the same stack as mentioned before. Therefore, the next generation biosensors are essentially single chip solution. The BEOL of the BiCMOS processes of IHP are passivated with a 400 nm thick layer of silicon nitride (Si_3N_4) and has a permittivity of 6.7. The intermediate dielectric between the metallization layers is silicon dioxide (SiO_2) with permittivity of 4.2. Therefore, the biological integration on top of the BEOL processes is separated from the transistors (at the FEOL of the BiCMOS process), by the above dielectric layers and hence, as mentioned previously, the biological interaction does not influence the operation of the transistors.

2.2.2 Influence of biological material and Integration

Planar interdigitated capacitors (IDC) fabricated on the topmost metal layer of the BiCMOS stack (TM1: top metal 1/TM2: top metal 2) are investigated as sensors in this thesis. In the immunosensor application explored in this thesis, the sensor is fabricated on the TM1 metal layer due to surface chemistry requirement for immobilization of biomolecules. While, for the applications of cytometry and single particle detection, the sensor is fabricated in TM2. Fabricating the sensor structure comes more from the aspect of biology; the biological compounds, for e.g., protein molecules in case of the immunosensors are immobilized on top of

the passivation layer of the topmost metal layer. In case of microfluidic interaction where fluids are analyzed, the microfluidic system is also heterogeneously integrated on top of the BEOL stack. Therefore, fabricating the sensor structure on the top metal layers ensures proximity of the sensor to the biological integration. This is significant for the overall sensitivity of the sensor system.

As mentioned in the previous section, the sensor architecture employed in this thesis is in the configuration of a resonator where the sensor capacitor is coupled with a pair of inductors. The schematic of the resonator is shown in Fig. 2.3 (a). The sensor capacitor detects the permittivity change in the bio-sample. The permittivity change can be brought about by concentration of particles in a suspension or concentration of immobilized biomolecules on the sensor, etc. This permittivity change causes a shift in the oscillation frequency of the resonant tank, and is read out by the CMOS oscillator circuit.

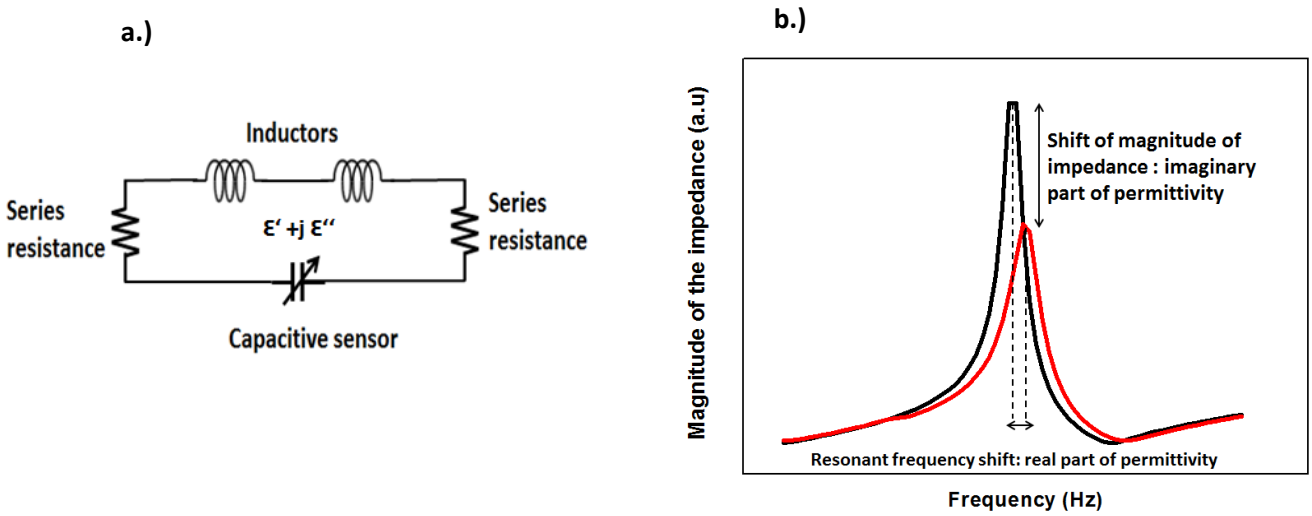

Figure 2.3 a) LC resonant tank circuit with the capacitor acting as the sensor b) quality factor of the LC tank circuit with and without loss.

The quality factor of the resonant tank is determined by the quality factors of the individual components. The fundamental definition of quality factor (Q) is defined as [106],

$$Q = 2\pi f \frac{energy\ stored}{average\ power\ dissipated} \tag{2.1}$$

where f is the resonance frequency of the LC tank. The frequency shift of the resonant tank is caused by the real part of the permittivity of the material. However, permittivity is a complex quantity with two components,

$$\varepsilon = \varepsilon' + j\varepsilon'' \tag{2.2}$$

where ε' is the real part of the permittivity and ε'' is the imaginary component of the permittivity [107]. The imaginary component of the permittivity determines the losses or degradation of electric field. Therefore, along with sensing of resonance frequency shift there is a variation of the output electric field power based on the complex permittivity of the material shown in Fig. 2.3 (b). The imaginary part of the permittivity, therefore, influences the quality factor of the resonator by affecting the loss and in turn the average power dissipation.

The biological suspension carrying the cells, proteins, and other bio-materials are often extremely lossy [108,109]. With respect to microwave passive structures, the lossy materials reduce the quality factor of the structure. This is seen in Fig. 2.3 (b), where the magnitude of the impedance of the tank is seen to reduce with the increasing losses. This is due to increase in average power dissipated due to the increase of losses.

At this juncture it is important to understand the influence of quality factor on the overall sensor system. With the reduction in the quality factor, the oscillations of the resonant tank are damped as shown in Fig. 2.4.

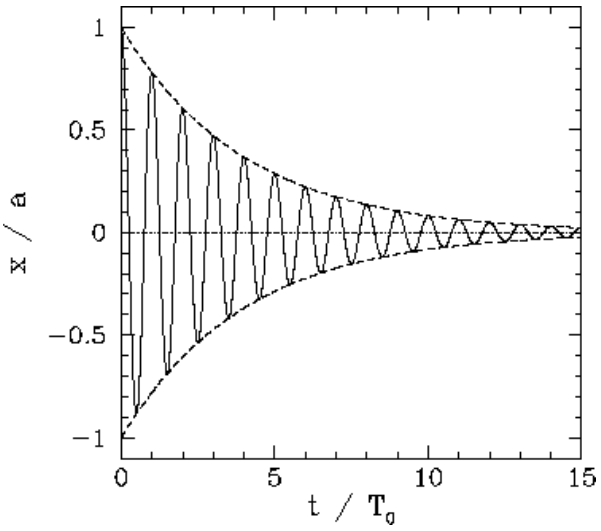

Figure 2.4 Damped oscillation due to loss. The losses are incurred due to the series resistance accompanying the inductors as well as the imaginary part of the permittivity of the biomaterial.

The damped oscillations already originate from the series resistance associated with the inductors due to finite conductivity of the metallization layers used for the inductor design. The additional material loss reducing the quality factor of the sensor system further enhances the loss and results in further damping of the oscillations. From the CMOS active circuit design (oscillator here) aspect, used to read out this oscillating frequency, there should be compensation mechanism for the losses. The active circuit of Fig. 2.5 is such a compensation mechanism. The CMOS oscillator topology employs the strategy of negative resistance to compensate for the

losses [110]. However, here it should be mentioned that the negative resistance compensation should be comparatively higher compared to the oscillators designed for communication circuits. In this case the dielectric loss on the sensor should also be taken into account. One can run into the problem of overcompensating the losses or in other words having a very high compensation for low loss materials. In that case, the output of the oscillator will not remain sinusoidal due to saturation of the oscillator. However, in this thesis the main objective is to determine the variation in the oscillation frequency of the oscillator, therefore, the loss of sinusoidal output of it is not of high significance. Water was considered to be the dielectric material with highest losses and air was considered to be with minimum dielectric loss. The oscillator design was performed to accommodate this range of losses.

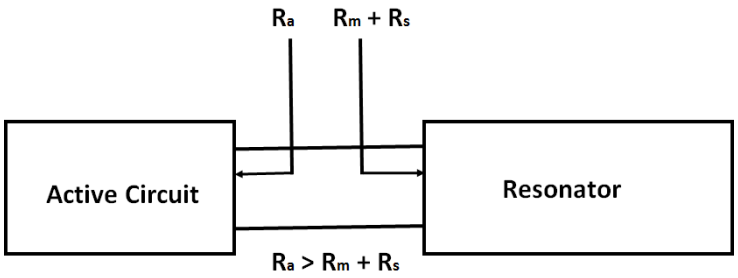

Figure 2.5 Negative resistance compensation done by the active circuit in order to sustain the oscillation of the resonance tank.

More on this is dealt within the subsequent section where the circuit design aspect in the thesis has been addressed. Therefore, the lossy biomaterial placed on top of the sensor structure plays a significant role in determining its quality factor and in turn in the performance of the overall sensor oscillator.

Now it is necessary to understand how the theoretical aspects affect the integration of the sensor system. As mentioned above the capacitive sensor is generally fabricated on the top metal layers for high sensitivity. However, if the inductors are placed very close to the sensor, the biomaterials might actively influence the performance of the inductors. The real part of the permittivity influences the parasitic capacitance of the inductor, therefore, detuning the value of the apparent inductance of the inductors. This effect modifies the oscillating frequency of the oscillator. Therefore, an unwanted parameter gets added to the sensor system, where the shift in the oscillating frequency has to be mapped to the change in capacitance of the sensor capacitor and the partial change in the inductance of the inductors, depending on the area of coverage of the inductor by the biomaterials.

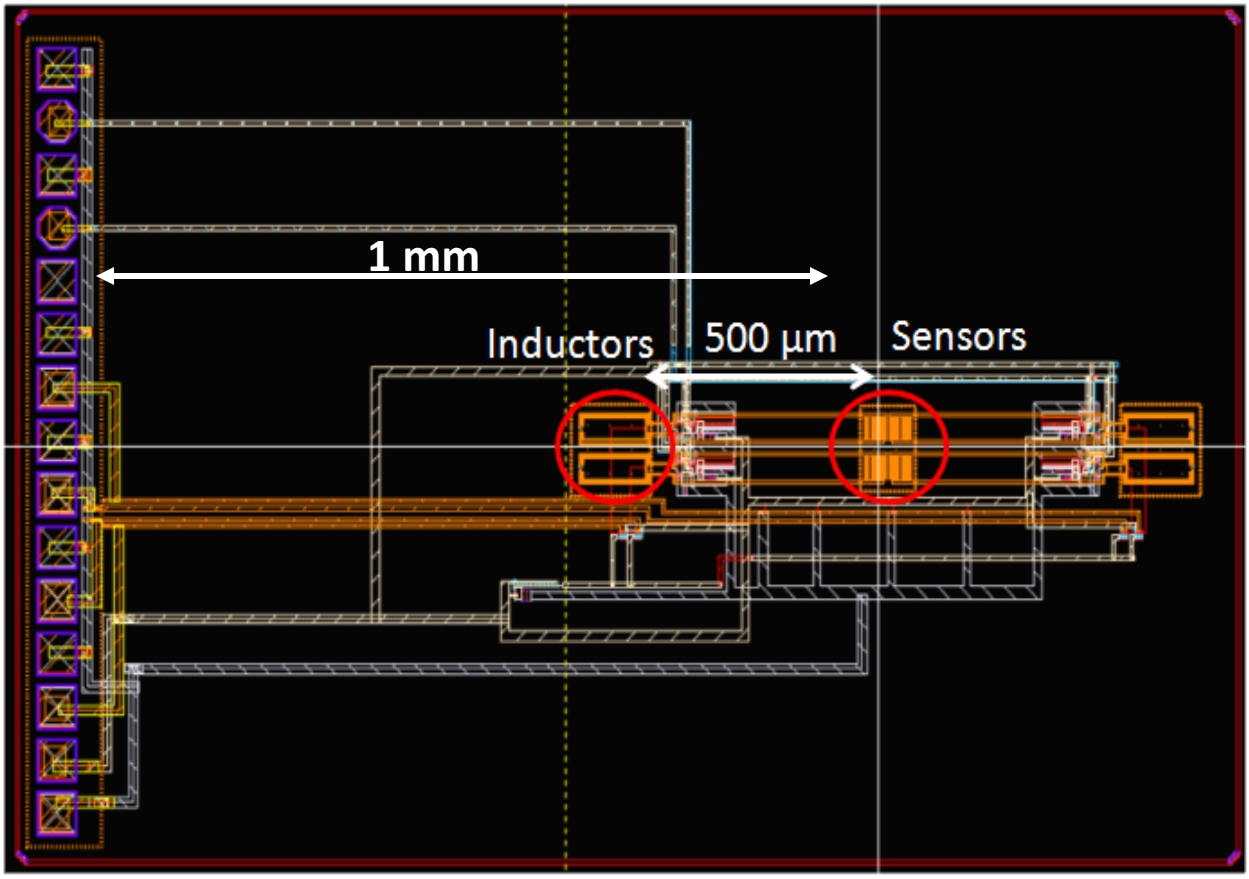

Figure 2.6 Typical layout of a sensor system. The distance of the inductors from the sensors is 500 µm. This evades the interaction of biomaterials with the inductors.

Qualitatively this might seem useful, as an additional parameter might increase the sensitivity of the sensor system, however, quantitatively this is an extremely tricky situation, where, extracting the true material parameters (concentration, type) from the oscillation frequency shift become difficult. The imaginary part of the permittivity on the other hand will influence the quality factor of the inductor. The quality factor of the inductors is degraded by the imaginary part of the permittivity. Hence, the overall degradation of the quality factor of the resonator is considerably high due to the degradation of quality factor of both the sensor capacitor and now additionally the inductors. These effects call for placement of the inductors far from the sensor capacitor. This is shown in Fig. 2.6 where the inductors are placed far from the sensor. This increases the area budget of the overall chip.

It is also seen from the sensor chip layout, that the pad-frame for electrical connections is placed on one side of the chip. And the placement of the pads is made at a distance of 1 mm from the sensor area. This is done for effective microfluidic integration without leakage. The microfluidic foot-print is made in a way such that the bonding area of the microfluidic system with the chip is substantially large to avoid any kind of fluid leakage from the microfluidic channel.

2.3 Design of planar microwave sensors

2.3.1 Coplanar Transmission lines

The model of coplanar transmission lines is used for analyzing the behavior of the interdigitated capacitor. Therefore, it is significant to delve into the analytical model of the coplanar transmission lines. The Fig. 2.7 shows a typical coplanar transmission line placed on a substrate and covered with a dielectric. Theoretical studies of coplanar transmission lines can be done using a full wave analysis or a quasi-static analysis [111]. The first theoretical analysis of coplanar structures was done by Wen et al. using conformal mapping technique. Since then, conformal mapping technique has been a useful approach in order to derive the parameters for coplanar transmission line.

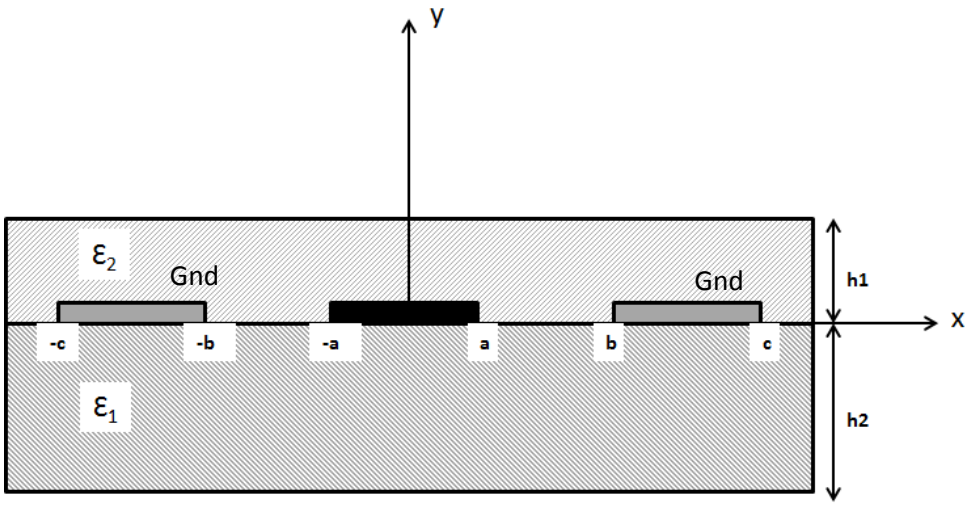

Figure 2.7 Coplanar transmission line sandwiched between two dielectrics.

Conformal mapping technique offers the advantage of converting open geometries into closed geometries [112], thereby, enabling the derivation of design equations. The Schwarz-Christoffel transformation method of conformal mapping is often used for the planar transmission lines like the coplanar transmission lines. The Schwarz-Christoffel transformation is used to map the the x-axis into a polygon and the upper half of z plane (that is y>0) is mapped as the interior of the polygon. This technique is extremely useful for mapping of the capacitance of the transmission line arising due to the fringing fields.

The partial capacitances of the coplanar transmission line shown in Fig. 2.7 can be written as follows:

C_0: This is the capacitance of the structure without any dielectric that is with air as the surrounding.

C_1: This is the capacitance of the structure with only dielectric $\varepsilon 2$ of height h_1

C_2: This is the capacitance of the structure with only dielectric $\varepsilon 1$ of height h_2

The total capacitance of the coplanar transmission line structure is given as:

$$C = C_0 + C_1 + C_2 \tag{2.3}$$

The individual configurations of the partial capacitances is shown in Fig. 2.8

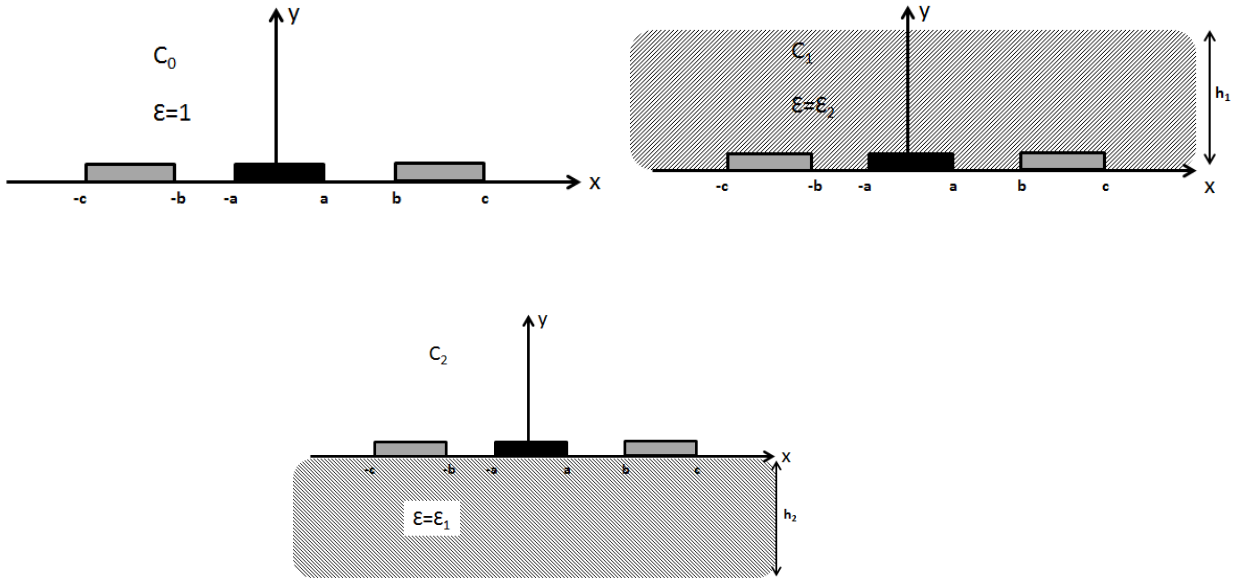

Figure 2.8 Partial capacitances of the coplanar transmission line showing the contribution of the individual dielectric layers

As described above, the partial capacitances can be obtained by the conformal mapping techniques [111,112]. The partial capacitance with no dielectric is given as,

$$C_0 = 4\varepsilon_0 \frac{K'(k)}{K(k)} \tag{2.4}$$

where, *K* is the first kind of complete elliptical integral and *K'(k) = K(k')*. The geometry of the coplanar structure defines the parameters *k* and *k'* and is given as,

$$k = \frac{c}{b}\sqrt{\frac{b^2-a^2}{c^2-a^2}} \tag{2.5}$$

$$k' = \sqrt{1-k^2} \tag{2.6}$$

The partial capacitances due to the dielectric layers can be calculated using similar conformal mapping techniques, however, the function for integral is dependent on the geometry of the coplanar transmission line and the height of the dielectric. The partial capacitance C_1 is given as

$$C_1 = 2\varepsilon_0(\varepsilon_2 - 1)\frac{K'(k_1)}{K(k_1)} \tag{2.7}$$

The same laws of complete elliptical integral applies. The function k_1 is give as

$$k_1 = \frac{\sinh(\frac{\pi c}{2h_1})}{\sinh(\frac{\pi b}{2h_1})}\sqrt{\frac{sinh^2(\frac{\pi b}{2h_1}) - sinh^2(\frac{\pi a}{2h_1})}{sinh^2(\frac{\pi c}{2h_1}) - sinh^2(\frac{\pi a}{2h_1})}} \tag{2.8}$$

On the same lines, the partial capacitance C_2 is given as

$$C_2 = 2\varepsilon_0(\varepsilon_1 - 1)\frac{K'(k_2)}{K(k_2)} \tag{2.9}$$

The k_2 can be derived in the same way as k_1 was derived.

2.3.2 Interdigitated Capacitor

The typical structure of an interdigitated capacitor (IDC) is shown in Fig. 2.9. The IDC relies on strip-to-strip capacitance of parallel conducting fingers. The fringing electric fields between the fingers of the IDC penetrates into the material placed on top of it and is varied based on the permittivity of the material.

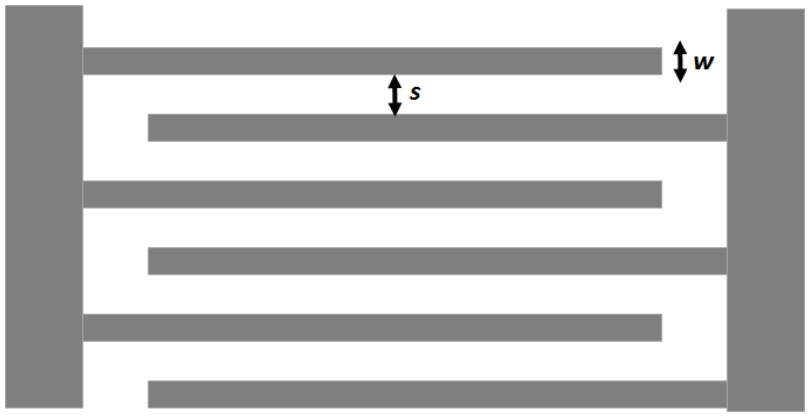

Figure 2.9 Geometry of the interdigitated capacitor showing the spacing and width of the fingers.

The significance of choosing IDC as the sensor element can be summarized as follows:

- at the operating sensor frequency, the dimensions of the IDC are of the order of micrometers, matching the dimension of biomaterials, for e.g., cells, fluid volume etc.
- feasible design of high quality factor IDC structures with high conductive top metal layers of the BEOL stack

- purely capacitive structure enables design of simpler read out techniques, for e.g., CMOS oscillators
- Penetration depth and capacitance density can be controlled based on the geometry of the IDC

The analysis of the IDC can be extended from the analysis done for the coplanar transmission lines in the previous section using the same conformal mapping technique. Conformal mapping technique can be used in the quasi-static condition. For quasi-static approximation the distance between the fingers of the IDC on the same electrode (also called the spatial wavelength of the IDC) has to be smaller than the operating wavelength of the IDC. In this thesis, the operating wavelength ranges from 60 mm to 20 mm (operating frequency: 5 GHz to 15 GHz). The spatial wavelength of the IDC being in the range of µm, enables the use of conformal mapping technique for establishing the governing equations of capacitance of the IDC. Analysis of IDCs has been done for decades now [112-114]. The conformal mapping, transforms the planar IDC structure into an orthogonal plane where the planar capacitance is translated to a parallel plate capacitor. However, in order to understand and correlate the results from the conformal mapping approach it is significant to understand the model of the IDC on the BICMOS platform used in this thesis.

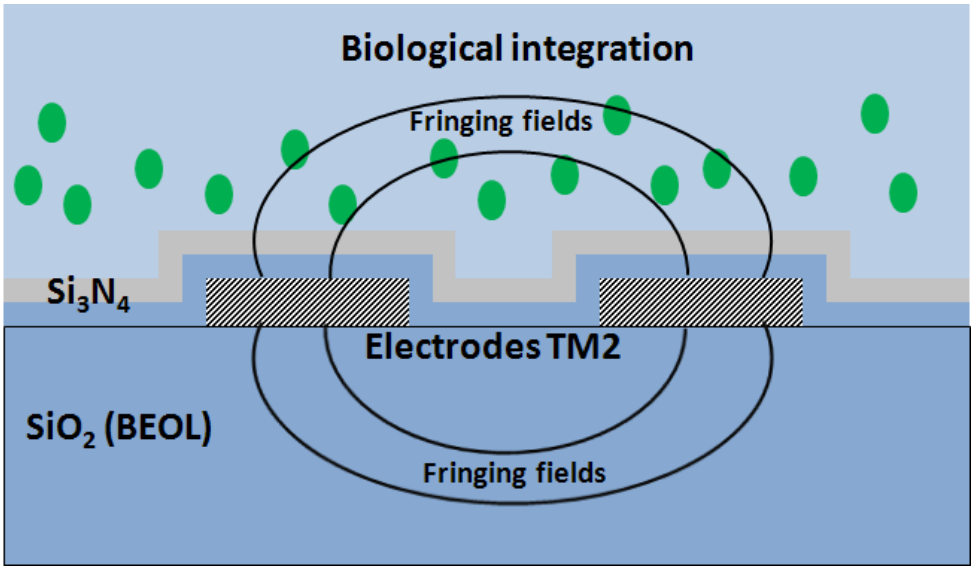

Figure 2.10 Cross-sectional schematic of the IDC fabricated on TM2 metallization layer of BEOL stack. The fringing fields penetrate into the biomaterial placed on top of the passivation layer.

Considering, the sensor is fabricated on the top metal layer as is the case in most of the thesis work, (for the case of immunosensor development, the IDC is in TM1 and the analytical expression is presented in the concerned chapter) the IDC configuration for sensor operation is shown in Fig. 2.10.

From Fig. 2.10 it is seen that the fringing electric fields penetrates into the BEOL SiO_2 dielectric at the bottom. On the top the fringing electric fields penetrate into the Si_3N_4 passivation layer and the material placed on top of it. Therefore, the IDC can be analyzed using conformal mapping technique by considering all the dielectric layers with specified heights. The model used for the analysis of the IDC is shown in Fig. 2.11

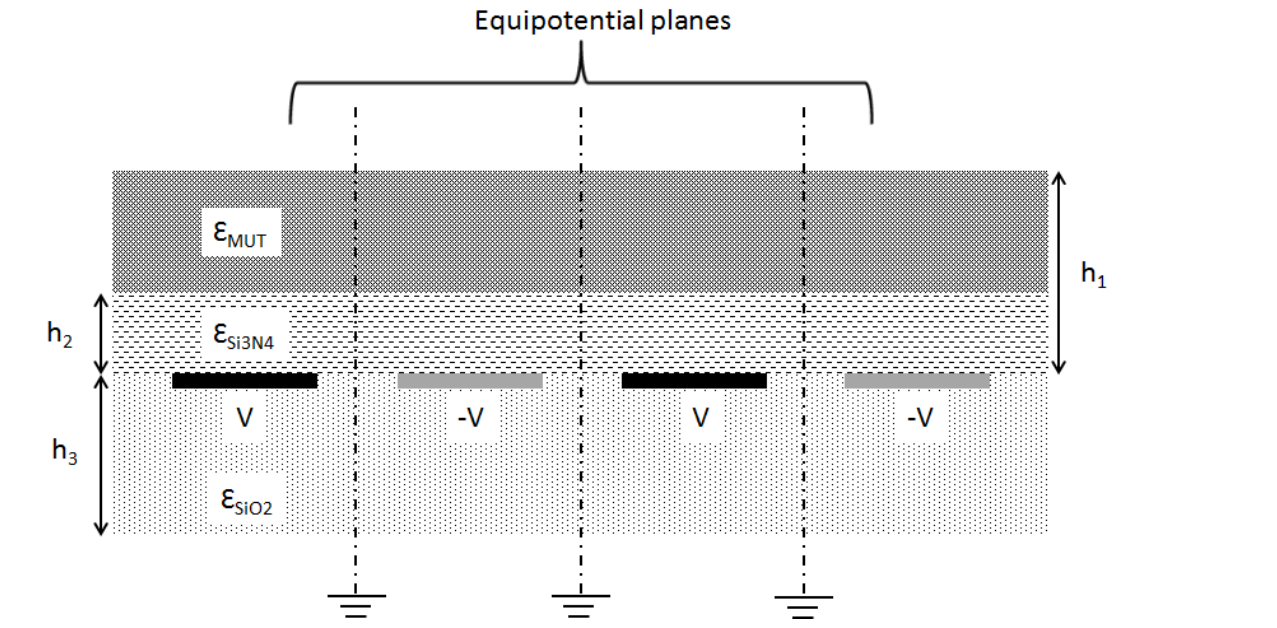

Figure 2.11 Model of IDC for evaluation of the capacitance fabricated on TM2 of the BiCMOS stack. The IDC electrodes have Si3N4 and MUT on top and SiO2 at the bottom. The equipotential surfaces are marked with vertical dotted lines. The two sets of electrodes are at the potential V and –V.

As seen from Fig. 2.11, the cross section of the IDC has two sets of electrodes with voltages V and –V respectively. The equipotential planes V=0, are the perpendicular planes half-way between the electrodes. The expression for the capacitance between the electrodes and the ground potential (equipotential plane) with a dielectric layer of height h can be established by mapping the planar surface to a parallel plate capacitor using the Schwarz-Christoffel transform technique. The overall capacitance of the IDC can be evaluated as follows

C_0: Capacitance with no dielectric layer, that is, air with infinite thickness

C_1: Capacitance with material under test of height h_1

C_2: Capacitance with Si_3N_4 passivation, of height h_2

C_3: Capacitance with SiO_2 below, of height h_3

The total capacitance is the sum of the partial capacitances multiplied by the length L of the fingers. Additionally, the parallel plate capacitance (C_{pp}) due to the thickness of the fingers needs to be taken into account.

$$C_{IDC} = L\,(C_0 + C_1 + C_2 + C_3) + C_{pp} \tag{2.10}$$

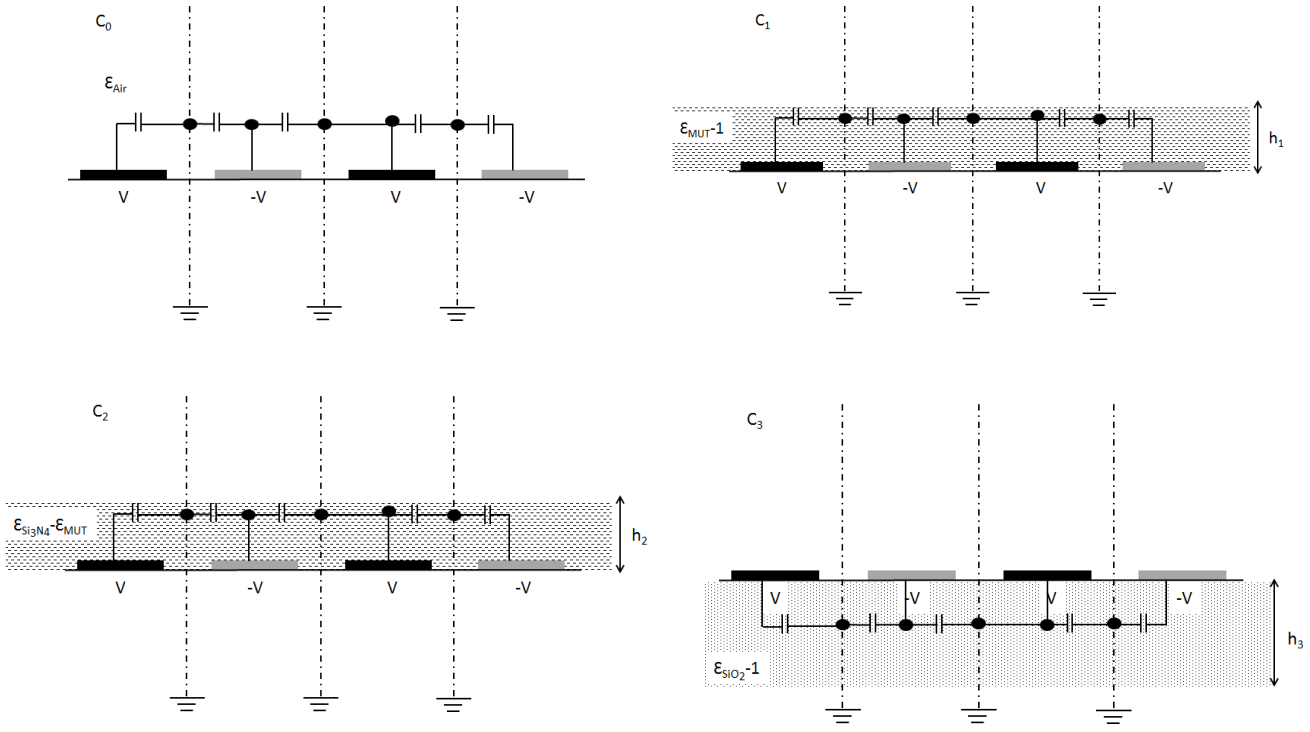

Figure 2.12 The partial capacitance components of the IDC for individual dielectric layers.

The partial capacitances can be derived in the same way as was explained in the previous section for coplanar transmission lines. For number of fingers N >3, the total capacitance is obtained by multiplying C_{IDC} with a factor (N-3).

The total capacitance can be approximated to,

$$C_{IDC\_Total} = 2\varepsilon_0(N-3)L\left(\frac{K'(k)}{K(k)} + (\varepsilon_{MUT}-1)\frac{K'(k_1)}{K(k_1)} + (\varepsilon_{Si3N4}-\varepsilon_{MUT})\frac{K'(k_2)}{K(k_2)} + (\varepsilon_{SiO2}-1)\frac{K'(k_3)}{K(k_3)}\right) + (N-3)C_{pp} \tag{2.11}$$

The term K is the complete elliptical integral function and k is the geometry and height of dielectric layer dependent term, as shown in coplanar transmission line derivations. The influence of the dielectric permittivity of the material under test (MUT) is seen in eq. 2.11. The

variation of this permittivity affects the fringing electric field between the fingers of the IDC and changes its capacitance.

Along with the geometry of the IDC determining the capacitance, another very significant parameter of the sensor structure designed for high-frequency sensing applications is the self-resonating frequency (SRF) of the structure. SRF of a structure is defined as the frequency at which the capacitive contribution of the structure is nullified by its self-inductive contribution and the structure is purely resistive. This phenomenon is analogous to the general resonant LC tank circuit operation; however, in the case of self-resonance the capacitive and the inductive contributions of the same structure are taken into account. The self-resonating phenomenon is shown in Fig. 2.13 (a).

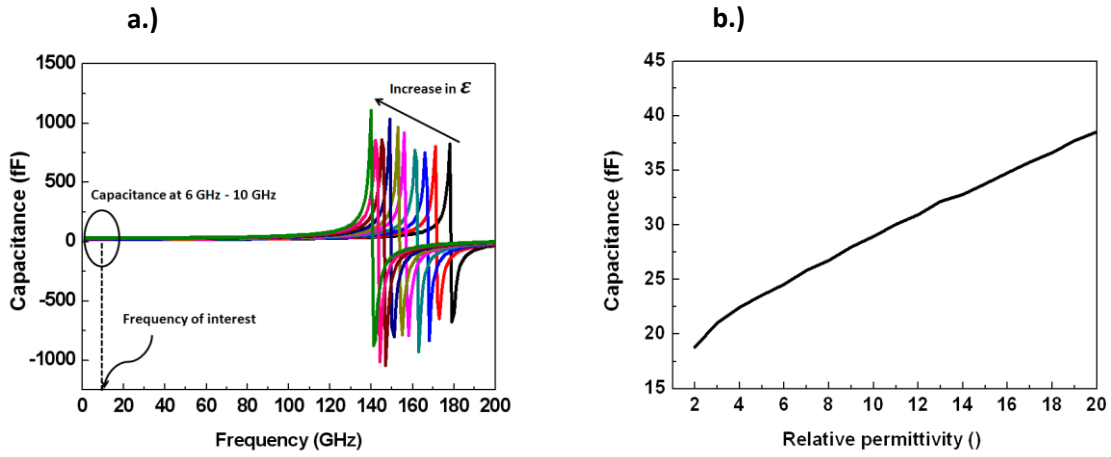

Figure 2.13 (a) Self resonance phenomenon of a typical IDC structure. The self-resonance frequency (SRF) is around 150 GHz (b) Variation of the capacitance of the IDC with respect to permittivity at the operating frequency range of 6 GHz – 12 GHz.

The resonance peak in the capacitance vs. frequency curve defines the frequency at which the IDC's self-inductance nullifies the capacitive contribution. Beyond the self-resonance phenomenon, as seen in Fig. 4.2 (a), the capacitance is negative, or in other words the structure is inductive. The SRF is dependent on the size of the sensor and also on the permittivity ambient of the IDC. The self resonating frequency of the IDC sensor structure decreases with the increase in its area. However, for a given geometry of the IDC on a specific substrate, the SRF is only dependent on the permittivity of the material placed on top of it (MUT). With the increase in the permittivity of the MUT the capacitance of the IDC increases and the SRF reduces as shown in Fig. 2.13(a). It is significant to design the operating frequency of the sensor system considerably lower than the SRF of the IDC. This is essentially because in such a condition the electric field in the IDC is rotation free and the structure is essentially capacitive. The simulated SRF of typical IDC structures used in this work is beyond 150 GHz and the simulation of one such IDC structure is shown in Fig. 2.13 (a). In this chapter three sensor systems operating in the frequency range of 6 GHz – 15 GHz are demonstrated. Therefore, the operating frequency range of the sensor systems is sufficiently below the SRF of the corresponding sensor IDCs. A typical

variation of the capacitance of the IDC with respect to the increase in permittivity of the MUT is shown in Fig. 2.13 (b). The direct proportionality of the IDC capacitance to the permittivity of the MUT can be seen in eq. 2.11, where the capacitance of the IDC was analyzed.

2.4 Design of sensor circuit

The sensor circuit is based on a standard cross-coupled oscillator topology where the sensor IDC is analogous to the varactor (variable capacitor) used in such a circuit. In a standard voltage controlled oscillator, the capacitance of the variable capacitor is tuned (varied) using a tuning voltage, resulting in the resonance frequency scaling of the oscillator. In this thesis, the resonance frequency of the oscillator is controlled by the variation of the permittivity on top of the IDC. The circuit topology can be seen in Fig. 2.14. An LC resonant tank structure is constituted by connecting the multi-fingered IDC in parallel to a couple of series connected inductors as shown in Fig 2.14. A pair of cross-coupled n-MOS transistors drives the oscillation of the LC resonant tank. This configuration is a typical negative transconductance oscillator.

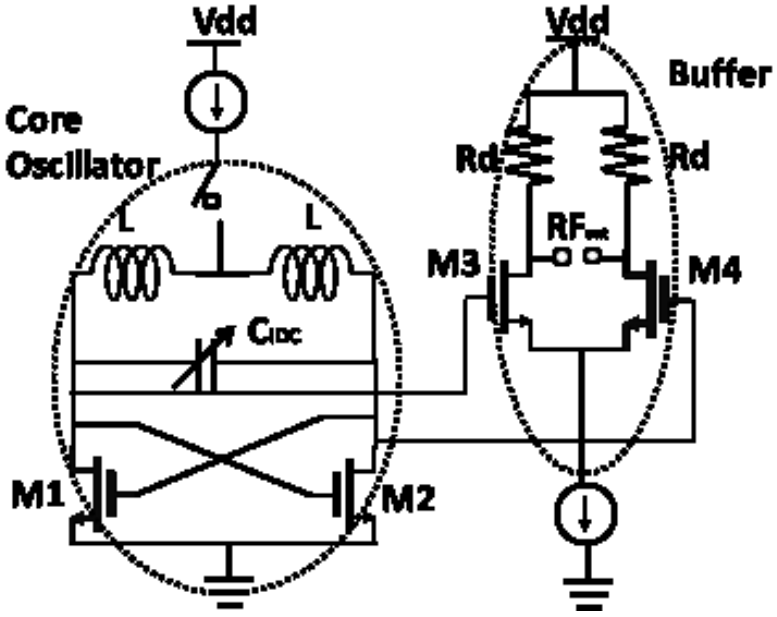

Figure 2.14 The sensor circuit with IDC sensor embedded in a cross coupled CMOS oscillator.

The model of the negative transconductance oscillator is shown in Fig. 2.15(a). The model represents the oscillator as two interconnected one-port networks: an LC tank which acts as the frequency selective resonator and an active network represented by the cross-coupled oscillator. In the steady state condition, loss conductance (G') generated in the tank circuit should be compensated by the negative transconductance generated by the active circuit, which enables

sustaining of the oscillations. The inductor being made from a metal of finite conductivity generates the losses due to the resistance of the metal.

The standard approach to represent an oscillator is given by a simple linear feedback system [110], with an overall transfer function given as,

$$\frac{Y(s)}{X(s)} = \frac{H(s)}{1-H(s)} \tag{2.12}$$

where, *X(s)* and *Y(s)* are the frequency domain representations of the input *x(t)* and output *y(t)* respectively. *H(s)* is the frequency transformation of the impulse response of the system *h(t)*. The commonly used Barkhausen's criteria for sustained oscillation at a frequency ω is written as,

1. Loop gain, |H(jω)| must be equal to unity
2. Total phase shift around the loop, must be equal to 0° or 180°

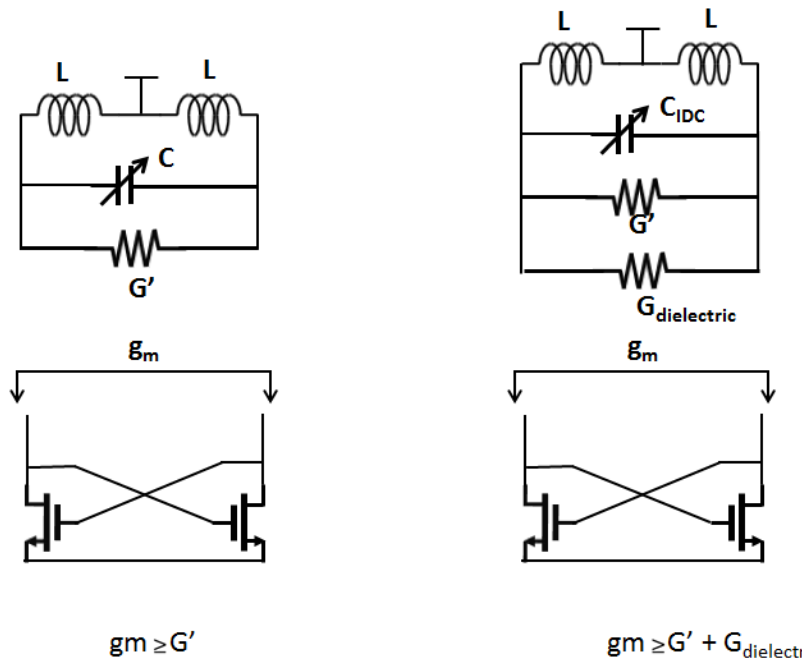

Figure 2.15 (a) Model for negative transconductance cross coupled oscillator without considering dielectric losses. (b) Model for negative transconductance cross coupled oscillator with considering dielectric losses.

The transconductance (g_m) of the transistor compensates the losses of the tank circuit. This is the negative transconductance used in this kind of oscillator design. From the energy point of view, the active circuit replenishes the energy dissipated periodically in G', thus, enabling a sustained

oscillation of the cross-coupled oscillator. Therefore, the transconductance of the cross coupled pair should be equal to or more than the negative value of G', ($g_m \geq$ -G').

In this thesis, the IDC sensor is used as the variable capacitor. The permittivity of the biomaterial placed on the top of the sensor is written as

$$\varepsilon_{MUT} = \varepsilon'_{MUT} + j\varepsilon''_{MUT}$$

As described in the previous section the real part of the permittivity influences the resonant frequency of the oscillator. The imaginary part of the permittivity accounts for the dielectric losses. This dielectric loss is in addition to the resonant tank losses mentioned above. This is modelled as the additional loss conductance in parallel to the tank loss conductance. This is shown in Fig. 2.14(b). Therefore, the negative transconductance required to compensate for the overall losses is higher than the negative transconductance required to compensate the tank losses. This requires designing of the cross coupled transistor pair with wider channel widths. The transconductance of a transistor is directly proportional to the width of the transistor [110]. The transconductance of the cross coupled pair should compensate for the maximum losses that can be incurred during the sensing process. In this thesis, biological samples are primarily measured in water, which acts as the aqueous suspension for measurement. The cross coupled pair of nMOS transistors is designed in such a way, that the transconductance of it compensates the losses for water. As addition of biological materials in water reduces the loss factor, the maximum loss for which the negative transconductance should be designed is water.

However, from the standpoint of the design of the oscillator, the high transconductance can lead to loss of sinusoidal nature of the output, for low loss materials. In that case there is an overcompensation due to the high transconductance of the cross coupled pair. This is however, not significant for the thesis work, as the resonant frequency of the oscillator is not affected by this loss of sinusoidal nature. In this work, the resonant frequency of the oscillator and its variation for different materials is of importance. The cross coupled nMOS pair brings in additional parasitic capacitance. The parasitic capacitance is determined by the width of the transistors and the biasing of the transistors. The additional parasitic capacitances affect the sensitivity of the sensor as the capacitance is in parallel to the sensor capacitor. The nMOS transistors at the following buffer stage also add parasitic capacitance. A buffer stage is used following the oscillator, in order to isolate the sensor circuit from additional circuitry following the sensor for advanced operations (see chapter 5). The resonant frequency of the oscillator is given as,

$$f = \frac{1}{2\pi\sqrt{2LC_{Total}}} \tag{2.13}$$

The total capacitance C_{Total}, is the sum of the capacitances due to the IDC and the parasitic capacitances due to the transistors.

The same oscillator circuit topology with the embedded IDC sensor is used all through-out the thesis work. In the subsequent chapters the use of the sensor and the oscillator circuit in total have been explained for various applications like immunosensors, cytometry, etc.

DIELECTRIC IMMUNOSENSOR

In this chapter* a CMOS high frequency direct immunosensor operating at 6 GHz (C-band) is discussed. The functioning of the sensor is shown by the label free determination of creatinine. The sensor is fabricated in standard 0.13 µm SiGe:C BiCMOS process. The ability to immobilize creatinine molecules on Si_3N_4 passivation layer of the standard BiCMOS/CMOS process evades any further need of cumbersome post processing of the fabricated sensor chip. The sensor is based on capacitive detection of the amount of non-creatinine bound antibodies binding to an immobilized creatinine layer on the passivated sensor. The chip bound antibody amount in turn corresponds indirectly to the creatinine concentration used in the incubation phase. The determination of creatinine in the concentration range of 0.88 – 880 µM has been successfully demonstrated. A sensitivity of 35 MHz/10-fold increase in creatinine concentration (during incubation) at the center frequency of 6 GHz has been manifested by the immunosensor. The results have been compared with a typical optical measurement technique and the sensitivity is of the order of established optical indication technique. The C-band immunosensor chip comprising an area of 0.3 mm^2 reduces the sensing area considerably, therefore, requiring sample volume as low as 2 µl. The small analyte sample volume and label free approach also reduce the experimental costs in addition to the low fabrication costs offered by standard fabrication technique of CMOS/BiCMOS process.

3.1 Introduction

ELISA (Enzyme Linked Immunosorbent Assays) has been established as the most standard technique in medical or clinical diagnostic processes over the last decade. The most common technique applied in the ELISA approach is based on chromatographic assays and is primarily used in point-of-care-testing (POCT) [115-118]. However, often such ELISA based techniques give qualitative or semi-quantitative analysis, therefore, limiting the applications to diagnose diseases depicting high changes in analyte concentrations. Hence, an ever increasing need for sensors with qualitative analysis is pressing. Immunosensors are such special "biosensors" based on selective antibody-antigen binding and providing concentration dependent or quantitative information. The fundamental scheme of an immunosensor is shown in Fig. 3.1, depicting the highly interdisciplinary approach of designing such specialized immunosensor. In the first step, antibodies or antigens are bound on a functionalized transducer. Selective pairing of a particular antigen-antibody pair in aqueous solution governed by a specific chemical reaction is sensed using one of the following generalized techniques: optical, chemical, amperometric, dielectric etc. The sensed signal is detected using a parameter change for the

- Parts of the chapter has been published as "Label free sensing of creatinine using a 6 GHz CMOS near-field dielectric immunosensor", *Analyst*, 2015, **140**, 3019-3027 DOI: 10.1039/c4an02194k

particular sensing scheme used: for e.g., fluorescence marker for optical technique, cyclic voltammetry signals for amperometric technique, capacitance shift for dielectric measurements, etc.

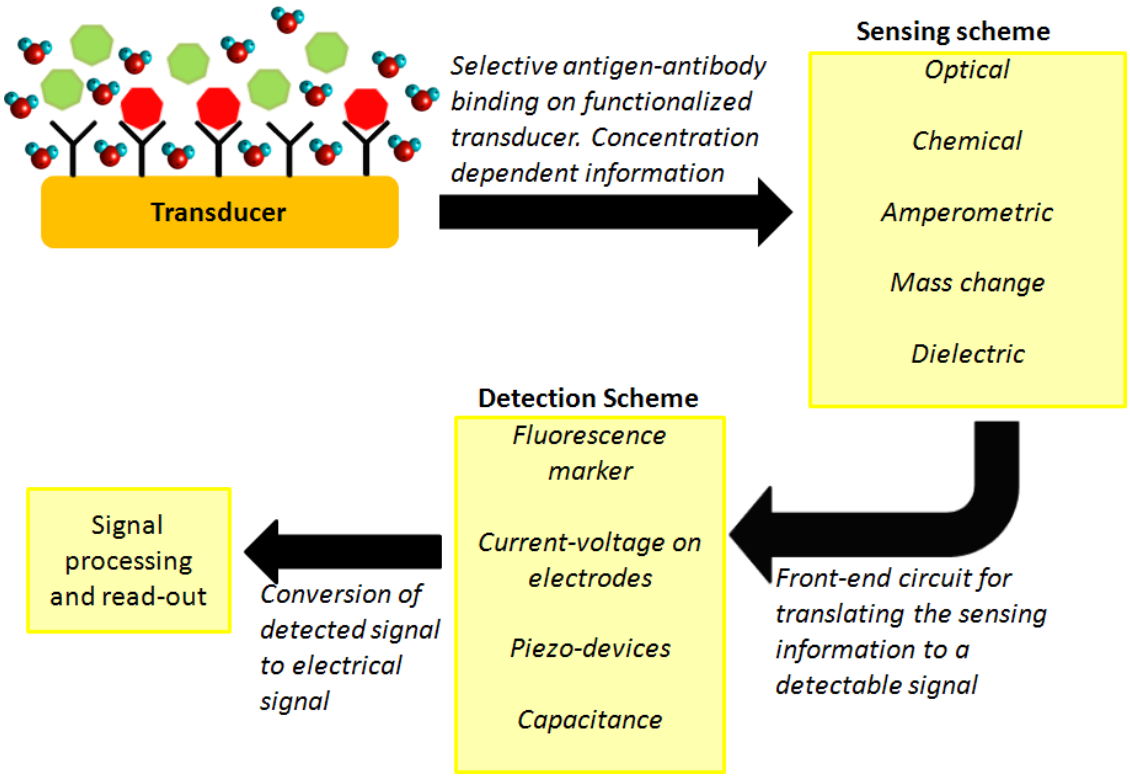

Figure 3.1 Schematic of a basic immunosensor. The first step includes immobilization of antibodies/antigens on a transducer surface followed by the binding of corresponding antigens/antibodies. A sensing scheme is employed to detect the antigen-antibody pair. A signal processing front-end circuit converts the detected signal to electrical signal.

The final step involves the conversion or amplification of the detected signal into a reasonable electrical signal for further signal processing and read-out or display. The cost and complexity of such a sensor system is often governed by one of the four steps described above. Optical sensing schemes are being investigated presently to establish immunosensors for POCT. The first approach includes ELISA-like immunosensor scheme for an autonomous LOC device containing all of the required reagents (e.g., buffers, enzyme or fluorophore antibody conjugates, etc.), separation units, pumps, channels and sensors [119, 120]. The second approach also incorporates labeling compounds (e.g., enzymes, fluorophores, redox mediators) but, in a one-step assay format [121]. In case of optical technique, the optical markers and the amount of antibodies used in the sensor system make the application expensive. The above class of immunosensors can be also classified as indirect immunosensors where the labeling compound aids in the sensing

scheme. Transduction techniques like surface plasmon resonance (SPR) is also being investigated recently. Such a technique evades labeling compounds as in the above techniques, and gives a direct indication of antigen-antibody binding, also referred to as direct immunosensor. The complexity and cost of such a system arise from the measurement test-bench and the necessary front end circuit [122]. In parallel to the on-going research for new immunosensor techniques, there already exists established commercial immunosensors, for e.g., BIAcore. Such established state-of-the-art immunosensors require incubation steps as well as manual pipetting steps [123, 124], therefore, increasing the overall development cost and complexity.

As a significant application of the developed high-frequency sensors for biomedical applications shown in this thesis work, establishing a miniaturized direct immunosensor has been a prime focus. Theoretical studies of microwave interaction with biological materials like biomolecules, cells, tissues, have been studied in detail over decades and there is considerable volume of related literature [125, 126]. In this part of the work we explore the design of a single chip immunosensor for the detection of creatinine molecules. The sensor is made to operate at the frequency range of 6 GHz. The choice of frequency is made 6 GHz, because the dielectric permittivity of the aqueous solution (water) used in this work is around 70. The dielectric permittivity of the given volume of antigens and antibodies in this frequency range is of the order of 2 to 3. This provides a considerable permittivity contrast for high sensitive immunosensor design.

3.2 Proposed CMOS compatible immunosensor approach

This section of the thesis demonstrates the development of fully integrated CMOS compatible immunosensor platform based on high-frequency (6 GHz) dielectric sensing; the sensor platform has been used to detect creatinine molecules. The primary advantage of using a high-frequency technique is the miniaturization of the overall sensor system leading to the use of extremely small sample volumes of the antigen and antibodies. As mentioned previously the “all-electrical” sensing approach nullifies the need of using labeling markers for detection and also the high frequency dielectric detection is independent of reference electrodes used for measurements. In order to develop real miniaturized LOC device, the above features of a high-frequency immunosensor based on dielectric detection is highly lucrative. The sensing approach is based on the capacitive detection of dielectric permittivity change. The capacitive sensor is embedded in a CMOS oscillator, where the sensor acts as a variable capacitor (varactor) and the capacitance change is translated to the resonant frequency shift of the oscillator.

The functionality of the sensor is determined by detection of the concentration of creatinine molecules in a competitive immunoassay technique. Creatinine is one of the most often determined parameters in clinical diagnostic. This is primarily because the concentration of creatinine in serum and urinary excretion is less influenced by dietary changes such as a high intake of a creatinine-free diet, unlike urea or nitrogen residues. Creatinine is the index for renal

glomerular infection; the concentration range in the plasma of a healthy adult person is around 25-150 µM or 2-17 µg mL^{-1} [127]. However, the concentration is dependent on the age, sex as well as the demography. This concentration range changes radically for patients with serious kidney disorders and general debilitation, in which the creatinine concentration increases in the serum/plasma and decreases in the urine. Standard chemical or optical techniques can be successfully used to determine creatinine concentration and are considered the gold standard, especially the Jaffe method [128,129] but with high cost and large complexities. In contrast, the proposed CMOS high-frequency immunosensor offers a flexible, easy to handle miniaturized solution with higher detection range of measurement and comparable sensitivity. The target of this work is to demonstrate the capability of the established CMOS dielectric immunosensor to detect and screen the increase in creatinine concentration in serum.

3.2.1 Fabrication and operation of the sensor

A multi-fingered planar interdigitated capacitor (IDC) is used as the prototype sensor for capacitive detection of concentration of creatinine molecules. The IDC along with embedding oscillator for read-out, has been fabricated in the standard 0.13 µm SiGe:C BiCMOS technology. The BEOL stack of the process with seven metal layers is shown in Fig. 3.2(a) as was described in chapter 2. The five lower metal layers are thinner (400 nm) compared to the top metal layers marked as TM1 and TM2 in Fig. 3.2 (a). The thickness of TM1 and TM2 are 1.5 µm and 2 µm respectively. The passivation layer of silicon nitride (Si_3N_4), of thickness 350 nm, on top of TM2 isolates the electrical circuit from the external environment. The planar IDC is fabricated on TM1 metal layer of the BEOL stack. The reason for fabricating the IDC on the TM1 metal layer stems from the need of immobilization of creatinine molecules. The surface chemistry developed for the immobilization technique is based on the dielectric stack comprising of a layer of Si_3N_4 and SiO_2. As seen from Fig. 3.2, the TM1 metal layer has a layer of SiO_2 and Si_3N_4 on top of it. The IDC is further coupled with a pair of inductors fabricated on TM2 metal layer to form a resonating tank. The sensor circuit, that is the cross coupled oscillator has been explained in chapter 2.

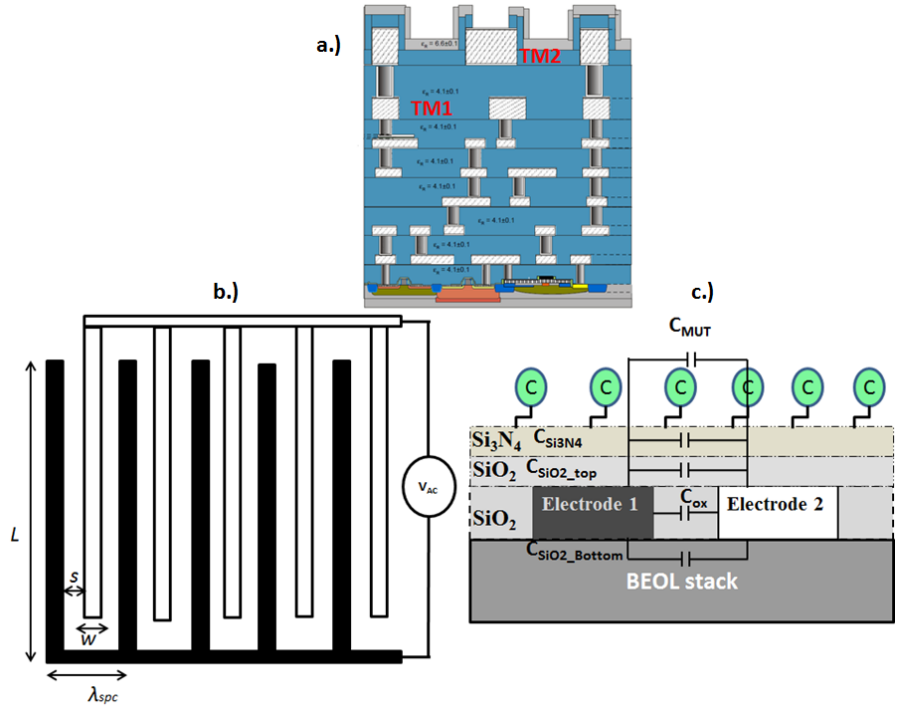

Figure 3.2 IDC sensor on BiCMOS back-end-of-line (a) Schematic of BiCMOS back-end-of-line stack with seven metallization layers. The top two metallization layers are thick and are less resistive. (b) Geometrical schematic of the IDC showing the length, spacing and width of the fingers. (c) Schematic of the immobilized creatinine on the sensor surface.

Fig. 3.2 (b) shows the geometry of the planar IDC sensor used in the immunosensor design. The IDC has five fingers (electrodes) with finger length (L) of 100 µm. The designed IDC has equal electrode width (w) and inter-electrode spacing (s) of 20 µm. The wider fingers and the gap is required for high penetration depth of the fringing fields. This is needed for the fringing fields to extend the SiO_2 and Si_3N_4 layers in order to sense the immobilized molecules on top of the Si_3N_4 layer. The thickness of the TM1 metal layer being 2 µm. The parallel plate capacitance between adjacent fingers with silicon dioxide (SiO_2) as the dielectric between the fingers, is shown as C_{ox} in the semi-infinite model of the IDC shown in Fig. 3.2 (c). The fringing electric fields between adjacent electrodes penetrating into the BEOL oxide layer in the bottom gives rise to the capacitance due to the substrate also shown as C_{SiO2_Bottom} in Fig. 3.2 (c). The fringing electric fields between the adjacent fingers on top penetrates into the top oxide layer (SiO_2), followed by the layer of Si_3N_4 passivation and the dielectric environment above that defined as the material under test (MUT). This fringing field gives rise to the capacitive contribution shown as C_{SiO2_top}, C_{Si3N4} and C_{MUT} in Fig. 3.2(c). Therefore, the total capacitance of a unit cell of the IDC (comprising two adjacent electrodes) per unit length is given as

$$C_{IDC} = C_{ox} + C_{SiO2\_Bottom} + C_{SiO2\_top} + C_{Si3N4} + C_{MUT} \quad (3.1)$$

The geometry of the IDC structure determines the penetration depth of the fringing electric field. The penetration depth (Pd) of the fringing fields from IDC is defined by the following equation [114].

$$Pd_{IDC} = \frac{w+s}{2\pi} \quad (3.2)$$

Pd_{IDC} is the penetration depth of the fringing fields from the IDC with finger width w and adjacent finger spacing of s. From the fabricated geometry of the IDC the penetration depth is calculated to be 8 µm. Therefore, the fringing fields in the bottom accounting for C_{sub} contribution in eq. (3.1) penetrate only into the oxide layer of the BEOL and do not extend to the silicon substrate. On the top, the SiO_2 above TM1 is 5 µm thick followed by the passivation layer of Si_3N_4 350 nm thick. Hence the fringing electric fields penetrate through the oxide and the passivation into the biomolecules immobilized on top of the passivated IDC surface. The capacitance of the IDC fabricated in TM1 can be derived following the same principles as was done in chapter 2. However, the correction term arising due to the SiO_2 layer on top of the TM1 has to be included. The equation obtained in eq. 2.11 is now replaced by the additional term included considering the influence of SiO_2 and is given as,

$$C_{IDC\_Total} = 2\varepsilon_0(N-3)L\left(\frac{K'(k)}{K(k)} + (\varepsilon_{MUT}-1)\frac{K'(k_1)}{K(k_1)} + (\varepsilon_{Si3N4}-\varepsilon_{MUT})\frac{K'(k_2)}{K(k_2)} + (\varepsilon_{SiO2}-\varepsilon_{Si3N4})\frac{K'(k_3)}{K(k_3)} + (\varepsilon_{SiO2}-1)\frac{K'(k_4)}{K(k_4)}\right) + (N-3)C_{ox} \quad (3.3)$$

This equation can be understood from the model of the IDC shown in Fig. 3.2 (c), depicting the various dielectric layers and the sensing layer. The immediate influence of fabrication of the sensor structure in the TM1 metal layer is the loss of sensitivity due to the influence of the oxide layer. The SEM image of the fabricated chip shown in Fig. 3.3 depicts the bond pads and the inductors on TM2 and a focused ion beam (FIB) cut was performed to demonstrate the IDC on TM1.

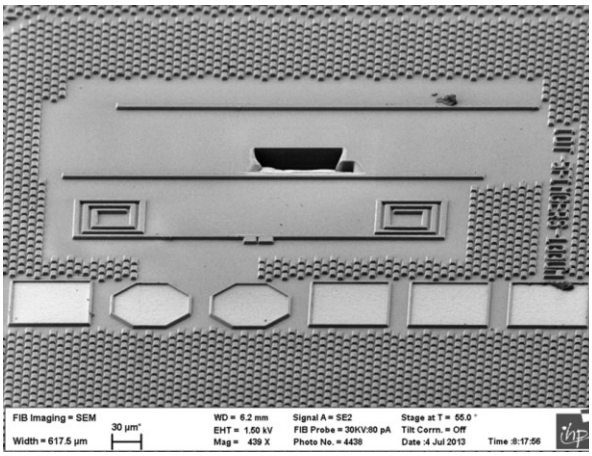

Figure 3.3 Scanning electron microscopy (SEM) image of the sensor chip showing the inductors on topmost metal layer. A focused ion beam (FIB) cutting is performed to expose the IDC sensor surface.

The creatinine molecules and the binding antibodies are of the order of 10 - 30 nanometers, and therefore, can be conveniently sensed by the IDC when on top of the passivation layer because of the penetration depth of the fringing fields.

The sensing scheme shown in Fig. 3.4 shows the condition of permittivity variation on top of the IDC. Following the fabrication of the sensor chip, creatinine molecules were immobilized on the passivated surface of the IDC as shown as the first step of the sensing scheme in Fig. 3.4. A competitive immunoassay like approach is used to detect the creatinine concentration. In such an indirect binding technique, initially, anti-creatinine molecules are incubated in different concentrations of creatinine, shown in the incubation phase in the Fig. 3.4. Four concentration levels of creatinine (0.88 µM to 880 µM) were chosen for incubation. This was done to demonstrate the wide detection range of the sensor. The resultant incubated solution is pipetted on top of the sensor IDC with previously immobilized creatinine molecules on top of it. Using a higher concentration of creatinine for incubation of the same amount of anti-creatinine antibodies would result in larger fraction of the antibodies binding to the incubating creatinine molecules. Therefore, a smaller fraction of the antibodies binds to the immobilized creatinine molecules on the IDC surface. An opposite effect is obvious when the concentration of the incubating creatinine is less.

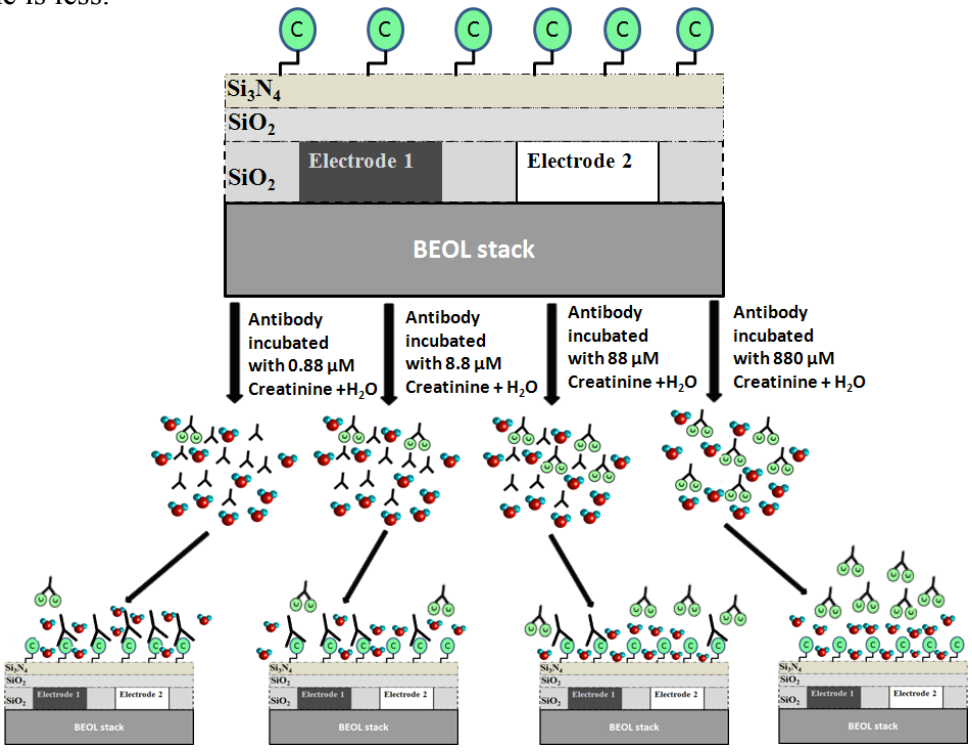

Figure 3.4 Sensor operation of the dielectric immunosensor. Creatinine molecules had been immobilized on the passivated surface of the sensor. Anti-creatinine antibodies were incubated in four different concentrations of creatinine molecules (pre-treatment phase). The four different antibody solutions are allowed to bind to the immobilized creatinine molecules. Antibody samples incubated with higher concentration of creatinine have less free antibodies left to bind to immobilized creatinine molecules.

This indirect binding technique of the previously incubated anti-creatinine antibodies has been utilized for the detection or sensing of the concentration of creatinine molecules used for incubation. The assay principle used here to bind the non-complexed free antibodies to a surface immobilized antigen is well established in clinical diagnostics. Many commercially available ELISA test kits for measurement of low molecular weight analytes are based on such principle. Following the phase of pipetting of the incubated anti-creatinine antibody solution, the chips were washed with water and dried. In order to test the binding of the antibodies to the chip immobilized creatinine molecules, anti-mouse-antibody peroxide conjugate was added to the chip. Binding of this conjugate to the anti-creatinine antibodies ensured that the anti-creatinine antibodies were bound by the chip immobilized creatinine molecules and not released by any process of denaturation occurring due to the drying phase as explained above.

An additional droplet of water has been added during the electrical measurement of the sensor chips and is shown in the sensing scheme as the water molecules. The use of additional droplet of water droplet causes intrinsic sensitivity amplification due to the stark permittivity contrast of water and the antibodies. When the anti-creatinine antibodies are incubated in higher concentration of creatinine, smaller fraction of the free antibodies bound to the chip immobilized creatinine. When lower amount of antibodies binds to the chip immobilized creatinine molecules, the molecules are surrounded by more amounts of water molecules. Therefore, the variation of the amount of non-creatinine bound antibodies binding to the immobilized creatinine varies the amount of water molecules surrounding the immobilized layer. Due to considerable contrast of permittivities between water and the antibodies this variation causes a sharp change in the C_{mut} contribution of the total IDC capacitance. If no water droplet is used in the electrical experiments, the immobilized creatinine molecules will be surrounded by air. The permittivity of the antibodies is of the very close to the permittivity of air when compared to their permittivity with respect to water. Therefore, from the sensing aspect not considerable permittivity change is seen if the antibodies bind to the immobilized creatinine or the immobilized creatinine molecules are surrounded by air. Hence, addition of water molecules ensures intrinsic sensitivity enhancement. It should be noted as well that immunosensors operate with real world samples in aqueous solution (serum/plasma) where multiple antibodies or antigens are suspended in the solution. Therefore, use of water molecule for sensitivity enhancement has been done without losing the generality of the immunosensor application. The capacitance change of the IDC can be translated to the concentration of creatinine used in the incubation phase. Thus, an indirect immunoassay based approach has been used in conjunction with an "all-electrical" sensing scheme.

3.2.2 Immobilization of creatinine

The immobilization surface chemistry of creatinine on top of the Si_3N_4 surface of the IDC was established on silicon test-structures passivated with Si_3N_4. The surface chemistry was established in co-operation with the Biotechnology group of University of Potsdam. Various

immobilization techniques based on creatinine butyric acid and a creatinine-bovine serum albumin conjugate (crea-BSA) were experimented on 1 cm^2 test structures or test chips. The structure of the creatinine molecule is shown in Fig. 3.5 (a). The preparation of creatinine butyric acid and a creatinine-bovine serum albumin conjugate (crea-BSA) has been dealt in detail by Benkert *et al.* [130]. The chemical structure of crea-BSA is shown in Fig. 3.5 (b).

Same procedure was followed for the synthesis of the above compounds. The best results for the immobilization of the creatinine molecules are obtained with the adsorption of crea-BSA to the Si_3N_4 surface. Crea-BSA (10 $mgml^{-1}$in standard phosphate buffered saline, PBS) was diluted in the ratio in the ratio 1:10 with aqua bidset. 2 µl of this solution was pipetted on the Si_3N_4 surface

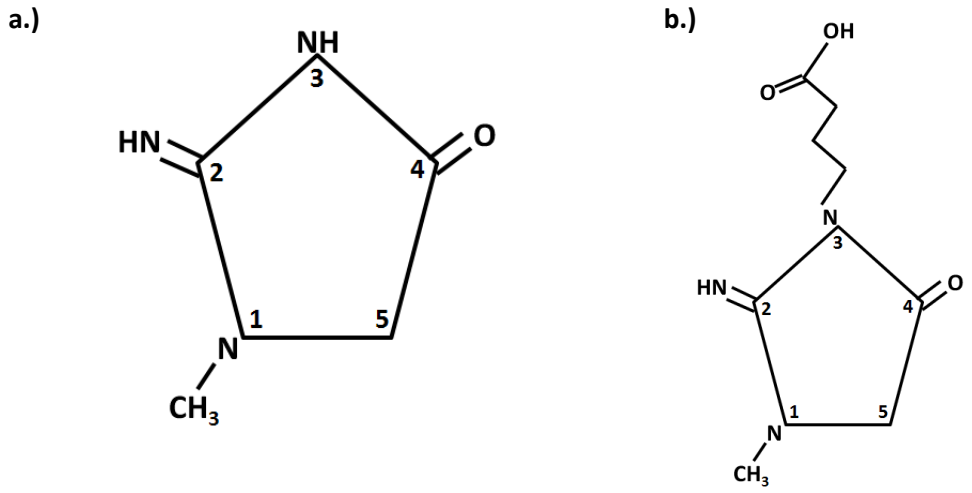

Figure 3.5 (a) Chemical structure of creatinine (b) Chemical structure of crea-BSA molecule.

of the test structures and was further incubated in a humid chamber for one hour. After six washing steps of the experimental with PBS and three washing steps with aqua bidset, the chip surfaces, the chip surfaces were blocked with 2.9 ml 3% BSA in PBS (BSA/PBS) for one hour. In order to establish a control experimental setup to determine the accurate immobilization of creatinine molecules, control chips were modified with 2 µl of a BSA solution in the same way as the experimental chips. For the detection of the immobilized creatinine, 0.1 ml of 3 µg ml^{-1} anti-creatinine antibody in BSA-PBS solution was added and incubated for one hour with 2.5 ml peroxidase-conjugated goat anti-mouse IgG (H+L) which was obtained from Dianova (Germany) and diluted in the ratio 1: 5000 in BSA/PBS. After six washing steps with PBS the chips were incubated with 2.5 ml of a peroxide standard substrate solution (3,3',5,5'- tetramethylbenzidine, H_2O_2 dissolved in 0.1 M acetate buffer pH 5) for one hour and the developed blue colour was compared visually. Since only in the case of chips with crea-BSA an antibody binding was observed, it can be concluded that the binding of the crea-BSA to the Si_3N_4 surface of the test

chip is very strong. Therefore, the same principle was used to immobilize the creatinine molecules on the Si_3N_4 surface of the sensor IDC.

A 3 mg sample of creatinine butyric acid was activated by a modified carbodiimde method with EDC amd sulfo-NHS (molecular ratio 1:3:1) in 0.05 M phosphate buffer (pH 5) for 30 minutes and coupled to 1 mg of carrier protein (KLH) in 0.1 M carbonate buffer at pH 8.5 for three hours. After gel filtration with PBS equilibrated PD-10 columns (Pharmacia Biotech, Sweden), the coupling efficiency was evaluated by determination of KLH-coupled creatinine via the Jaffe method in relation to the protein concentration. In addition, the decrease in free amino groups of KLH was controlled by 2,4,6- trinitrobenzenesulfonic acid. Monoclonal antibodies were obtained by immunization of mice with synthesized creatinine-KLH conjugate and the hybridoma technique with mouse myeloma cell line SP2.

3.2.3 Sensor circuit design

The oscillator circuit with the embedded IDC sensor described in chapter 2 is the sensor circuit. In this work of immunosensor, the exclusive variation of capacitance in the sensor circuit is caused due to the variation of the IDC capacitance brought about by the binding of different concentrations of anti-creatinine antibodies to the immobilized creatinine molecules on the IDC. For the developed prototype immunosensor operating at 6 GHz, 1 nH inductors were used. The capacitance of the IDC is simulated using ADS Momentum and is obtained to be 100 fF. The inductors are fabricated on the TM2 (topmost metal layer) of the BEOL stack, and have a simulated quality factor of 15 at 6 GHz aiding the overall quality factor of the LC resonance tank. The "all-electrical" immunosensor requires a 3.3 V external DC power supply for operation and as measurement equipment an X band spectrum analyzer from Rhode and Schwarz is used.

3.3 Results and discussion

The capacitance variation of the sensor IDC due to binding of anti-creatinine antibodies to the immobilized creatinine molecules in an aqueous environment was simulated in COMSOL 4.2a. The effect of the permittivity of the aqueous solution on the sensitivity of the IDC was simulated to establish the idea of intrinsic sensitivity enhancement as was proposed in the previous section. The immobilized creatinine molecules were modeled as circular structures with effective diameter of 10 nm and permittivity of 1 gm/dl 3-4 [131,132]. The antibodies were modeled as cylindrical pillars of height 30 nm and effective diameter 10 nm and a relative permittivity of 2 for same sample volume. The size of the antibodies is considerably larger when compared to the creatinine molecules.

The inclusion of the aqueous environment replicates the electrical experimental scenario where a droplet of water is added during the measurements. Four simulation environments were established for four different concentrations of creatinine molecules used in the incubation of the anti-creatinine antibodies. The simulations then indicate that for an aqueous solution

environment with sufficiently high permittivity compared to the antibodies and creatinine molecules, the IDC shows considerable increase in its capacitance with increase in concentration of creatinine molecules used during the incubation phase. The maximum increase of capacitance is seen when the aqueous solution has the permittivity of water and the least variation when the aqueous environment is modeled with the permittivity of air. The results are shown in Fig. 3.6. This is in line with the proposed theory although the theory appears counter-intuitive initially. The combined effect of the permittivity of the aqueous environment along with the antibodies

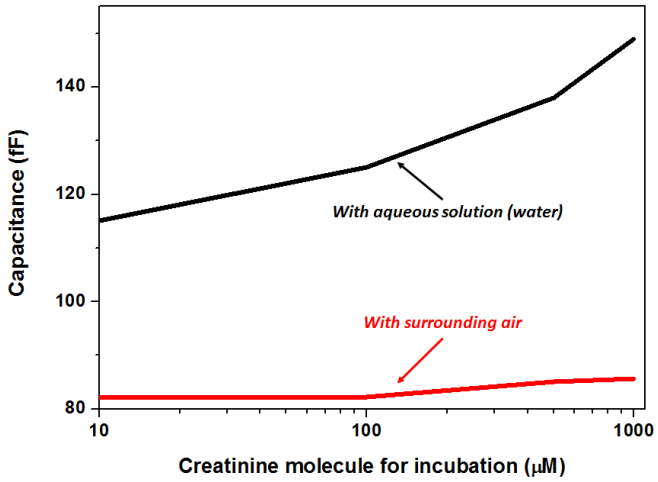

Figure 3.6. Typical variation of IDC capacitance as a function of concentration of creatinine molecules used in the incubation of antibodies. The capacitance increases with increase in creatinine molecule concentration used during incubation. The capacitance variation is strong when the surrounding medium for experiment is water while with air the variation is negligible.

and creatinine molecules has to be taken into account. A higher concentration of creatinine molecules used for the incubation of anti-creatinine antibodies translates to the fact, more number of anti-creatinine antibodies bind to the creatinine during the incubation phase (see Fig. 3.4). Thus, the number of free antibodies in the incubated solution reduces with the increase in the concentration of creatinine used during the incubation phase. On pipetting the samples on the sensor, different concentrations of antibodies bind to the immobilized creatinine molecules. The same has been simulated. When few antibodies bind to the immobilized creatinine, it indicates higher concentration of creatinine molecules used for incubation. In case of fewer binding antibodies, the immobilized creatinine molecules are surrounded by the molecules of the aqueous environment. When, the permittivity of the aqueous solution is high, this translates to a higher capacitance of the IDC when lower number of antibodies bind to the immobilized creatinine. The same is observed in the simulation. In case of water as the aqueous medium, with permittivity of 70 at 6 GHz, the variation in capacitance of the based on the binding antibodies is quite high

(shown in the black curve of Fig. 3.6). However, when the permittivity of the aqueous medium is replaced by the permittivity of air that is 1, the variation in capacitance is negligible. This can be accredited to the permittivity contrast. With air, the permittivity was similar to the permittivity of the antibodies. Therefore, not much variation in capacitance was seen in case of fewer antibodies binding and more air molecules around the immobilized creatinine molecules and vice versa. While in the case of the water molecules, whose permittivity was considerably high when compared to the antibodies, a high variation of capacitance is seen with the binding of the antibodies. Therefore, it can be stated that, higher concentration of creatinine molecules used for incubation of the antibodies results in higher capacitance of the IDC while the experiments are conducted in a relatively high permittivity aqueous environment. From the CMOS oscillator sensor circuit outlook, this change of capacitance translates to a decreasing resonant frequency with increasing concentration of creatinine molecules used for the incubation phase.

3.3.1 Optical measurement of creatinine concentration

Prior to the conduction of the "all-electrical" measurements using the sensor circuits, optical measurements in a standard ELISA like approach is conducted on test chips, primarily for two reasons: ELISA-like assay procedures and the optical measurements are established reliable measurement technique and can be used as an independent standard method to compare the results with the "all-electrical" method; secondly, in order to find the best immobilization and binding condition which should be later applied to the sensor chips.

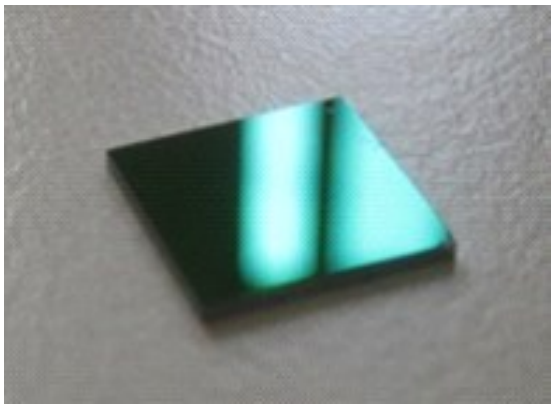

Figure 3.7. Chip photograph of Si_3N_4/Si test chip for optical measurement. Chip size is 1 cm x 1 cm.

Initially several methods in order to immobilize Si_3N_4 passivated silicon test chips were compared regarding the anti-creatinine antibodies binding. Hence, creatinine butyric acid and crea-BSA were covalently or non-covalently immobilized onto different modified test chips. 2 µl of the immobilization solution was pipetted to the Si_3N_4 surface, which was the same amount needed to cover the IDC sensor area. One such test chip is shown in Fig. 3.7.

The immobilized creatinine was then detected with the mono-clonal anti-creatinine antibody B90-AH5 and a peroxidase-conjugated anti-mouse IgG. The peroxidase activity was detected via a standard color reaction using 3,3',5,5'-tetra-methylbenzidine and hydrogen peroxide. Most of the chips generated no color. Only chips with adsorptive immobilized crea-BSA generated the typical blue color, whereas, the chips with immobilized BSA generated no color.

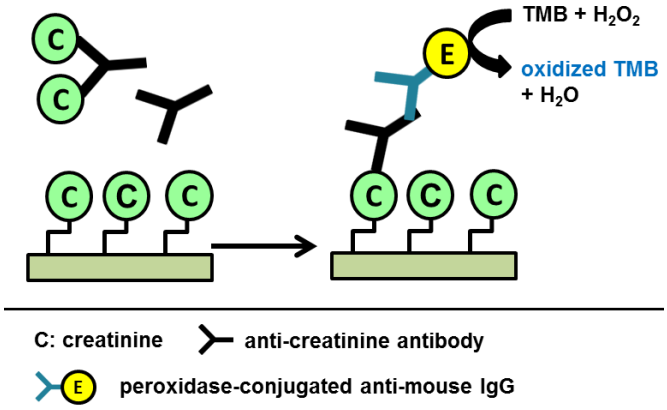

Figure 3.8. Indirect competitive assay principle for optical creatinine determination with creatinine-modified Si_3N_4 test chips

.

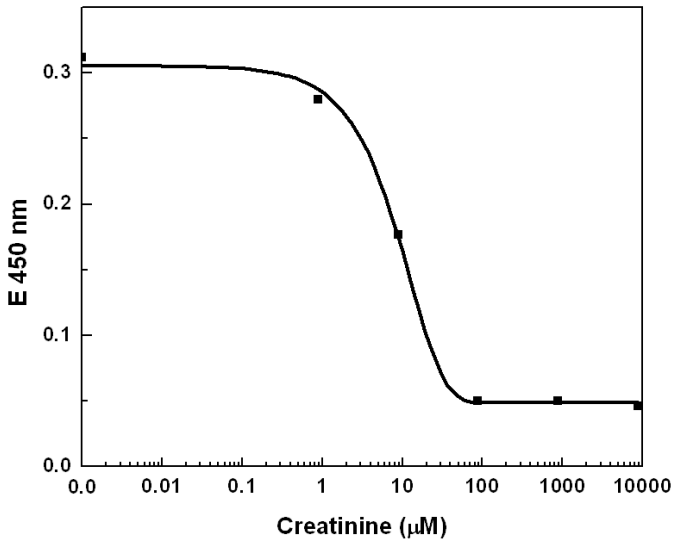

Figure 3.9. Optical measurement of creatinine concentration. The response slope of the optical measurement in the range 0.88 to 88 µM shows the dynamic range of the standard measurement technique.

This result shows that the anti-creatinine antibody was specifically bound to the immobilized crea-BSA. For creatinine determination an indirect competitive immunoassay principle as shown in Fig. 3.8 was applied.

The crea-BSA modified Si_3N_4 test chips were incubated with different creatinine concentration (0-8.8 mM) with a defined and optimized antibody concentration (0.1 µg ml^{-1}). As mentioned above, the optical measurements were conducted to compare the standard technique with our proposed "all-electrical" approach. The detection range of the established optical technique although covers the concentration ranges of creatinine which is of clinical relevance, but is saturated beyond 88 µM of creatinine concentration. On comparing the detection range of both measurement techniques, the electrical approach shows an order of magnitude increase in detection range, as is demonstrated in the subsequent section.

3.3.2 Dielectric measurement of creatinine concentration

Characterization of sensor

The sensor chip showing the IDC sensor in conjunction with oscillator circuit is shown in Fig. 3.10.

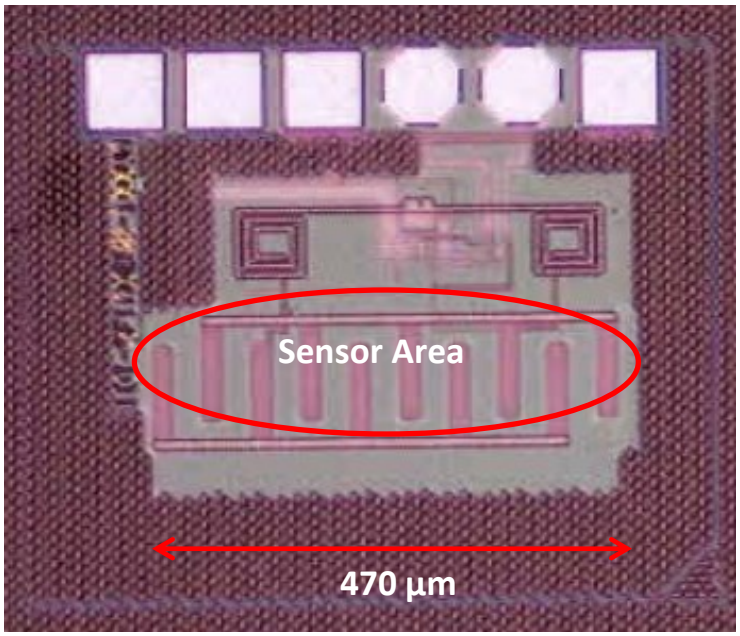

Figure 3.10. Chip photograph of dielectric sensor. The sensor area (IDC) is marked in red.

The chip was characterised initially to analyse the electrical performance and was followed by a calibration step with the measurement of glucose solution (see chapter 4 for glucose solution measurement). The sensor chip draws a current of 27 mA from 3.3 V DC power supply. The resonance frequency of the sensor oscillator is 6.01 GHz in air that is with no material placed on top of the sensor. The overall chip area is 0.3 mm^2. The miniaturized sensor area as mentioned above reduces the volume of the probe sample used in the analysis of the creatinine.

The performance of the sensor oscillator showing resonance frequency shift for varying IDC capacitance was characterized with glucose solution measurements. Fig. 3.12 shows the measurement of various concentrations of glucose solutions using the sensor oscillator. Different concentrations of glucose solutions are pipetted on the sensing area and the resulting frequency is measured and compared with simulations.

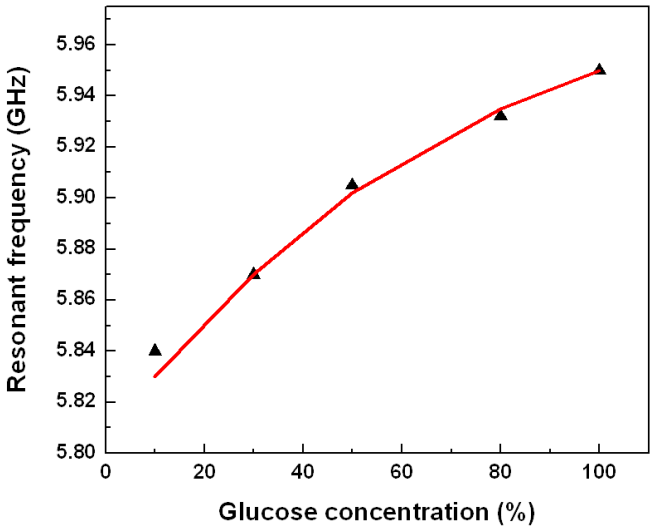

Figure 3.11. Calibration of sensor circuit with glucose solution. The red curve shows the simulation and the black triangles are the measurement results. The resonant frequency up-shifts with increasing glucose concentration.

The resultant permittivity of the glucose solution for different concentration of glucose is calculated analytically using the mixture rules (see chapter 4). It is observed that the resonance frequency of the sensor oscillator up-shifts with increasing concentration of glucose in the homogeneous solution of glucose in water. This is attributed to the decrease in resultant permittivity of the solution with the increasing concentration of glucose as glucose has lower permittivity as compared to water. With lower glucose concentration the permittivity of the resultant solution is close to water and the same can be seen in Fig. 3.11. The resonance

frequency of the sensor oscillator is with pure water on top of the IDC is 5.81 GHz. This measured behavior of the sensor is in close agreement with the theoretical and simulated behavior of the sensor. Thus, the calibration technique well establishes the operation of the sensor. The sensor is now extended to the direct measurement of the creatinine.

Creatinine concentration measurement

Several chips from the same wafer need to be characterized in order to determine the reproducibility and the yield of the fabricated direct immunosensor. Multiple chips on the same wafer were characterized to estimate the on wafer process variation. The variation observed in the resonance frequency of the sensor oscillator is not more than 3 MHz. This depicts the high yield and reproducibility of the sensor chip. The creatinine molecules were immobilized on the sensor area only, using the surface chemistry on top of the sensor area. The surface chemistry was used only to modify the sensor area, leaving the inductors. Therefore, the creatinine molecules did not detune the inductors.

Eight chips with the same resonance frequency of 6.01 GHz were chosen and treated later in order to immobilize creatinine molecules on the IDC sensor surface. This is followed by the pipetting step of 2 µl of the pre-treated anti-creatinine antibody samples on the Si_3N_4 based surface of the IDC sensor area marked in red in Fig. 3.10. It was mentioned above for the purpose of electrical measurement with strong permittivity contrast and a better sensor response a drop of water (1 µl) was added on the sensor area. Fig. 3.12 shows the resonance frequency shift of two chips treated with two different incubated antibody samples.

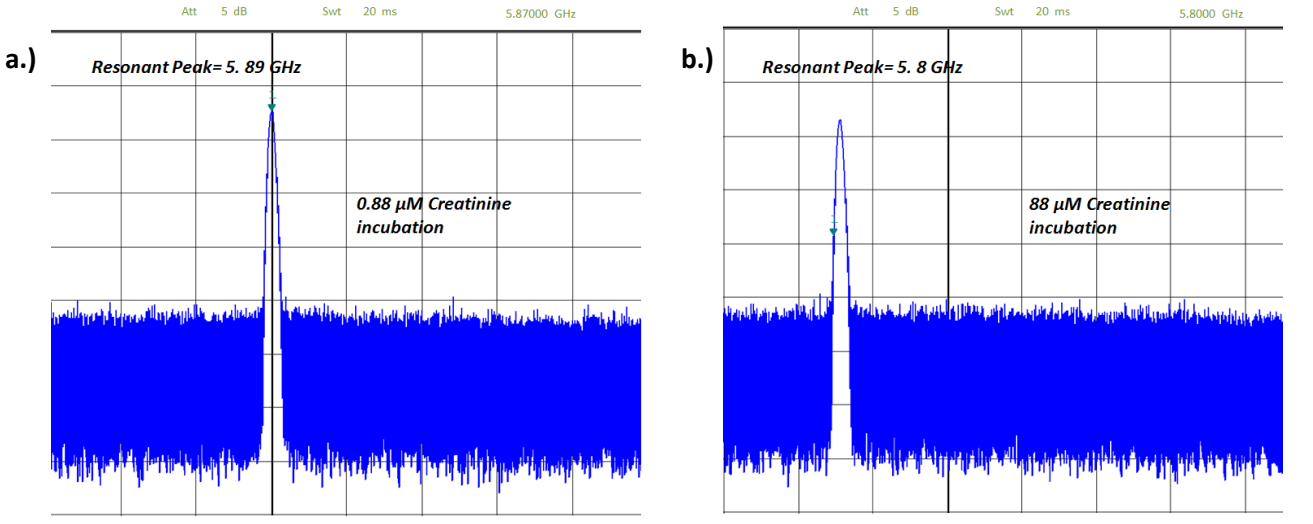

Figure 3.12. (a) Resonant frequency peak for chip treated with antibodies incubated with 0.88 µM creatinine. (b) Resonant frequency peak for chip treated with antibodies incubated with 88 µM creatinine.

The measurement results of the chips with four different samples of antibody are shown in Fig. 3.13. The higher the concentration of creatinine in the pre-incubation the lower is the concentration of antibody binding to the immobilized creatinine molecules on the IDC. The black curve shows the measurements done with an additional droplet of water of approximate volume of 1 µl carefully pipetted on the sensing area.

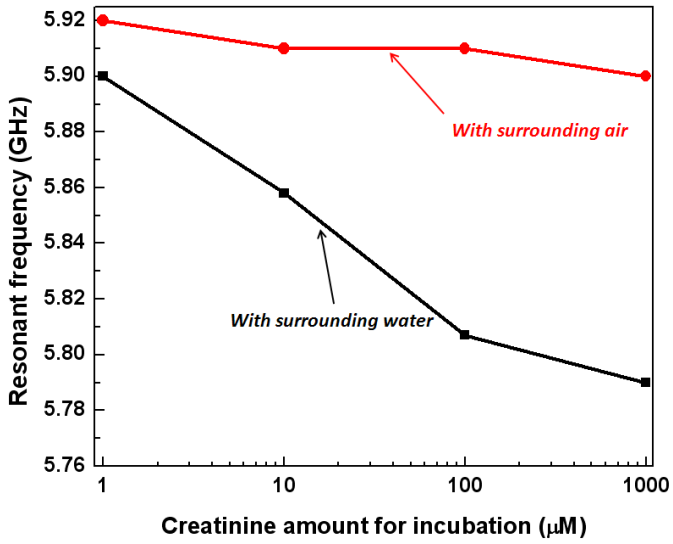

Figure 3.13. Measured variation of resonant frequency as a function of creatinine concentration used in the incubation of antibodies. The black curve shows the resonant frequency for four samples with increasing concentration of creatinine used in incubation while the experiment was done in aqueous (water) environment. The resonant frequency downshifts with increasing creatinine concentration. The red curve shows the same experiment done with air as the surrounding medium.

It is seen, with lower concentration of creatinine used in pre-treatment (higher amount of antibodies binding to the immobilized creatinine), higher is the resonant frequency. This is in line with the proposed theory and simulation results shown above. As seen from the measurements, for each step variation of the concentration of the creatinine, the resonant frequency varies by approximately 35 MHz. With highest creatinine concentration during the incubation phase, least amount of antibodies binds to the immobilized creatinine molecules on the IDC. Therefore, the resulting resonant frequency tends towards the frequency of the oscillator with pure water on top of it 5.73 GHz). The red curve shows the same experiments done on the same chips with air as the surrounding medium.

As seen from the results there is negligible variation of the resonant frequency of the oscillator although there is a tendency of frequency downshift. The measurement results agree closely with our proposed model and simulation. The capacitance variation of the IDC is strongly dependent on the permittivity contrast between the antibodies and the

surrounding medium and hence, suited for biosensor, immunosensor applications as most often a buffer solution is used for such measurements.

It can also be noted from the above measurements that in aqueous solution, the sensor has a detection range higher than the optical measurement technique. It was shown in Fig.3.10 that the measurement response with optical technique saturates beyond 88 μM of creatinine concentration used in the incubation phase. However, in the proposed sensor, the curve although seems to have a saturating effect, but have considerable sensitivity from 88 μM to 880 μM. Therefore, the sensor is sensitive beyond the clinically relevant range of 0.88 μM – 88 μM as well. The increase in the sensitivity range, makes the sensor useful for other clinical diagnostics as well. The variation of frequency in this range is 25 MHz and is considerably higher than the process variation of 3 MHz, therefore, showing an order of magnitude higher detection range compared to the established optical technique. This can be attributed to the contrast of permittivity between water molecules and the anti-creatinine antibodies. When comparing the sensitivity of the two approaches, the percentage change of frequency per 10-fold increase in concentration of creatinine with respect to the total frequency shift over the entire detection range (~42%) is comparable to the percentage change in E_{450nm} intensity (~ 40%).

In order to determine the error bar in the measurement and also to determine the reproducibility of the sensor system from the measurement perspective, several sets of chips with same samples of pre-incubated antibodies were measured at the same time in aqueous solution. The maximum normalized standard deviation in the resonant frequency for similar measurement condition is 0.223. The frequency response of two sets of chips showing maximum measurement variations was plotted. The resonant frequency contrast for the two sets of chips was observed for all the four antibody samples incubated with different amounts of creatinine. The maximum drift in the resonant frequency of two chips with same sample of antibodies was observed to be 4 MHz, shown in Fig.3.14. This drift in the resonant frequency is approximately a tenth of the measured sensitivity of the sensor. The observed variation being considerably less than the sensitivity shows high reproducibility of the immunosensor system.

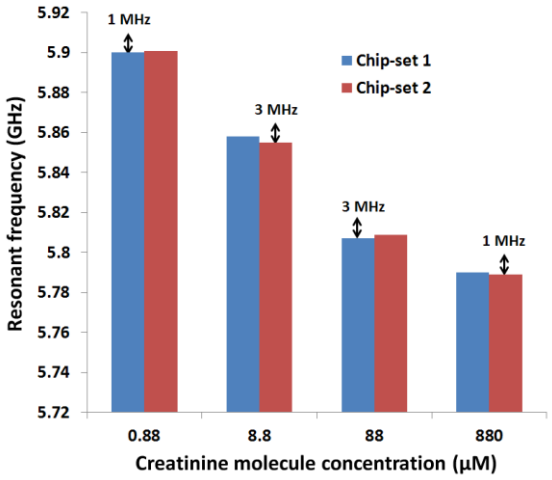

Figure 3.14. Error bar measurement for two sets of chips. The maximum frequency drift does between two chips does not exceed 4 MHz.

3.4 Conclusion

The results show that creatinine can be measured with the developed CMOS high frequency dielectric immunosensor in the clinically relevant concentration range. The electrical measurement results show close agreement with an optical standard measurement technique. The measurement capability in the order of nanomolar concentration level shows that such a high frequency sensor can be successfully used for relevant measurements in clinical diagnostics. The measured frequency shift of 35 MHz in the clinically relevant regime of creatinine concentration of 0.88 µM to 88 µM is much higher than the effect of process variation. The effect of process variation was measured and was shown negligible in comparison to the sensitivity of the sensor. This was shown in the error bar measurement conducted with two sets of chips. Therefore, it can be deduced that the demonstrated CMOS high frequency sensor has considerable stability for clinical measurements. The miniaturized sensor design and the exclusion of any labelling compounds will reduce the costs in comparison to other antibody-based creatinine assays enormously. Additionally, the capability of immobilization of creatinine molecules on standard passivation layer of CMOS process (Si_3N_4) evades the need of any post processing techniques of the silicon chip required for immobilization of creatinine molecules. This result is very significant for future CMOS immunosensors for creatinine and can be adapted to other antigen antibody couples

Since the already published creatinine enzyme immunoassays and indirect immunosensors can specifically measure creatinine in real human serum samples it can be assumed that the developed immunosensor which uses the same antibody is also able to measure real samples Since nanomolar analyte concentrations can be determined it can be stated that in future the developed technology can be adapted for other clinically relevant analytes as well.

DETECTION of ANALYTE CONCENTRATION

This section* of the thesis presents a high-frequency (X-band) CMOS dielectric sensors applied to various biological applications; primarily to detect concentration of suspended particles in a solution, to detect concentration of glucose in homogeneous glucose solutions, dielectric imaging of biomaterials and detection of fat and calcium in blood. Three sets of sensor chips in the frequency range of 6 GHz to 12 GHz are demonstrated in this chapter. The sensor chips are fabricated in 0.25 µm or 0.13 µm SiGe:C BiCMOS technology of IHP. Two approaches for fluid handling are shown in this chapter. The first approach includes using of a typical polymer based microfluidic system and the second approach includes creation of an insulating wall around the sensor area of the chip. The post-processing steps required for the microfluidic integration is explained in this chapter. In that context, the influence of silicon nitride and silicon dioxide passivation layers on the sensor chip is analyzed. The dielectric sensitivity of the chips is characterized and calibrated using different organic fluids (alcohols); sensitivity of the sensor chips were found to be a strong function of the passivation layers on the top of the sensors. The sensors are further applied to detect fat and calcium present in blood samples, as a first step to develop minimally invasive technique for plaque characterization in arteries. Further, a prototype of a typical sensor array system is demonstrated for imaging of biomaterials and can have potential applications in analyzing cancerous tissues form healthy ones.

4.1 Introduction

The key features that a state-of-the-art biosensor should possess are the capability of *in situ* and label free detection of molecules and biological cells within extremely small volumes of the probe sample with a reduced measurement time. Chapter 3 dealt with one such special biosensor (immunosensor), the functioning of which required extremely small sample volumes of antigens and antibodies. On similar lines, there is an increasing demand for developing miniaturized fast non-invasive systems for detection of molecular concentrations, concentration of cells and particles in biological suspension [133, 134] which will use significantly less amount of probe samples as compared to the established sensing systems. Applications like detection of oral squamous cell carcinoma [135], determining the sickle red blood cells in serum [136], discrimination of leukemia cells (HL-60) [137], require rapid label free sensing techniques.

*Parts of this chapter have been published as "Integrated high-frequency sensors in catheters for minimally invasive plaque characterization", European Microelectronics and Packaging Conference and Exhibition, September 2015, Friedrichshafen, Germany

"12 GHz CMOS MEMS lab-on-chip system for detection of concentration of suspended particles in bio-suspensions", Biodevices, January 2015, Lisbon, Portugal

"An 8 GHz CMOS near field bio-sensor array for imaging spatial permittivity distribution", IEEE-MTT-S International Microwave Symposium, May 2014, Tampa, USA DOI: 10.1109/MWSYM.2014.6848459

As shown in Fig. 4.1 a typical LOC device should have microfluidic sensing system with integrated autonomous control and detection circuits on the same measurement and sensing platform. The medical industry has unprecedented possibilities to extract advantages out of the developing LOC technology, as it rightly corresponds to the perfect size to reach biomolecules and cells properties.

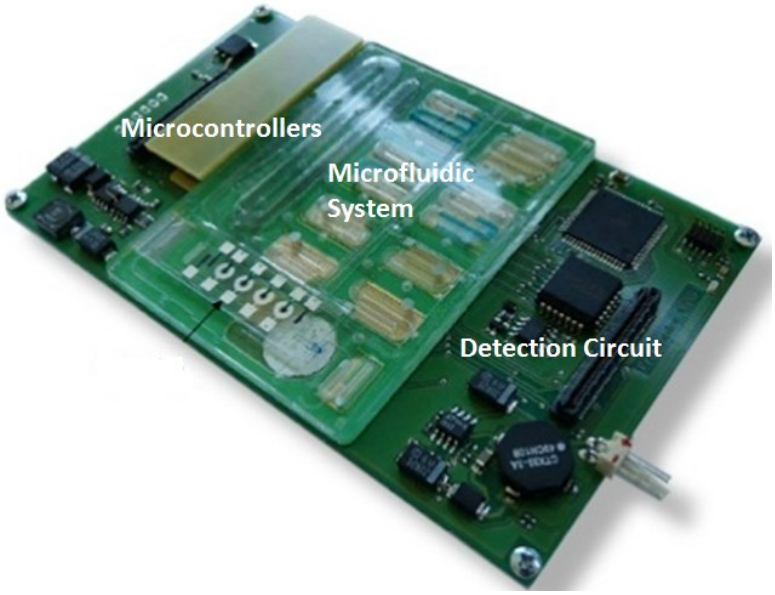

Figure 4.1 Typical schematic of a lab on a chip system showing the microfluidic and detection system. The same platform houses the microcontroller and the detection circuits (IHP internal).

The development of such LOC device is analogous to the miniaturization of the age old computing systems of 1960s to the hand held smart phones with higher computing powers. The dream of establishing LOC system is to miniaturize the functionalities of the state-of-the-art biotechnology laboratories to a hand held autonomous compact device.

In this chapter, we report a complete CMOS/microfluidic system for dielectric detection of suspended particles in biological suspensions in the frequency range of 6 GHz to 12 GHz. Hybrid integration of the microfluidic system to the CMOS chip is performed as a post process step after the chip fabrication. Simultaneous electrical and optical measurements of suspended particles in a solution depict close correlation of both the measurement. The X-band sensor described in this work aids in avoiding low frequency dispersion mechanisms described previously. As mentioned previously low-frequency dispersion mechanisms are useful to determine other properties of the particles but can be problematic for detection of concentration of particles.

4.2 Sensor parameters for microfluidic integration

As mentioned before, the sensor architecture (permittivity controlled oscillator) is the same for all the application and also the sensor module, IDC. The sensing principle is based on the variation of fringing field capacitance between the fingers of the IDC, due to the change of permittivity on top of it. The operation of such a sensor based on a unit cell model has been explained in chapter 2. In this section of this chapter a more detailed analysis of the sensor for the microfluidic integration is taken into account: which is the effect of passivation layer on the sensitivity of the sensor.

The sensor systems are fabricated in the standard BiCMOS process lines of IHP (0.13 µm for 6 GHz sensor system and 0.25 µm for 8 GHz and 12 GHz sensor system). As was explained in chapter 2 the choice of metal layer stems from the biological integration need. One major implication of the choice of the metal layer for designing the IDC, along with the influence on its quality factor is the influence of passivation layer. Passivation layer in micro-fabrication or CMOS technology is an insulation layer deposited on top of the metal layers (electrodes) to protect the metal layers from external environment. The passivation layer for a standard BiCMOS process is 400 nm of Si_3N_4. The influence of passivation layer is a significant parameter to be analyzed due to the two different approaches considered here for characterizing bio-suspensions. The first approach involves using a conventional polymer based microfluidic system suitable for analysis of fluids in a flow assisted fluid system. Chemical mechanical polishing is employed in order to planarize the Si_3N_4 surface for better bonding of the polymer microfluidic system to the silicon chip. Such a planarization results in the reduced thickness of the passivation layer. The second approach includes fabricating a non-conductive wall around the sensor structure for biological suspension. Such an approach is suitable for analysis of fluids in static condition. In this approach, the thickness of the passivation layer is not reduced. Fig. 4.3 shows the variation of the capacitance of the IDC with increasing permittivity of MUT for varied thickness of the passivation layer. The variation of the capacitance with increasing permittivity given by the slopes of the curves in Fig. 4.2 is seen to reduce with the increasing thickness of the passivation layer. The slope of the curve defines the sensitivity of IDC alone. Such a result is understandable, as the strength of the fringing electric field tends to decay exponentially along the z direction. This has been discussed in detail in the analysis of the penetration depth of electric fields of IDC, in chapter 3. If the IDC is designed on the TM1 metallization layer of the BiCMOS stack, the passivation layer has a thickness of approximately 5 µm. This is the combined height of SiO_2 on TM1 and Si_3N_4 on TM2.

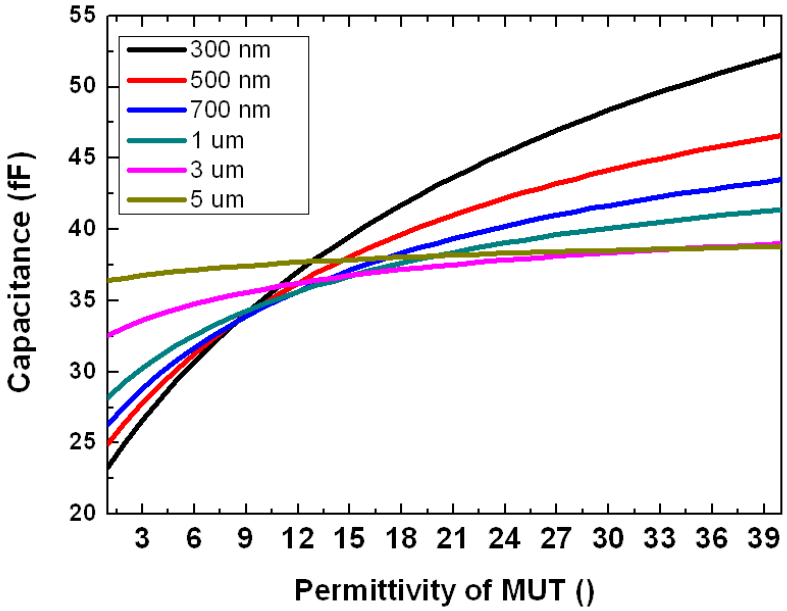

Figure 4.2 Variation of capacitance of the IDC with respect to permittivity of MUT for different thicknesses of passivation layer on top of the IDC. The variation of capacitance reduces with increasing thickness of passivation layer.

This is the case for the sensor system operating at 6 GHz where the IDC is designed on the TM1 metallization layer. For this sensor system we use the non-conductive wall approach for fluid characterization in order to analyze the limits of the sensitivity of the sensor system in terms of passivation layer thickness. The effect of passivation is of wide interest for near field bio sensing, as often the electrodes are passivated to prevent them from coming in direct contact with the bio materials. It is shown with simulations that the sensor is sensitive up to a passivation thickness of 5 µm and thus can be efficiently used in near field bio sensing applications. The same has been shown with the measurements using the 5 GHz sensor system.

4.2.1 Planarization of silicon chip

As mentioned above, in order to analyze biological suspensions using the CMOS sensor chip, two approaches were considered. In the first approach, where a polymer based microfluidic system is used to handle the bio-suspension, planarization of the silicon chip is required for precise binding between the polymer microfluidic channels and the silicon chip. This requires post processing of the chip after fabrication. Chemical mechanical polishing (CMP) step is employed in order to planarize the Si_3N_4 passivation surface [138].

The chip fabrication involves the production process of the silicon wafer consisting of the sensor circuit in a standard BiCMOS process (0.25 µm for 12 GHz sensor chip). As shown in Fig. 4.3

(a) the BEOL of the 0.25 µm BiCMOS process has five metal layers aluminum/tungsten metallization with silicon dioxide as the interlayer dielectric.

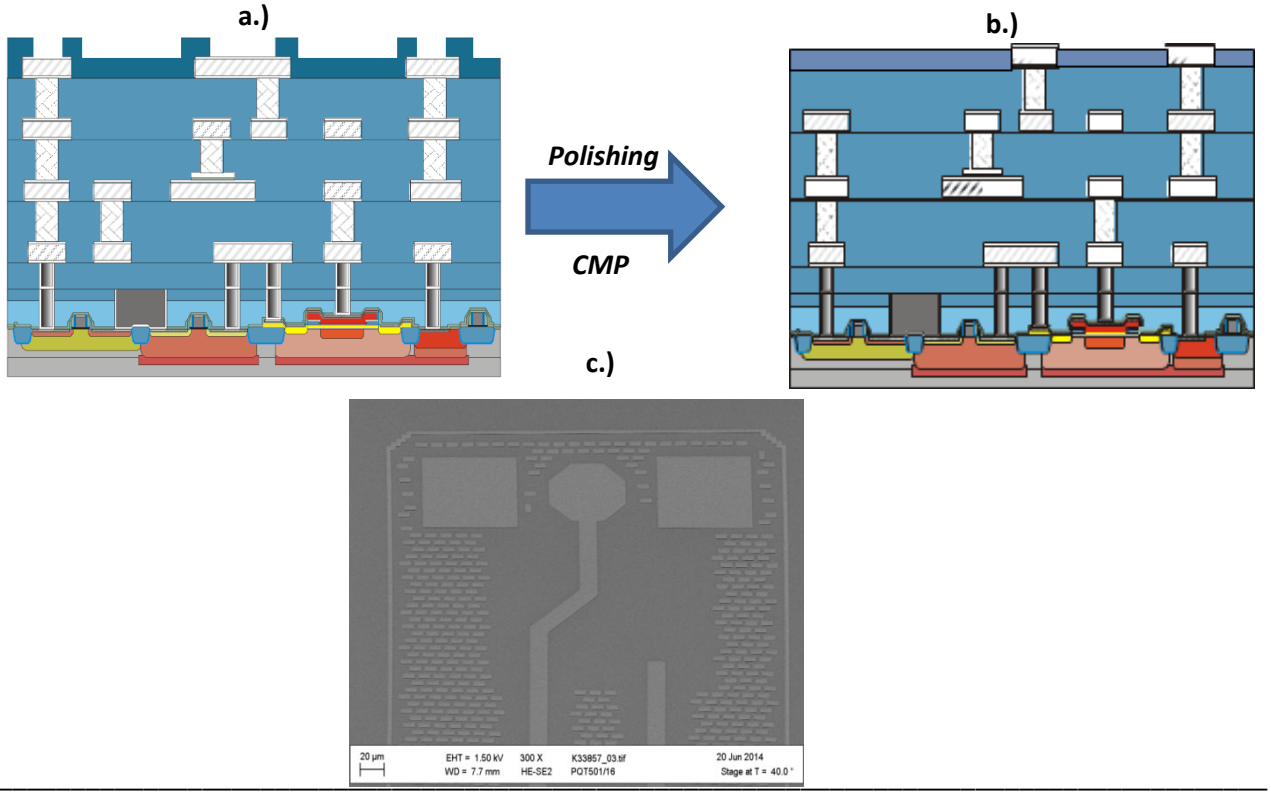

Figure 4.3 Planarization of the BiCMOS stack for microfluidic integration. (a) Schematic of the back-end-of-line stack. (b) Schematic of the stack followed by planarization (c) SEM image of a typical planarized chip.

As was mentioned in the passivation analysis in the previous section, the back-end-of-line stack is topped with Si_3N_4 passivation surface. The thickness of the TM2 layer is 3 µm as is shown in Fig. 4.3 (a). Therefore, the topography of the finished sensor chip is at least 3 µm high. There are stringent requirements for the planarity of the surface of the (Polydimethylsiloxane) PDMS and the silicon chip for bonding purposes. Therefore, the fabricated sensor chip is not suitable for the bonding process with an irregularity in the topography of the order of µm. The processing of the chip is modified for the planarization of the chip surface. The gaps between the TM2 structures are filled with silicon dioxide and planarized using the CMP technique. High density plasma (HDP) chemical vapor deposition (CVD) was used to deposit this silicon dioxide. HDP is used because of its good gap filling properties. The CMP process was stopped several hundred nanometers above the TM2 layer. Then the oxide was etched back using reactive ion etching without a resist mask until the TM2 surface was exposed. Fig. 4.3 (b) shows the BEOL stack after the CMP process. The top Si_3N_4 layer is completely planarized and TM2 metallization layer is exposed to the external environment. The gap between the TM2 metal structures is filled with SiO_2 as mentioned above. A scanning electron microscopy image of a planarized chip is shown in Fig. 4.3 (c).

4.2.2 Microfluidic integration to silicon Chip

PDMS microfluidic channels of width 500 µm and height 50 µm were fabricated using SU8 master mold using soft lithography technique. This technique of polymer based microfluidic system was first introduced by the group of Whitesides of the department of Chemistry in Harvard University [139]. The same procedure is followed here. The PDMS channel was further bonded to the CMOS chip using oxygen plasma bonding technique. Fig. 4.4 shows the schematic view of the CMOS microfluidic system.

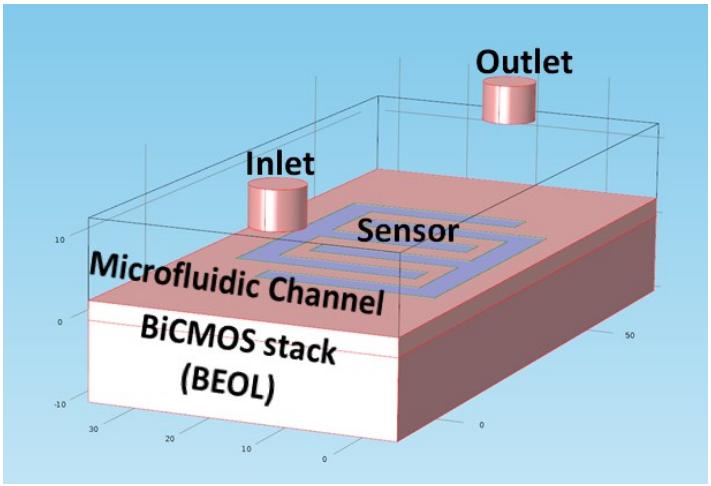

Figure 4.4 Schematic of the microfluidic integration with the CMOS sensor chip.

The master mold was fabricated from SU8 photoresist patterned on a 4 inch silicon wafer. SU8 is most commonly used for such fabrication techniques because of the capability of manufacturing high aspect ratio structures with it. PDMS was prepared using Sylgard 184 silicone elastomer base (Monomer) and its curing agent (hardener). The monomer and the hardener were mixed in the ratio 10:1. Other ratios of monomer to hardener were also tried for different values of elasticity of the PDMS structures. However, the above combination of monomer and hardener was chosen as it gave the best bonding strength. After thorough mixing, the solution was poured on the master mould and cured at a temperature of 70°C for ninety minutes. Room temperature curing is also possible but takes a longer time of approximately a day. The obtained PDMS structure was carefully peeled off from the mold and stored in a salinized chamber.

Oxygen plasma bonding of the PDMS microfluidic channel to the CMOS chip was performed in the Reactive Ion Etching (RIE) chamber. Plasma pressure of 16 Pa was used for a time of 30 seconds with an RF power of 65 Watt.

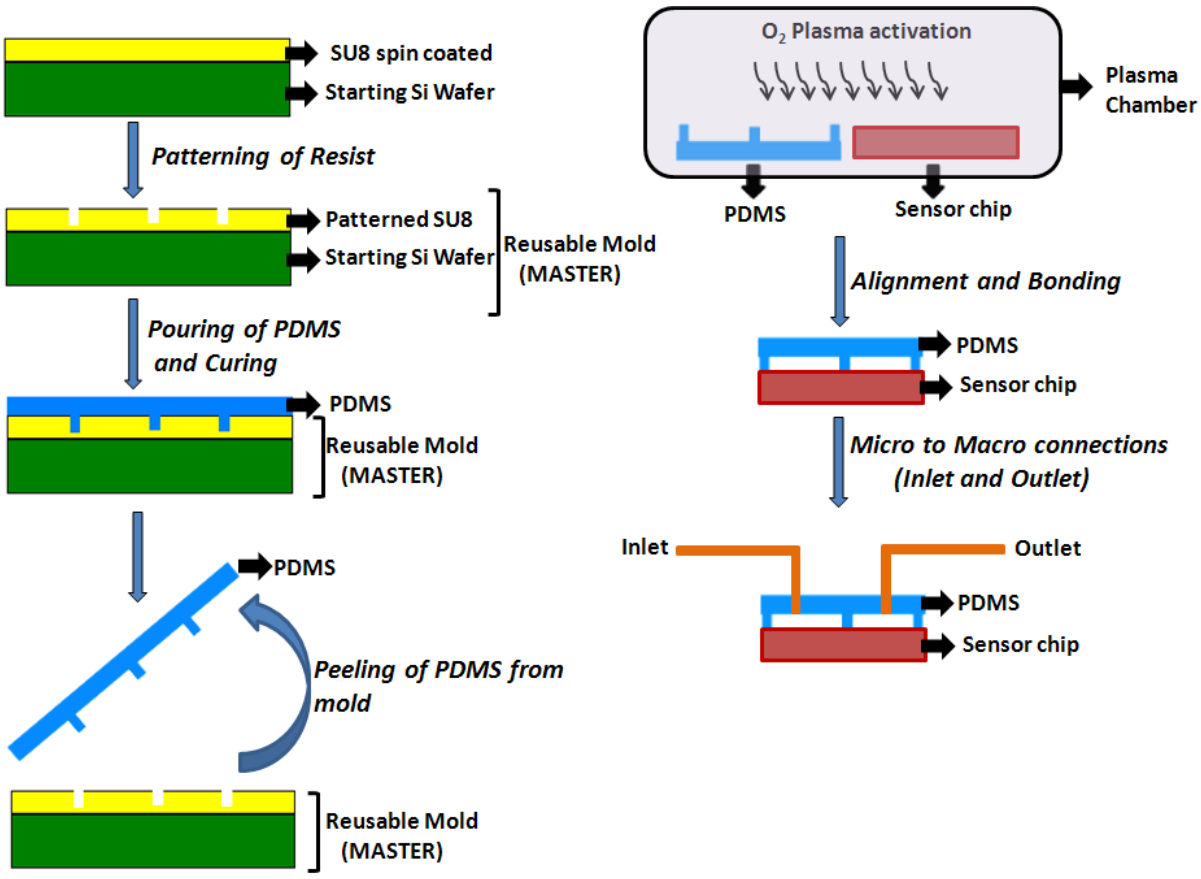

Figure 4.5 Fabrication and bonding of PDMS microfluidic channel with the CMOS sensor chip. The PDMS microfluidic system is fabricated using soft lithography approach. Oxygen plasma bonding is used to bond the PDMS microfluidic channel to the silicon chip.

Using higher RF power reduces the bonding strength as the PDMS surface which is changed from hydrophobic to hydrophilic due to the plasma action, to enable the bonding process, is transformed back to hydrophobic with higher RF power. Careful alignment of the channel on top of the sensor was the limiting factor of the bonding time. The bonding time was kept within one minute in order to keep the PDMS in the activated state. Fig. 4.5 shows the process steps of the PDMS/CMOS hybrid microfluidic system.

4.3 Results and discussion

4.3.1 Calibration of sensors

Organic alcohols and glucose solutions have been used to calibrate the sensors. In the frequency range of 6 GHz to 15 GHz the dispersion of water can be used to calibrate the sensor. In this frequency range a small change in the concentration of glucose in the solution can change the permittivity considerably of the solution. This is due to the dispersion slope of water. The

frequency dependent dielectric constant of pure water is characterized by a single Debye relaxation mechanism with the relaxation frequency approximately at 17 GHz shown in eq. 4.2. The variation of the dielectric constant of water with respect to frequency is shown in Fig. 4.6 [140]. The static dielectric constant of water as seen from Fig. 4.6 is around 78 and the permittivity at infinite frequency is 4.

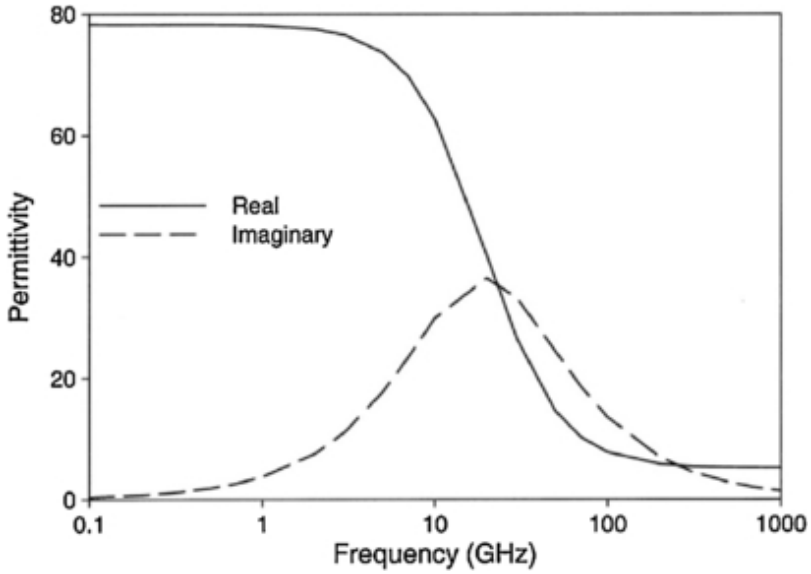

Figure 4.6 Permittivity of water with respect to frequency. The static permittivity of water is 78 while the infinite frequency permittivity is 4. The characteristic frequency of the Debye relaxation process is 18 GHz [140].

The dielectric permittivity of water due to the single Debye mechanism is seen to reduce with frequency. The dispersion mechanism is given by the equation,

$$\varepsilon_f = \varepsilon_\infty + \frac{\varepsilon_s - \varepsilon_\infty}{1+(\frac{f}{f_c})^2} \tag{4.2}$$

ε_f is the permittivity at the operating frequency f. ε_s and ε_∞ are the static and infinite frequency permittivity respectively. The characteristic frequency of the relaxation mechanism is given by f_c. At 6 GHz the permittivity is 70 and at 12 GHz the permittivity is 60. The permittivity of water at the above frequencies is considerably higher when compared to glucose. With the increase of water content in the glucose solution, the overall permittivity of the solution increases. Therefore, the concentration of glucose in a suspension can be characterized based on the variation of the average dielectric concentration of the suspension depending on the glucose concentration.

As mentioned in the previous section as one of the approaches for fluid handling, a non-conductive dielectric wall was fabricated around the sensor to analyze the glucose suspensions. Fig. 4.7 shows a typical sensor chip mounted on board with dielectric wall for fluid handling.

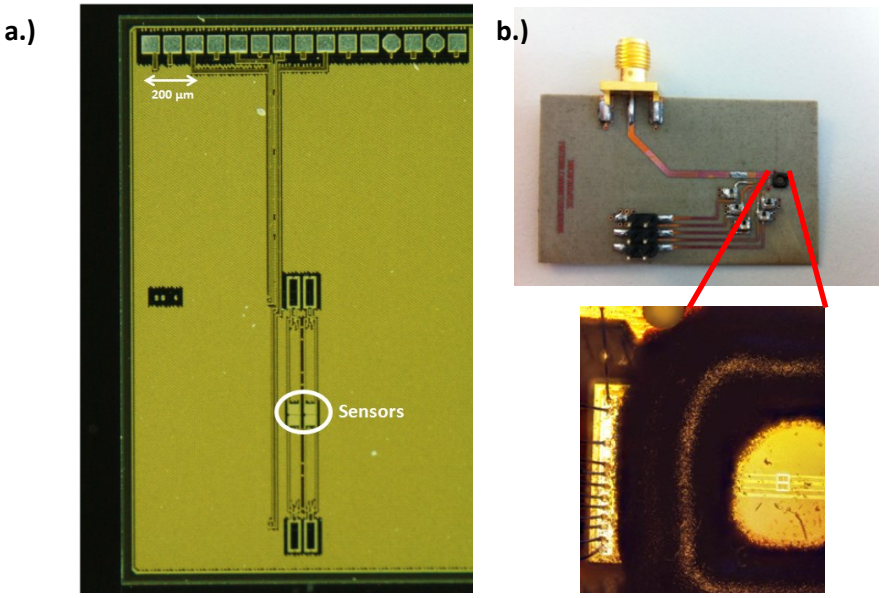

Figure 4.7 Sensor with non-conductive wall around the senor for fluid handling. (a) Typical sensor chip (b) Sensor mounted on board with non-conductive wall.

The sensor chip shown in Fig. 4.8(a) has four sensors with a switched architecture. At a given time only one sensor is operated by turning on the switch for the respective sensor. The glucose solution is pipetted on top of the enclosed sensors as shown in Fig. 4.8. The sensor circuit is similar to the one described in chapter 2.

The 6 GHz glucose sensor has the IDC designed on the TM1 metallization layer of the BEOL stack. As mentioned in the previous section, this design was adopted to characterize the feasibility and the detection limit of the sensor system in terms of its sensitivity based on the thickness of the passivation layer. A systematic way to characterize the sensor was to first analyze the dielectric permittivity of solutions of known permittivity. The calibration of the sensor is done with organic fluids of known permittivity. The resonance frequency of the sensor oscillator is 6.02 GHz with no material placed on top of the sensor, however, with dielectric wall built around the sensor. The liquids used for calibration of the sensor were PMMA ($\varepsilon = 2.67$), PDMS ($\varepsilon = 2.63$), Ethanol ($\varepsilon = 3.2$), methanol ($\varepsilon \sim 12$). Fluids with such permittivity values were chosen in order to determine the resolution of the sensor.

Fig. 4.8 shows the variation of the resonant frequency of the oscillator during the calibration phase. It is noted that the resonant frequency downshifts with the increasing permittivity of the fluids and the same is expected from the sensor performance. This is due to the increase in the

capacitance of the IDC. It is also noted that the PDMS and PMMA having similar permittivity values at 6 GHz, varying only in the second decimal place and therefore, show identical frequency shifts.

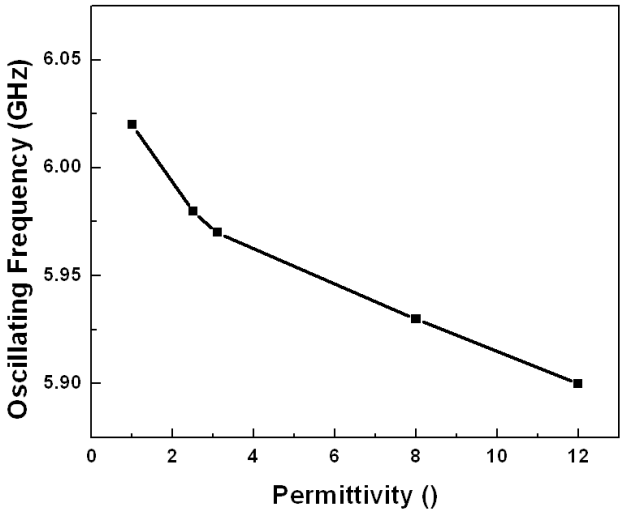

Figure 4.8 Variation of the resonance frequency of the oscillator with materials of different permittivities. The oscillating frequency downshifts with increasing permittivity.

The sensor shows a sensitivity of 20 MHz/permittivity in the permittivity range of 1 to 20, as extracted from the measurements. For error bar measurements, several chips are measured and a variation of 2 MHz to 3 MHz in the normalized (with air on top) resonance frequency is observed. Therefore, combining the sensitivity and the error bar measurements it can be concluded that the sensor system shows a detection resolution of 0.5 in the permittivity values. The same was seen in the PMMA and the PDMS measurement as mentioned above. The sensor was then used to characterize the concentration glucose in a homogenous solution. Fig. 4.9 shows the variation of the resonance frequency of the sensor oscillator with the concentration of water in glucose solution. For a 90% saturated glucose solution (10% water), the permittivity as obtained from the literature is approximately 10. Water, which has a considerably higher permittivity as shown in the previous section, increases the permittivity of the solution when added to the saturated glucose. The same trend is noted in the measurement, as seen in Fig. 4.9. As the water content in glucose solution was increased the resonance frequency of the sensor was reduced or in other words, the resonance frequency of the oscillator has a direct proportionality to the glucose concentration as increasing glucose concentration reduces the permittivity of the solution. The sensors show a sensitivity of 15 MHz downshift per 10% increase in concentration of water in the glucose solution. In Fig 4.9, the 0% concentration of water indicates super saturated glucose solution. All the other measurements are normalized to

this super saturated glucose solution. The increase in concentration of water is done by incrementally adding fixed volume of water in the saturated glucose solution.

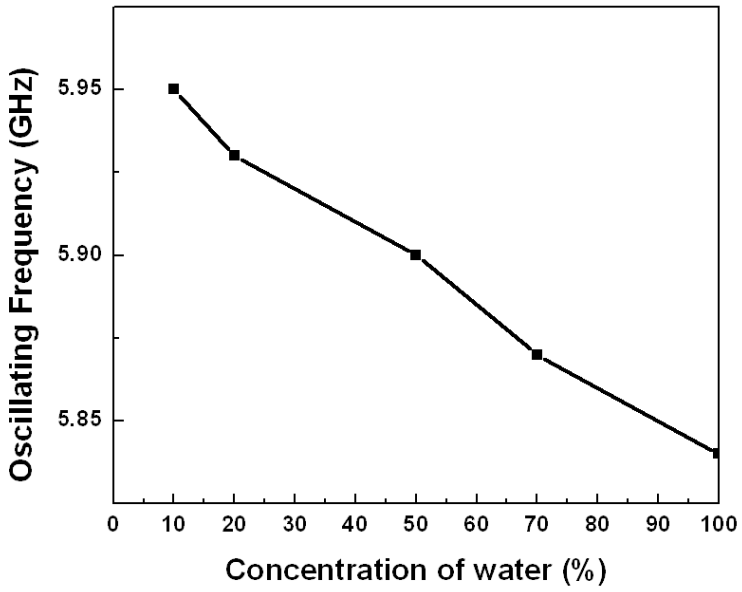

Figure 4.9 Variation of oscillating frequency of the sensor with increasing concentration of water in glucose solution.

From the above measurements, it is shown that the IDC although fabricated on TM1 metal layer of the BEOL stack, with 5 µm of passivation of combined Si_3N_4 and SiO_2 dielectrics, is sensitive to the change of permittivity on top of it. The fabrication of the sensor in TM1 metal layer was needed for immunosensor application as was mentioned in chapter 3. The results of glucose solution calibration of the 5 GHz sensor are presented here to show the difference in the sensitivity for the two metal layers of the sensor, TM1, TM2. The sensitivity and the resolution can be dramatically enhanced with the removal of the passivation layer and shifting the IDC on the TM2 metal layer, thus, bringing the sensor close to the analyte. The same has been done using the 12 GHz sensor.

The 12 GHz sensor is used in conjunction with a microfluidic system for the characterization of the biological suspensions. As was mentioned before, the passivation layer is planarized in order to obtain a sufficiently precise bonding between the chip and the microfluidic system. The IDC is designed in the TM2 metallization layer and hence, has close exposure to the analyte. The CMOS chips were characterized electrically prior to microfluidic experiments. The current drawn by the chip was 12 mA at an operating voltage of 3 V. The oscillating frequency was measured to be 12.32 GHz with an output power of -5 dBm. Further characterization of the chip was performed after plasma bonding of the PDMS microfluidic channel with the chip. The DC operating values of the chip remained unaltered, while the oscillating frequency was measured to

be 12.20 GHz. The 100 MHz shift of the oscillating frequency was accounted for the influence of the PDMS on the inductor coils used in the design of the oscillator. This resonant frequency served as the reference for further measurements, as the microfluidic channel was empty.

The variation of oscillating frequency of the dielectric sensor with materials of different permittivities was characterized by using organic fluids in the microfluidic system. A downshift of oscillating frequency was observed with increasing permittivity of the organic fluids, in this case alcohols. Fig. 4.10 shows the variation of the resonant frequency for different alcohols. At 12 GHz isopropanol and ethanol have almost the same permittivity (Ɛ= 3.8~4.2), as shown by Belrhiti *et al* [140] and can be seen in the frequency output plot to be close to each other. When compared to the 5 GHz sensor, already a better selectivity is noticed. It is also noted that although the static permittivity of methanol is higher than the static permittivity of acetone, at 12 GHz, the permittivity of methanol is less than the permittivity of acetone described by Kung *et al* [141] and the corresponding shift of resonant frequency shows the same.

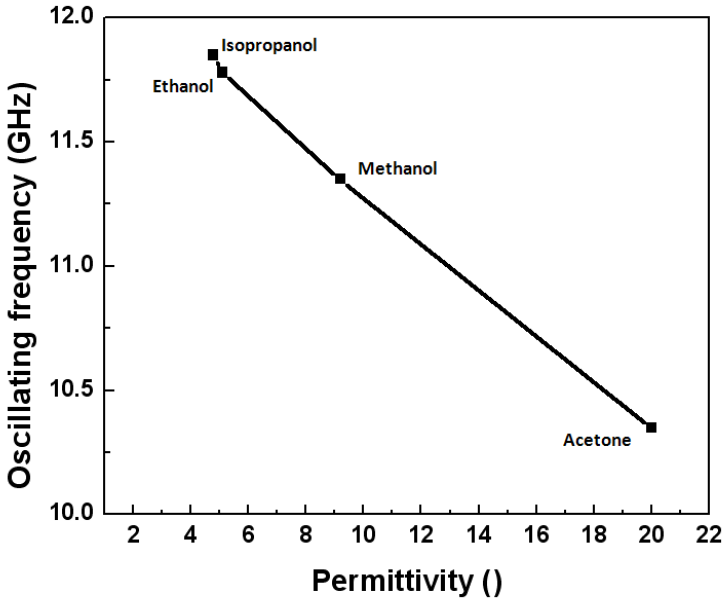

Figure 4.10 Variation of the oscillating frequency for different organic alcohols. The resonance frequency downshifts with increasing permittivity and has a sensitivity of 100 MHz/permittivity.

Sensitivity of 100 MHz/permittivity was observed with the measurements performed with the organic alcohols. This sensitivity is considerably higher when compared to the 5 GHz sensor oscillator. In order to estimate the measurement reproducibility microfluidic channels were bonded to five different sensor chips from the same wafer. Maximum frequency variation of 2 MHz was observed for same measurements and was negligible compared to the sensitivity of the sensor. The detection limit of the sensor can also be estimated with the measurement of isopropanol and ethanol. The alcohols have a permittivity difference of 0.7 at 12 GHz and still

show a considerable frequency shift as shown in Fig. 4.10. The CMOS/microfluidic system was then used to study the effect of water in a homogeneous glucose solution. The variation of resonant frequency with different concentration of water depicts the variation of permittivity of the glucose solution with water content. Fig 4.11 shows the downshift of resonant frequency of the oscillator with increasing water content. Saturated glucose solution has a permittivity of 8 at 12 GHz given by Meriakri *et al* [142]. The corresponding oscillating frequency is measured to be 11.52 GHz. This is close to the value measured for methanol (ε= 9.2) during calibration. The obtained results can be extended to determine permittivity of the glucose solution with different concentration of water. Every 10% increase in the water content shows a frequency down-shift of 250 MHz, which indicates a permittivity increase of approximately 2.5. The increase in water concentration is obtained by incremental increase of water volume in the super saturated glucose solution

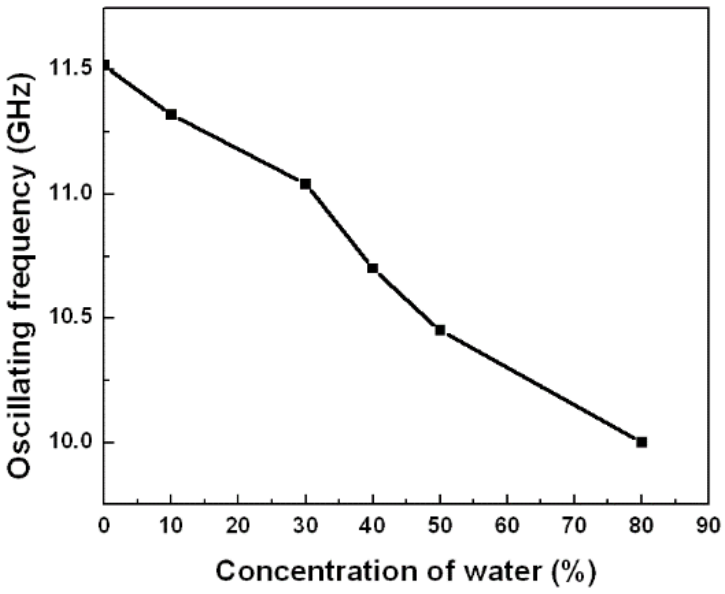

Figure 4.11 Variation of oscillating frequency of the sensor with increasing concentration of water in glucose solution.

Comparing the sensitivity of the two sensors, it is intuitive that the 12 GHz sensor has a higher sensitivity when compared to the sensor operating at 6 GHz due to the closer proximity of the sensor to the analyte. This is also observed while determination of the change in permittivity of the glucose solution with varying concentration of glucose. The glucose solution when measured using the 12 GHz sensor, shows an increase in permittivity of 2.5/10% increase in water concentration. This is significantly higher when compared to the measurements performed using the 6 GHz sensor oscillator. The actual change of the permittivity in the solution due to concentration of glucose was hidden by the permittivities of SiO_2 and Si_3N_4.

4.3.2 Particle concentration measurement

The 12 GHz sensor in conjunction with microfluidic system was utilized to determine the concentration of suspended microbeads in acetone. The influence of micro-beads or particles in a solution can be understood by the hindrance of molecular motion given by the Stokes-Einstein Debye equation [143]. The presence of the particles in an aqueous solution (for e.g., acetone in this case) influences the Debye relaxation process observed in aqueous solutions as described previously for water, thus impacting the overall permittivity of the solution. This can be utilized as a sensing parameter in order to determine the concentration of particles in a solution. Such a technique is lucrative for *in situ*, label-free molecular detection in extremely small sample volumes as well as cytometric applications. A typical biological cell suspension shows the dispersion mechanisms as shown in Fig. 4.12.

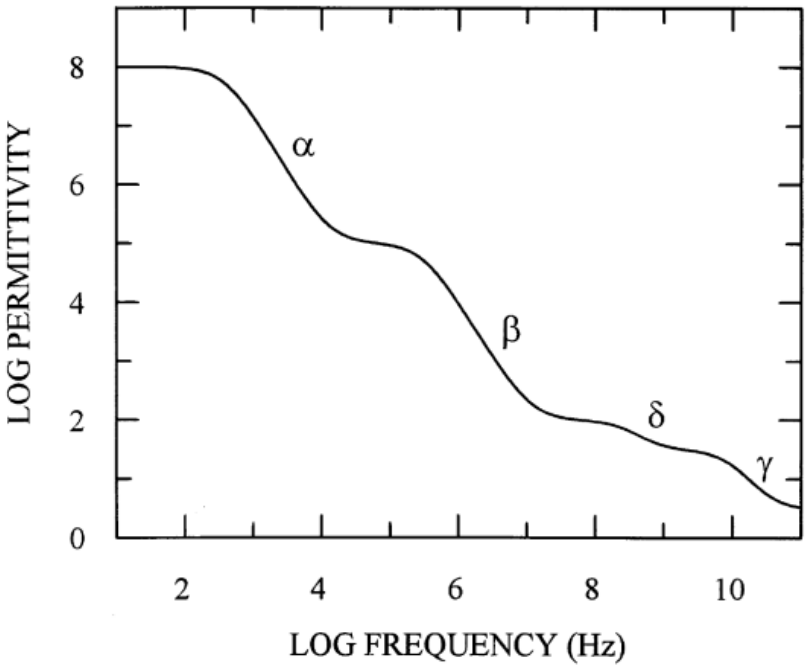

Figure 4.12 Dielectric dispersion curve for biological cell suspension.

The α and β dispersion mechanisms are low-frequency phenomena. As mentioned previously, the low-frequency dispersion mechanisms can be utilized to understand other parameters of the particles or biological molecules.

At high frequency regime (GHz range) γ dispersion dominates and as described above, can be utilized to determine the concentration of particles in a solution. From the mathematical relation it can be understood that the characteristic Debye relaxation time increases or the characteristic frequency reduces with increasing concentration of particles in a suspension [143].

$$\tau = \frac{\pi \eta r l^2}{k_B T} \tag{4.4}$$

r is the radius of the particle, l is the hopping length, η is the viscosity of the particle k_B is the Boltzmann's constant and T is the temperature. Viscosity is directly proportional to the number of particles.

The effective permittivity of the solution with particles can be approximated with Maxwell-Garnett equation [144] or Bruggeman's approach [145]. Using the Maxwell-Garnett equation the effective permittivity of the solution of acetone and microbeads in this work can be expressed as,

$$\varepsilon_{eff} = \varepsilon_a \left(1 + \frac{3\sigma(\varepsilon_{mb} - \varepsilon_a)}{(\varepsilon_{mb} + 2\varepsilon_a)}\right) \tag{4.4}$$

ε_{eff} is the effective permittivity of the solution and the permittivity of acetone and the microbeads are given by ε_a and ε_{mb} respectively. σ is the volume fraction of the microbeads given by

$$\sigma = NV/V_{tot} \tag{4.5}$$

N is the number of microbeads with volume V and V_{tot} is the total volume of the solution. In our measurement system we used micro-beads of diameter 10 μm in different concentrations in a fixed volume of acetone 2 ml.

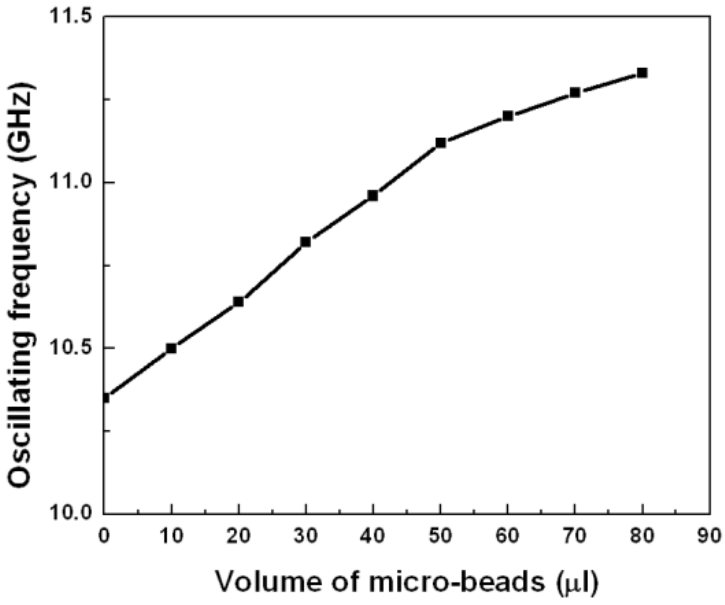

Figure 4.13 Variation of oscillating frequency of the sensor with varying concentration of microbeads in acetone.

The beads were thoroughly mixed in order to prepare a homogeneous solution. The variation of the resonance frequency of the sensor oscillator with respect to the concentration of microbeads in acetone is shown in Fig. 4.13. Equation (3) shows that effective permittivity of the solution

has a direct proportionality with concentration of particles in the solution. However, the second term of the equation ($\varepsilon_{mb} - \varepsilon_a$) renders a negative term when the permittivity of acetone is higher than the permittivity of the particles. Therefore, the overall term has a value less than 1 and the value reduces with increasing concentration. Thus, the overall permittivity of the solution decreases with increasing concentration of particles. Therefore, as observed in Fig. 4.14, the resonance frequency of the oscillator increases with increasing concentration of particles due to reduced capacitance. The diameter of the beads are 10 µm with average permittivity of 2. Frequency up-shit of 125 MHz/10 µl increase in bead content in acetone is measured.

4.3.3 Fat and Calcium characterization in blood

Atherosclerosis is the intravascular condition where the artery walls are hardened due to deposition of calcified fat on its walls [146, 147]. Such hardening of artery walls leads to extreme medical conditions and is often rated as one of the primary reasons for death due to heart failure, stroke, etc [148]. Compact CMOS compatible sensors can serve as an interesting alternative to the state of the art detection techniques of calcified fat which include intra-vascular-ultrasound-imaging (IVUS), optical-coherence-tomography (OCT) of arteries etc [148, 149]. Although, IVUS is an established technique using high frequency acoustic signals, the image quality and the axial resolution is still a concern. On the other hand, OCT systems overcome the shortcomings of IVUS, at the expense of high packaging cost. In this regard, high-frequency or microwave sensors compatible to CMOS technology are a possible solution. CMOS high-frequency sensors offer compact low-cost miniaturized solution for efficient imaging of intravascular modalities with axial resolution in the order of µm. However, development of such sensors for applications in the area of medical diagnostics like plaque characterization is still on the horizon.

In order to establish such high-frequency sensors for *in-situ* applications, initial *ex-vivo* validations of such sensors with same materials (blood, fat and calcium) are mandatory, in order to establish the feasibility of such sensors in the real environment. In this part of the chapter, we present a CMOS sensor operating at 12.6 GHz, used to discriminate pure blood samples form blood samples infested with fat and calcium in the liquid phase.

The sensor chip draws a current of 12.5 mA from a 2.5 V power supply. The normalized resonant frequency of the oscillator with no material on top of the IDC is 12.6 GHz with output power of -5 dBm. The measurements were conducted in two phases. A calibration step is performed with organic alcohols to estimate the sensitivity and the selectivity of the sensor. The second phase of the measurements is performed with the blood samples. The functionality of the sensor is characterized using organic alcohols. The resonant frequency of the oscillator scales down with increasing permittivity of the organic alcohols as shown in Fig. 4.14. Selectivity of the order of 0.5 in absolute permittivity value is demonstrated with detection of isopropanol and

ethanol (Ɛ= 3.5 and 4 respectively). However, with the measured error limit of 3 MHz and sensitivity of 100 MHz/permittivity, the limit of selectivity is extended to the order of 0.1 in absolute permittivity value. The calibration step was followed by the measurement of binary mixtures of fat and calcium in blood. A similar control experiment was performed using water as the suspending medium for different fat and calcium concentrations.

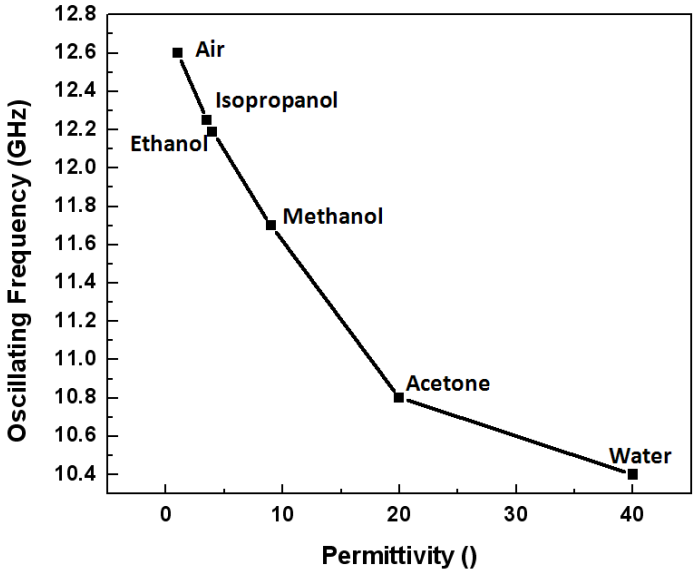

Figure 4.14 Calibration of the sensor system. Resonant frequency downshifts with increasing permittivity of alcohol.

Pure pig-blood samples were procured and binary mixtures were prepared with varied concentrations of liquid fat and calcium. The suspending medium was blood.

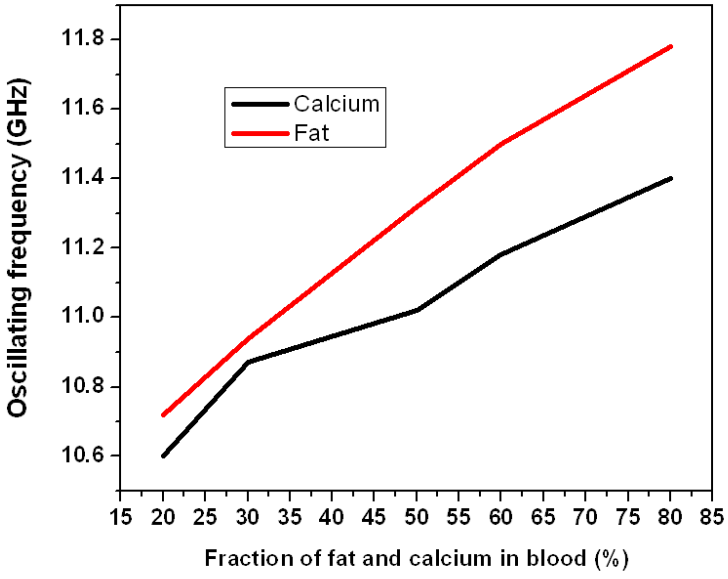

Figure 4.15 Variation of the resonant frequency of the oscillator with varying fraction of fat and calcium in blood. The resonant frequency scales up with increasing concentration.

Fig. 4.15 shows the resonant frequency scaling of the oscillator with respect to the fat and calcium concentration in the mixture samples. The resonant frequency of the oscillator scales up with increasing concentration of fat and calcium in the mixture. Permittivity of the suspending medium, blood Ɛ = 46), is higher (when compared to calcium (Ɛ = 9) and fat (Ɛ = 4.5) [109]. As far as the specificity of the sensor is concerned, it should be kept in mind that the sensor will be used to screen calcified fat. Therefore, detection of calcified fat from blood is the main focus of the sensor.

Therefore, increasing concentration of fat and calcium lowers the overall permittivity of the mixture, lowering the IDC capacitance resulting in up scaling of the oscillating frequency. The permittivities extracted from the above measurements along with the aid of the calibration step fit precisely with the analytically obtained values from binary mixture laws governed by Lichtenecker equations below.

$$\in_{res} = \exp[v_1 ln \in_1 + v_2 ln \in_2] \tag{4.6}$$

Where v_1 and v_2 are the volume fraction of the two materials in the mixture with permittivity values $\mathcal{E}_1$ and $\mathcal{E}_2$ respectively and $\mathcal{E}_{res}$ is the effective permittivity of the mixture. Fig. 4.16 shows the fit of the extracted permittivity values from the measurements with the analytical equation. The error in the extracted permittivity values is 0.4 % when compared to the theoretically calculated value.

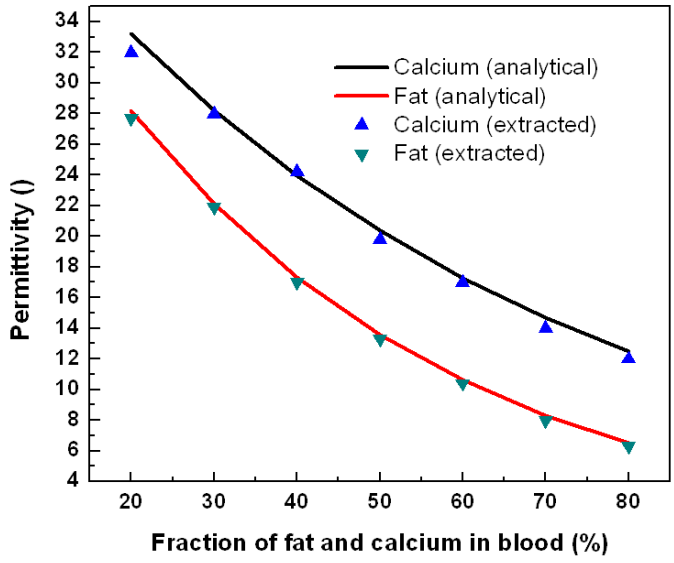

Figure 4.16 Permittivity of binary mixture: fat and calcium in blood. The extracted permittivity values are fit to the analytically calculated permittivity values.

A similar control experiment was established with binary mixtures of calcium and fat prepared in water in order to show the detectability of the sensor is dependent on the permittivity contrast of the suspending medium and calcium and fat. The frequency response of the oscillator is shown in Fig. 4.17. As expected, the resonant frequency increases with increasing concentration of fat and calcium in the mixture. It is noted that the discrimination window is much higher when the suspending medium is water. This can be attributed to the higher permittivity contrast between water, and calcium and fat, when compared to blood. Therefore, it can be deduced that the detection of varying concentration of foreign material in a suspending medium is highly dependent on the permittivity contrast of the two. However, in the real environment where such sensors will be used for plaque characterization, more than the concentration of fat and calcium in blood, the composition of plaque would vary. Therefore, detection of high calcium and fat content in blood is a sufficient criterion for the feasibility of the sensor system.

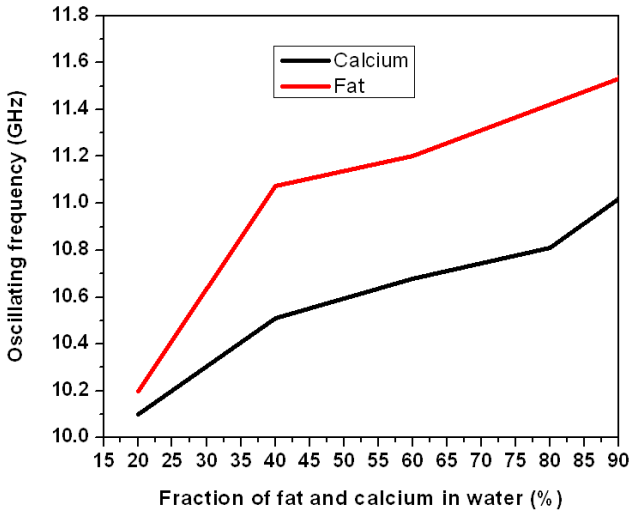

Figure 4.17 Variation of the resonant frequency of the oscillator with varying fraction of fat and calcium in water. The resonant frequency scales up with increasing concentration.

4.3.4 Dielectric imaging of biomaterials

There is an increasing need for spatially localized characterization of biomaterials for effective analysis of test samples, for example, analysis of different protein molecules on same test plate. Thus spatial imaging of permittivity for an area of a biological test sample would provide an accurate understanding of the properties of the test sample. This section of the chapter is dedicated towards establishing a frequency shift biosensor array for accurate spatial dielectric imaging of a given area of a biological test sample. In addition, sensor arrays allow characterization of biomaterials without need of precise positioning of the sensor or of the biological sample, as a complete area will be scanned.

The CMOS sensor oscillator described above has been used in switched array configuration, for dielectric imaging of biomaterials. Fig. 4.18 shows the architecture of switched four element sensor array system: a common current source is used for all the oscillators and is connected to one oscillator at a given point of time with the switches shown in the figure.

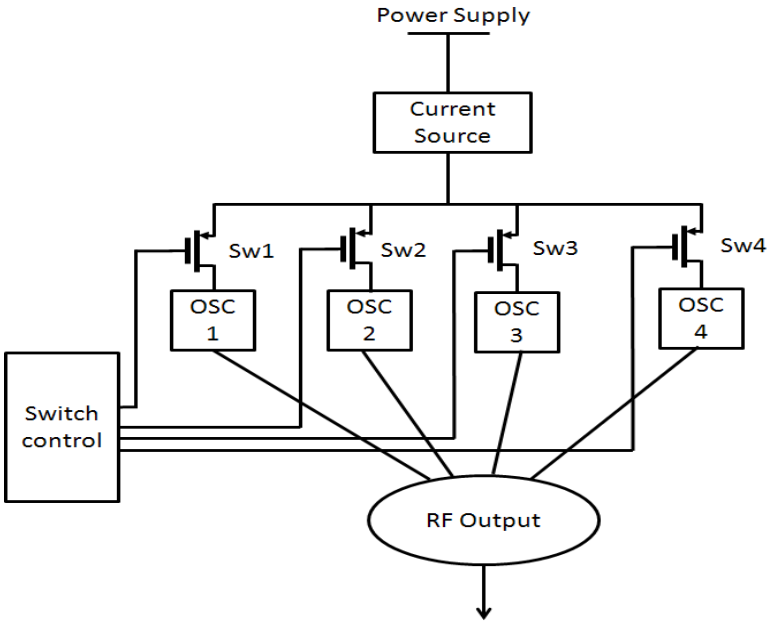

Figure 4.18 Four unit switched sensor array. PMOS transistors are used as switches to a common current source supplying the sensor oscillators. A digital control for the switches is shown.

In this work pMOS switches were used. The switches were turned off with the bias voltage of 2.5 V applied to the gates of the pMOS transistors. Individual sensor units were activated by applying 0 V bias to the gates of the corresponding pMOS transistors. The corresponding chip micrograph is shown in Fig. 4.19.

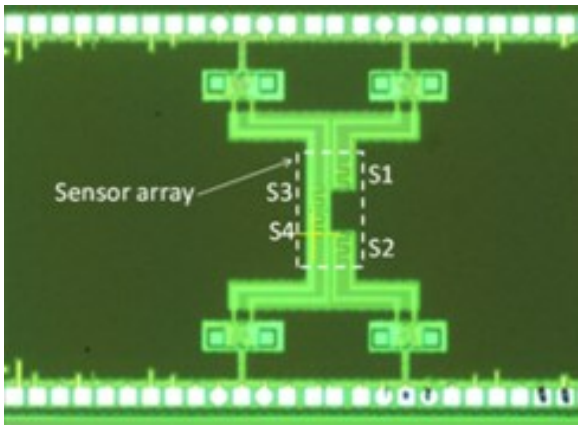

Figure 4.19 Chip micrograph of four unit sensor array.

As a prototype a four unit sensor array was demonstrated. The sensors are marked on the chip as S1, S2, S3 and S4. Sensors 1 and 2 (S1 and S2) operate at the same frequency of 8.28 GHz and sensor 3 and 4 (S3 and S4) operate at 7.8 GHz with power levels of -6 dBm. The chip was fabricated in 0.25 µm BiCMOS process and the IDC was fabricated on the TM1 of the BEOL stack; therefore, the sensitivity is of the same order as 6 GHz sensor, of 22 MHz/permittivity. As an outlook the sensor array is proposed to be used for spatial imaging of immobilized molecules. Therefore, for future surface chemistry need, the sensor is fabricated in TM1. Three different materials (glue, air, saturated glucose solution) have been used to demonstrate the functionality of the imaging approach. In a first step, each of these materials was put on all the sensors simultaneously. After these first experiments, the sensor array was further used to map different materials on top of different cells of the sensor array. Fig. 4.21 shows the dielectric mapping of the biomaterials.

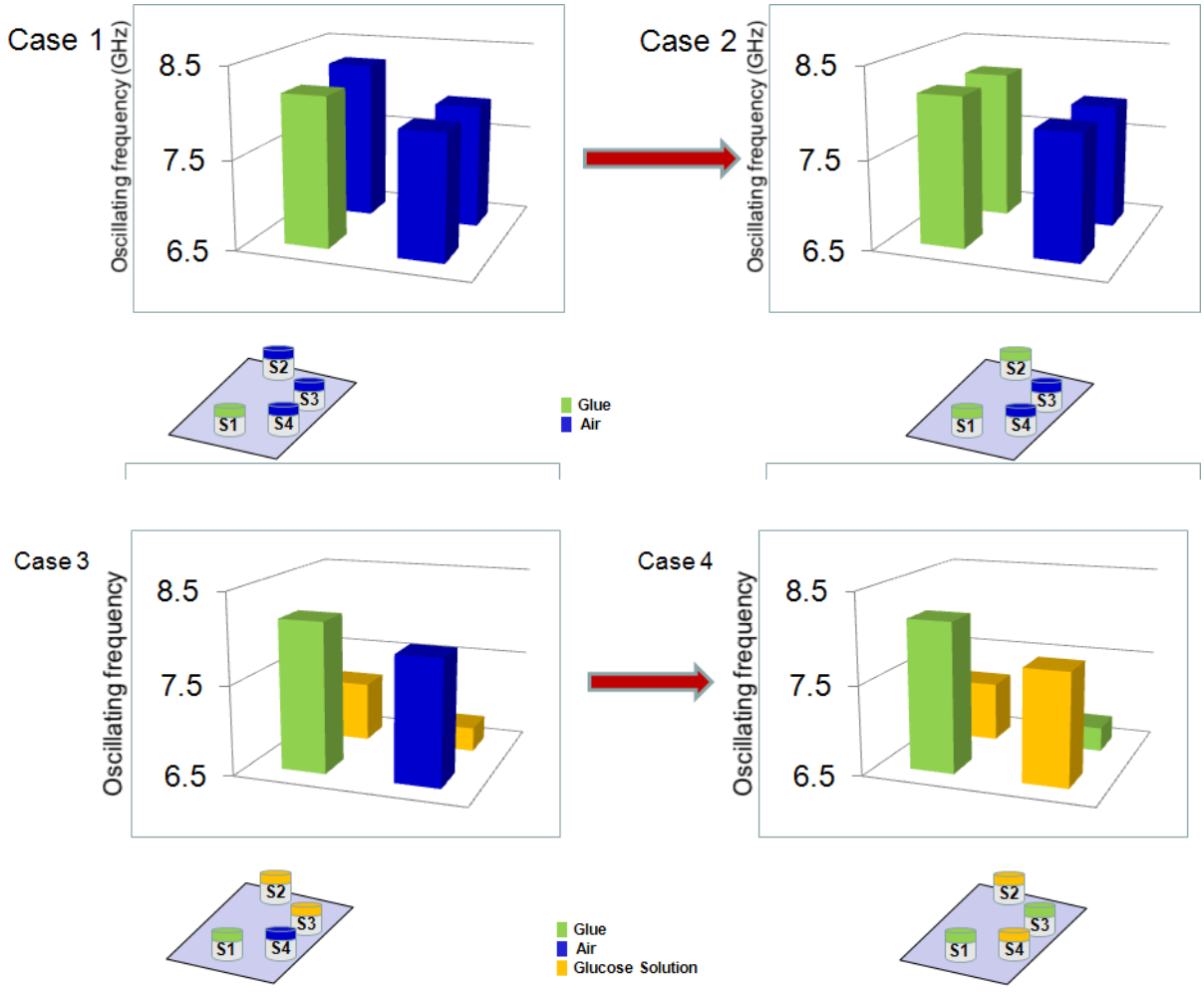

Figure 4.20 Imaging of dielectric distribution as tabulated in table 1; Green: glue, Orange: honey, Blue: air.

Fig. 4.20 shows the mapping scheme. The materials on one sensor have negligible influence on the sensitivity of the neighboring sensors. The four cases shown in Fig. 4.21 have been summarized in table 4.1.

Table 4.1: Four sensor imaging scheme

Case	Senosr1	Sensor 2	Sensor 3	Sensor 4
1	Glue 8.137 GHz	Air 8.28 GHz	Air 7.79 GHz	Air 7.8 GHz
2	Glue 8.137 GHz	Glue 8.137 GHz	Air 7.79 GHz	Air 7.794 GHz
3	Glue 8.132 GHz	Glucose 8.03 GHz	Air 7.78 GHz	Glucose 7.6 GHz
4	Glue 8.13 GHz	Glucose 8.03GHz	Glue 7.74 GHz	Glucose 7.6 GHz

Careful spotting of the sensors using needles with diameter of the order of 50 μm was used to spot the sensors with respective materials. The inductors as seen from the chip photograph have been placed far away from the sensors in the layout. Therefore, the spotting of the sensors does not influence the inductors. In terms of lateral resolution, the first results show that the resolution is of the order of the sensor dimension (in order of 50 μm). The sensor array can be further extended to multi-element array; however, the output architecture should be completely decoupled and a corresponding frequency counter for the oscillator sensors will be an ideal architecture.

4.4 Conclusion

In this chapter high-frequency CMOS compatible sensors are demonstrated for various biomedical applications. The utilization of such a sensor in the detection of concentration of glucose in a homogeneous glucose solution is demonstrated at two frequency range namely 12 GHz and 6 GHz. The sensitivity of the sensor is shown to be dependent on the proximity of the sensor to the analyte sample to be probed. Post processing (chemical mechanical polishing) step to bring the sensor close to the fluid samples has been demonstrated. Such post-processed sensor chips have been shown to operate in conjunction with polymer based microfluidic systems, therefore, demonstrating hybrid CMOS/Polymer based sensing platform. The sensor systems were shown to have sufficient sensitivity and resolution even without the post-processing or polishing step. When the sensor is placed at a sufficient distance from the fluid sample, (IDC fabricated on TM1 for 6 GHz sensor) the sensor could distinguish 10% increase in glucose

concentration in the solution. Therefore, the sensing platform can be used with or without post processing steps.

Cytometric applications especially characterization of cells and molecules in a suspension is of prime focus of today's biosensors. In this chapter the 12 GHz sensor system has been used to detect the concentration of polystyrene microbeads in a suspension. The advantages of using high-frequency sensor approach for detection of concentration of particles in a biological suspension have been shown in this chapter. Therefore, CMOS compatible high-frequency sensors can be used for cytometric applications, for e.g. distinguishing living cells from dead cells in suspensions, detection of concentration of white or red blood corpuscles in serum etc.

There is an endeavor to establish microwave sensor modalities for minimally invasive detection of plaques in arteries in order to offer a cheap and robust alternative to the established optical approaches. A section of this chapter deals with the establishment of the proof of concept of microwave sensors that can be developed in the future to detect plaque in arteries. In this chapter calcium and fat in their liquid phase have been detected in blood. Various concentrations of calcium and fat in blood have been precisely sensed. The measurement was verified by extracting the permittivity of the mixtures from the measurements and fitting it to the analytically obtained values. The fit of the measurement with the analytical results demonstrates the feasibility of establishment of microwave sensors for intravascular imaging modalities. In the final application of the high-frequency biosensors, an array of such sensors applied to dielectric imaging of biomaterial is demonstrated. With the sensor prototype described in this work, precise discrimination of biomaterials based on their permittivity values is demonstrated.

All in all the main focus of the chapter was to demonstrate the capabilities of CMOS compatible high-frequency sensors for various biological and medical diagnostic applications. Such sensors are fast, require no labeling and are easy to handle because of simple front-end circuit platform; therefore, they are termed as the next generation biosensors ahead of the established optical sensor platforms.

TOWARDS PARTICLE COUNTING

In this chapter* we propose a sensor architecture and a corresponding read-out technique for detection of dynamic capacitance change that can be applied to rapid particle counting and single particle sensing in a fluidic system. The sensing principle is similar to the previous chapters and is based on capacitance variation of an interdigitated capacitors (IDC) structure embedded in an oscillator circuit. The capacitance scaling of the IDC results in frequency modulation of the oscillator. A demodulator architecture is employed to read-out the frequency modulation caused by the capacitance change. A self-calibrating technique is employed at the read-out amplifier stage. The capacitance variation of the IDC due to particle flow causing frequency modulation and the corresponding demodulator read-out has been analytically modelled. Experimental verification of the established model and the functionality of the sensor chip were shown using a modulating capacitor independent of fluidic integration. Initial results show that the sensor is capable of detecting frequency changes of the order of 70 parts per million (PPM) which translates to a shift of 1 MHz at 14.3 GHz operating frequency. It is also shown that a capacitance change every 3 µs can be accurately detected.

5.1 Introduction

Detection and analysis of single cell and particle in aqueous solution is of high relevance in biosensing applications. Single cell based biosensors have come into prominence primarily due to emerging field of POCT in the area of disease monitoring and control and medical diagnostics. The capability of the inclusion of transducers, sensors, detection circuits and microfluidic platform provides unprecedented advantages to POC devices and has been shown in chapter 3 and chapter 4. An alternative CMOS "all-electrical" approach for standard ELISA based immunosensors has been shown in chapter 3. On the same lines, CMOS/BiCMOS based biosensors applied to single particle (cell) analysis can be an attractive alternative to detection methods based on fluorescence, acoustic, surface plasmon resonance based, amperoemetric, etc. From the circuit design aspect, designing of CMOS/BiCMOS compatible single particle sensors requires highly sensitive sensing circuit and at the same time flexible read-out approach. Hybrid integrated circuits for easy read-out have been demonstrated by research groups [151].

- Parts of this chapter have been published as "Self-calibrating highly sensitive dynamic capacitance sensor towards rapid sensing and counting of particles in laminar flow systems", *Analyst*, 2015, **140**, 3262-3272 DOI: 10.1039/C5AN00187K

In this chapter, a compact BiCMOS high sensitive capacitive sensor approach is proposed, where the sensing principle exploits microwave frequencies and at the same time provides a pseudo DC output. The sensor system shows very high sensitivity of the order of 70 parts per million (PPM) and is in the range of detection single particles in a suspension as well as depicts excellent flexibility in handling due to DC output. An analytical model is established to depict the operation of the capacitive sensor in conjunction with a flow assisted fluidic system. The functioning of the sensor system is further demonstrated using a modulating capacitor emulating the flow of particles in a fluid system. Therefore, the proposed system is suitable for particle counting and single particle sensing applications, as the capacitance modulation due to particle flow in a fluid system is analogous to modulating capacitor used in this work. The sensing principle is based on the previously demonstrated (chapter 3, chapter 4) capacitive sensor embedded in an oscillator circuit. The operating frequency of the sensor is in the range of 12 GHz to 14.5 GHz, thus exploiting the advantages of high-frequency sensing approach. The frequency modulation of the oscillator due to the capacitance change is read out using a demodulator circuit. Therefore, the output of the sensor is a pseudo DC (few KHz) signal, thus making handling of the sensor extremely flexible. All in all, the proposed sensor system adds the advantages of high-frequency detection technique, miniaturization and simultaneously keeps the output handling capability simple. Moreover, the topology opens the possibility of integrating functionalities such as in-situ signal processing, making these chips even more lucrative. The measurement time of the sensor is dependent on the settling time of on-chip circuit blocks and can be reduced to the order of few micro seconds. Therefore, the measurement time can be reduced considerably compared to other aforementioned techniques.

The theory has been further extended to address the problem of noise in such integrated microfluidic systems. Noise from the sensor circuit and also from the external biological environment plays a crucial role in such devices. Noise can be eliminated by using a correlation technique using two such demodulator architectures with the same integrated system. The recent integration possibilities of such sensor chips with MEMS-based microfluidic systems add more relevance to such sensors being used in biosensing [98, 152]. Therefore, high-frequency microelectronics-based fluidic sensor circuits with DC output handling can be suggested as a promising tool for the miniaturization of conventional biological cell detection techniques.

5.2 System dynamics analysis

The capacitive sensors demonstrated so far in this thesis work were suited for detecting dielectric variation in the IDC environment, however, in a static condition. When embedded in an oscillator circuit, the capacitance changes of the IDC resulted in the resonance frequency shift of the oscillator and was used to determine the concentration of biomarkers like creatinine, concentration of glucose or concentration of suspended particles in an aqueous solution and more. As mentioned above the sensors were operated in a static condition, even with the aid of

microfluidic systems, average concentration of particles in the suspension was detected. In this work, we propose an advanced circuitry and an analytical theory to extend the capacitive sensing technique based on frequency shift sensor towards a flow assisted fluidic system.

Applications of flow assisted systems range from analysis of single particles (for e.g., cells) to counting of particles in a solution. The extension to a dynamic approach is brought by the inclusion of a demodulator circuitry to detect the frequency modulation that would be caused by the dynamic capacitance shift due to flow of particles in the fluid system. The sensor is designed to operate in the frequency range of 12 GHz to 14.3 GHz, with the demodulator output in the range of few kHz.
The system is modelled in two steps: in the first step the dynamic capacitance change of the IDE due to particle flow in an aqueous solution is modelled and simulated. In the subsequent step the demodulator circuitry for detection of the dynamic particle flow is mathematically modelled and simulated.

5.2.1 Modelling of dynamic capacitance sensor

The modelling of the capacitive sensor in a fluid flow environment where the flow of particles causes capacitance modulation of the IDC is done using a long fluid channel approximation. In the long channel approximation, the sensor is assumed to be considerably far from the inlets and the outlets of the fluid system. Such a sensor configuration is fabricated for particle concentration analysis in chapter 4. Fig. 5.1 shows a test structure of the same.

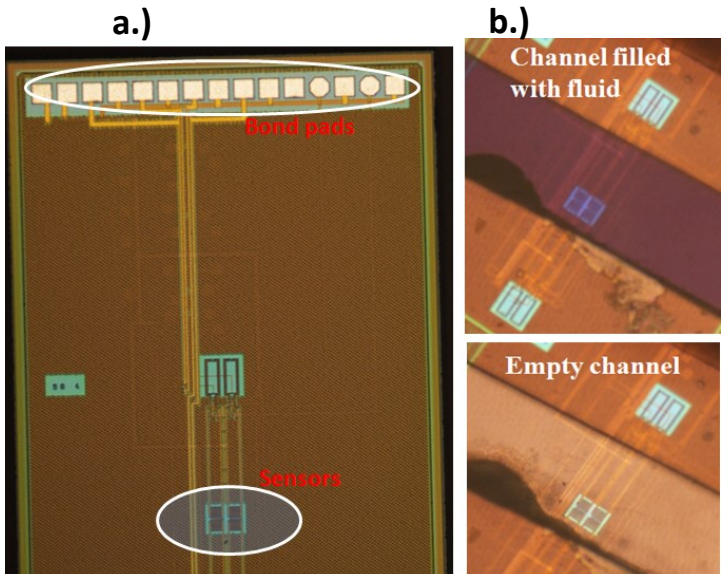

Figure 5.1 Fabricated sensor chip with long channel microfluidic system integration. a) High-frequency sensor chip showing the sensor arrangement. b) A long channel microfluidic channel is aligned on top of the sensor. The two conditions depict the channel with and without the fluid.

In such a condition, the suspended particles in a laminar flow of the aqueous solution are in a steady state when they reach the sensor. The velocity of the particles can be approximated to the mean velocity of the fluid on top of the sensor. This is significant in order to determine the flow rate of the particles.

The inflow and outflow of particles on top of the sensor creates a capacitance modulation. Fig. 5.2 (a) shows the model for the flux of the particles on top of the IDC sensor, in the fluid system. The permittivity contrast between the aqueous medium and the particles determine the height of the capacitance modulation. The 2D geometry of the IDC sensor structure along with the simulated variation of its capacitance due to a particle flowing on top of it is shown in Fig. 5.2 (b). IDC sensor employed in this work to design the sensor oscillator has finger width equal to finger spacing of 5 µm. A particle of diameter 8 µm (diameter of a standard *yeast* cell) and permittivity 20 is considered, flowing in an aqueous solution (solution of water) of permittivity 60. In the previous chapter the permittivity of water with respect to frequency was shown. At the frequency range of operation of the sensor system (12 GHz-14.5 GHz), the aqueous solution of water should be around 40. Therefore, the assumed permittivity values are pragmatic, as the aqueous solution which is generally a solution of water.

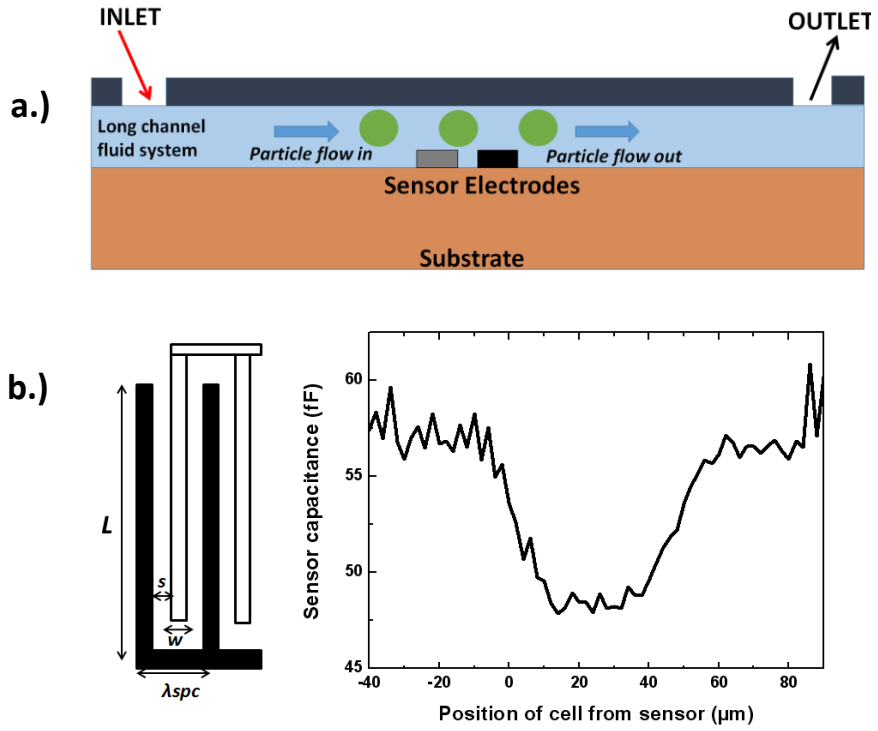

Figure 5.2 a) Schematic depiction of particle flow in a long channel fluid system aligned on top of the sensor. b) Geometry of IDE sensor considered in this work. Simulated variation of sensor capacitance due to flow of particles. The capacitance of variation is plotted with respect to position of particle on top of the sensor.

As the particle migrates on top of the sensor, the capacitance reduces as shown in Fig. 5.2 (b). This can be attributed to the lower permittivity of the particles compared to the suspending aqueous solution. The IDC regains its capacitance value once the particle moves away from the sensor. This is defined as the capacitance modulation. A steady flow of such particles will, therefore, cause capacitive pulses. The simulation was carried out on COMSOL multi-physics software. The irregularities in the simulated curve come from the meshing of the structure with the moving particle.

Embedded in the oscillator these capacitive pulses will translate to resonance frequency modulation of the oscillator circuit. The fluid velocity in the channel and the concentration of particles in the fluid determine the modulation rate. From the sensing aspect, detection of this frequency modulation will enable particle counting. This dynamic behaviour of the capacitive sensor based on the particle flow can be sensed using an integrated phased-locked loop (PLL) demodulator in conjunction with the sensor embedding oscillator circuit.
A typical PLL circuit stabilizes the resonance frequency of a voltage-controlled oscillator (VCO) using a reference, typically a crystal oscillator [110]. In the designed sensor system, a permittivity-controlled oscillator replaces the VCO in the PLL, where the variable capacitor (IDC sensor) in the oscillator is a function of permittivity instead of voltage, as explained in previous chapters. When the resonant frequency of the oscillator is modulated by a moving particle, or by particles of different type the PLL output frequency is stabilized by a control voltage, which serves as the demodulator output. The significant aspect of the PLL used in the sensor system is the constant gain; this enables a self-calibrating feature of the sensor architecture enabling detection of extremely minute capacitance change. A detailed analysis of the self-calibrating feature of the sensor system is done in the subsequent sections.

5.2.2 Design of sensor circuit

The oscillator sensor circuit has the same topology as was described in the previous chapters; a cross-coupled CMOS oscillator using the IDC sensor as the variable capacitor. However, for the design of the complete sensor system additional variable capacitors are used as shown in Fig. 5.3. The CMOS cross-coupled oscillator is further embedded in a PLL to demonstrate the proposed technique of frequency modulation-demodulation. The sensor IDC is employed along with three variable capacitors (varactors) in order to modify the oscillation frequency. The varactors consist of two pMOSFETs, the sources and drains of which are connected to the control voltage.

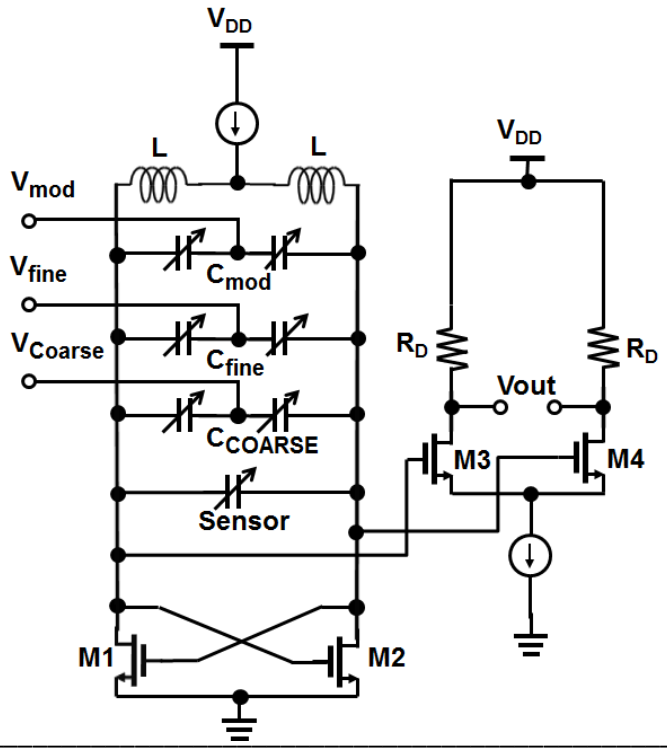

Figure 5.3 Schematic of the sensor circuit. The sensor is embedded in the oscillator circuit. The variable capacitor C_{mod} is used for experiments without fluid integration.

A large coarse-tuning capacitor C_{coarse} is responsible for compensating Process-Voltage-Temperature (PVT) variations. The MOSFETs used for the C_{coarse} is 8 fingers, with W/L ratio of 12 for each gate finger. The value of the on chip C_{coarse} is 137 fF. PVT variations are brought about by uncontrolled variations in the CMOS processing altering the properties of the active devices (transistors), minor variations in the supply voltage altering the operating point of the circuits or variation of on chip temperature varying the circuit conditions. Hu *et a*l [153] deals with the influence of PVT variations on circuit performance and corresponding compensation techniques. A small fine-tuning capacitor C_{fine} is used to detect small frequency changes. For the C_{fine}, single finger MOSFETs has been used with the same W/L ratio of 12. The value of the C_{fine} is 3.2 fF. Moreover, an additional small varactor, C_{mod} is used to emulate the dynamic capacitance change for the initial measurements independent of an integrated microfluidic channel. The C_{mod} has the same dimension and value of the C_{fine}. The buffer stage is used to isolate the oscillator from the subsequent circuit chain following the oscillator. The following table shows the values of the individual components used in the sensor circuit design.

Table 5.1 Component parameters for sensor circuit

Name of the component	Value
Inductor (L)	320 pH
Fine Capacitor (Cfine)	3.2 fF
Coarse Capacitor (C_{COARSE})	137 fF
Modulating capacitor (Cmod)	3.2 fF
Sensor Capacitor (IDC): simulated	50 fF

The rationale behind this topology of the sensor oscillator is to use a relatively slow coarse tuning loop with a high gain together with a fast fine tuning loop with a relatively small gain. This makes the detection of fast dynamic changes in the sensor capacitor easy. This will be explained in the subsequent section.

5.2.3 Frequency demodulator architecture

Figure 5.4 shows the frequency demodulator architecture with the sensor circuit embedded in the demodulator architecture.

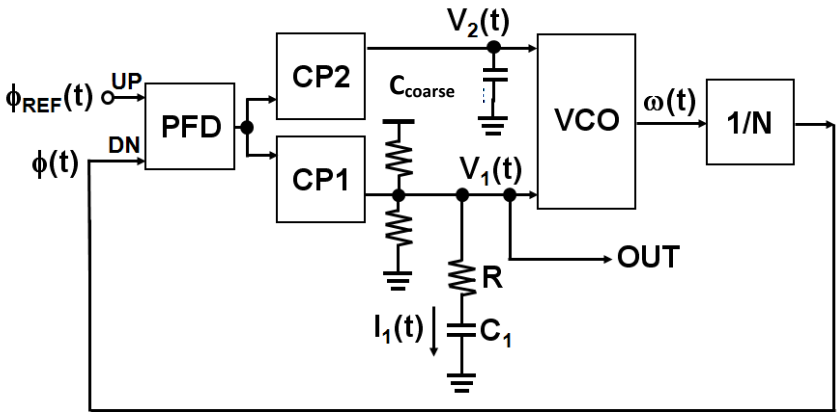

Figure 5.4 Demodulator architecture block diagram. The output of the demodulator is taken from the fine-tuning loop containing C_1 and R. The VCO shown in the block represents the oscillator with sensor.

The readers should refer to works of Hu *et al* and Herzel *et al* [153, 154], for detailed understanding of the circuit blocks used in the frequency demodulator architecture. However, in this section of the chapter a brief description of the circuit blocks will be presented. The main focus is on the derivation of the analytical equations governing the frequency demodulation architecture.

A second-order charge pump (CP) PLL is considered as was shown in the work of Herzel *et al* [155]. The oscillator circuit is controlled by two sets of tuning voltages: V_1 supplying the C_{fine} varactor of the oscillator circuit also referred to as fine-tuning voltage; V_2 supplying the C_{coarse} varactor and is referred to as the coarse tuning voltage. The voltages are controlled by the two CPs shown as CP1 and CP2 in Fig. 5.4. The CPs are current sources with switch supplying the control voltage to the oscillator, based on the input from the phase frequency detector (PFD). The UP input of the PFD is driven by a reference signal with phase φ (t) in the range of MHz. The oscillator output frequency is divided by the appropriate dividing ration (N), shown by the 1/N block. This is done to equate the frequency output of the oscillator to the reference input at the normal condition (when no frequency tuning of the oscillator occurs). The divider output is connected with the DN input of the PFD. The PFD compares the frequencies of the divided oscillator output and the reference signal. When the oscillator output is tuned due to the variation of permittivity of the IDC sensor, the PFD will generate the required signal for the CPs to generate the appropriate voltage for the restoration of the original resonance frequency of the oscillator.

The fundamental idea of designing the PLL are:

- Large gain of the detector
- Constant gain of the detector

The detector gain is inverse of the oscillator gain. The above requirements translate to the fact that that the oscillator gain should be small and constant. This requires the capacitor C_{coarse} to be sufficiently large such that the coarse tuning loop has a weak influence on the loop dynamics. Since the detector gain is basically the inverse VCO gain [105], the FM detector is highly linear. The settling time of the overall loop should be fast enough in order to detect the dynamic capacitive changes. The bias voltage on V_1 (t) which stabilizes the oscillator frequency by tuning the C_{fine} varactor, will be taken as the output of the demodulator. This output is fed to an operational amplifier for the amplification of the output signal.

We can now proceed with the mathematical analysis of the frequency demodulator architecture.

We consider a PLL with an FM input signal

$$\omega_{REF}(t) = \omega_0 + m\omega_0 \sin(\omega_m t) \tag{5.1}$$

where ω_m is the modulation angular frequency, ω_0 is the mean reference angular frequency, and m is the modulation index. We define the phase error at the phase frequency detector (PFD) input by,

$$\varphi_e(t) = \varphi_{REF}(t) - \varphi(t) \tag{5.2}$$

Its first derivative is given by

$$\frac{d\varphi_e(t)}{dt} = \omega_{REF}(t) - \frac{d\varphi(t)}{dt} \tag{5.3}$$

Substituting eq. 5.1 in eq. 5.3 we obtain the second derivative given by

$$\frac{d^2\varphi_e(t)}{dt^2} = m\omega_0\omega_m \cos(\omega_m t) - \frac{d^2\varphi(t)}{dt^2} \tag{5.4}$$

This equation will be useful to eliminate *φ (t)* from the differential equation describing the dynamics of the demodulator architecture.

In the following, we consider a linear, time-invariant continuous-time model (CTM) to keep the analysis of the FM-induced phase error simple. Describing the governing equations of the other blocks in the demodulator architecture is necessary in order to derive the output voltage of the demodulator. Considering C_{coarse} tending to infinity, the PLL corresponds to a single-loop operation as far as the small signal behavior is considered. In that condition, the gain of the PFD is defined as,

$$K_{PFD1} = \frac{I_{CP1}}{2\pi} \tag{5.5}$$

where Icp_1 is the charge pump (CP) current in the fine tuning loop containing C_1 in the ON state. The average CP current is obtained as

$$I_1(t) = \varphi_e(t) K_{PFD1} \tag{5.6}$$

The resulting voltage across the R-C_1 filter in the fine-tuning loop is given as,

$$V_1(t) = RI_1(t) + \frac{1}{C_1}\int_0^t I_1(\tau)d\tau + const. \tag{5.7}$$

Here, we used the first-order loop filter composed of C_1 and R in order to simplify the analysis. A more detailed analysis would include the biasing resistors and bypass capacitors. The loop filter has been described following the overall analysis of the demodulator. However, the simplification does not imply loss of generality in the derived equation. The derivative of (5.7) is obtained as,

$$\frac{dV_1(t)}{dt} = R\frac{dI_1(t)}{dt} + \frac{I_1(t)}{C_1} \tag{5.8}$$

The equation governing the oscillator output is given as,

$$\frac{d\omega(t)}{dt} = 2\pi K_1 \frac{dV_1(t)}{dt} \tag{5.9}$$

Where K_1 is the oscillator gain. Substituting (5.8) into (5.9) we obtain,

$$\frac{d\omega(t)}{dt} = 2\pi K_1 R \frac{dI_1(t)}{dt} + 2\pi K_1 \frac{I_1(t)}{C_1} \tag{5.10}$$

The PFD input phase obeys

$$\frac{d^2\varphi(t)}{dt^2} = \frac{1}{N}\frac{d\omega(t)}{dt} \tag{5.11}$$

Substituting (5.10) into (5.11) we obtain

$$\frac{d^2\varphi(t)}{dt^2} = \frac{2\pi K_1 R}{N}\frac{dI_1(t)}{dt} + \frac{2\pi K_1 I_1(t)}{NC_1} \tag{5.12}$$

Replacing the average value of I_1 (t) obtained in (5.6) into (5.12) we obtain

$$\frac{d^2\varphi(t)}{dt^2} = \frac{2\pi K_{PFD1} K_1 R}{N}\frac{d\varphi_e(t)}{dt} + \frac{2\pi K_{PFD1} k_1 \varphi_e(t)}{NC_1} \tag{5.13}$$

φ (t) can be eliminated from the above equation by utilising (5.4) resulting in

$$\frac{d^2\varphi_e(t)}{dt^2} + \frac{2\pi K_{PFD1} K_1 R}{N}\frac{d\varphi_e(t)}{dt} + \frac{2\pi K_{PFD1} k_1 \varphi_e(t)}{NC_1} = m\omega_0\omega_m \cos(\omega_m t) \tag{5.14}$$

Now we incorporate the coarse tuning loop consisting C_{coarse} in the analysis. According to the block diagram of the demodulator architecture shown there is no additional resistor as was present in the fine-tuning loop. Therefore, the obtained voltage equation at the coarse tuning node corresponding to equation (5.8) is

$$\frac{dV_2(t)}{dt} = \frac{I_2(t)}{C_{coarse}} \tag{5.15}$$

It can be seen from the demodulator architecture, the two charge pumps are driven by the same PFD such that the waveforms V_1 (t) and V_2 (t) are the same, except for the constant factor given by the ratio of the charge pump currents in the ON state. Therefore, the voltage equation at the coarse tuning loop is given as

$$\frac{dV_2(t)}{dt} = \frac{I_1(t)}{C_1}\frac{I_{CP2}C_1}{I_{CP1}Ccoarse} \tag{5.16}$$

The oscillator frequency is the sum of the control voltages weighted by the gains of the oscillator for individual loops,

$$\frac{d\omega(t)}{dt} = 2\pi K_1 \frac{dV_1(t)}{dt} + 2\pi K_2 \frac{dV_2(t)}{dt} \tag{5.17}$$

Including the above constraints of two loops, we obtain a similar equation as (13), and is given as,

$$\frac{d^2\varphi_e^d(t)}{dt^2} + 2\gamma\frac{d\varphi_e^d(t)}{dt} + \omega_n^2\varphi_e^d(t) = F\cos(\omega_m t) \tag{5.18}$$

where we introduced the following abbreviations

$$\gamma = \frac{I_{CP1}K_1R}{2N} \tag{5.19}$$

$$\omega_n^2 = \frac{I_{CP1}K_1}{C_1N}\left(1 + \frac{I_{CP2}K_2C_1}{I_{CP1}K_1C_{coarse}}\right) \tag{5.20}$$

$$F = m\omega_0\omega_m \tag{5.21}$$

Equation 5.18 is a well-known differential equation describing a damped harmonic oscillator driven by external force. In our case, the driving force is the variation of the capacitance due to flow of particles on top of the sensor. The solution of such a differential equation has been well discussed and can be used further to obtain the demodulator output voltage, which serves as the output of our sensor system.

The solution of the differential equation yields,

$$V_1(t) = V_{dem}\cos(\omega_m t + \varphi_1) \tag{5.22}$$

Solution for V_{dem} shows that it can be expressed as

$$V_{dem} = \frac{m\omega_0}{2\pi(\frac{K_1}{N})} \tag{5.23}$$

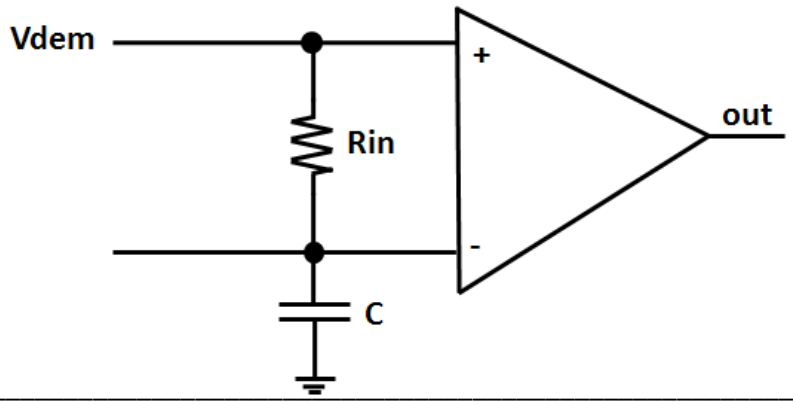

Figure 5.5 Differential operational amplifier with RC biasing for self-calibration.

The V_{dem} output is fed to the operational amplifier as shown in Fig. 5.5. A resistance R_{in} of value 5 MΩ was used and the corresponding RC biasing of the referenced input results in the same DC values of both the inputs to the amplifier. The V_{dem} output serves as one of the inputs to the amplifier, while the other input is the time averaged value of V_{dem} due to a very large value of the biasing capacitance used. This technique eases the amplification of very small signal changes at the demodulator output regardless of PVT variations. The transistors were sized as 20 µm for the amplifier stage. The device mismatch between the two transistors of the amplifier does not influence the operation of the amplifier. It requires no further external calibration often needed

for differential amplifiers, therefore, depicting the self-calibrating feature of the sensor architecture.

It is important to understand the filter that is used in conjunction with the charge pump. Fig. 5.6 shows the architecture of the loop filter. The coarse capacitor C_{coarse} is large enough and as mentioned above has no influence on the loop dynamics. Therefore, the coarse loop can be ideally considered not active, and the loop filter then is a third order loop filter. The transfer function of the loop filter is given as,

$$G(s) = \frac{1}{sC_3}\frac{1/Z_2}{1/Z_2+1/Z_1} \tag{5.24}$$

where,

$$Z_1 = (R + \frac{1}{sC_1}) \parallel \frac{1}{sC_2} \parallel R_{bias1} \parallel R_{bias2} \tag{5.25}$$

$$Z_2 = R_3 + \frac{1}{sC_3} \tag{5.26}$$

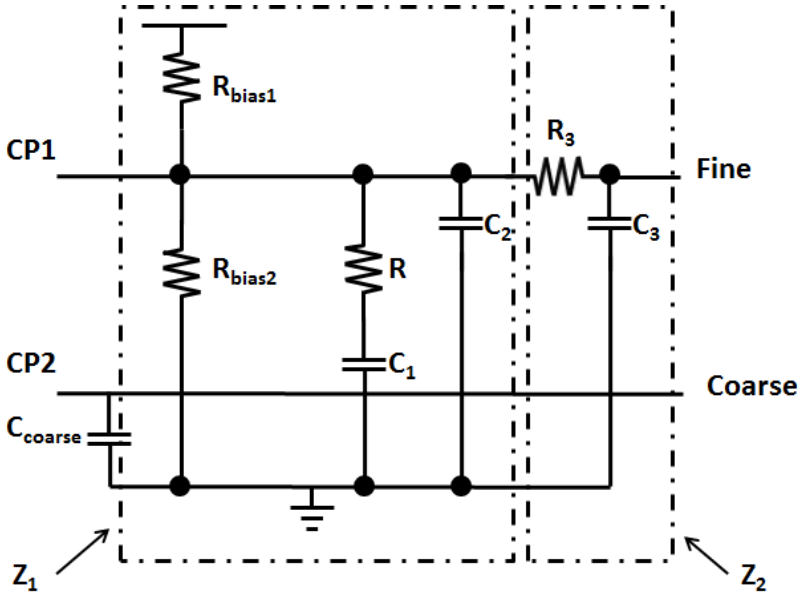

Figure 5.6 Loop filter showing the coarse and fine tuning loop.

The voltage divider incorporated with with the resistors R_{bias1} and R_{bias2} are significant in terms of the dual loop operation of the PLL. This arrangement keeps the fine tuning voltage at a value where the gain is constant. A large capacitor used in the coarse tuning loop (C_{coarse}) acts as the filter for the coarse tuning loop. For the approximation of the large coarse capacitor to be valid, the value of Ccoarse should be

$$C_{coarse} \gg \frac{I_{CP2}K_{PFD2}}{I_{CP1}K_{PFD1}}C_1 \tag{5.27}$$

The primary filter parameters R and C1 are chosen for this operation as, R = 1KΩ and C_1 is chosen to be 1 nF and is implemented on board. The loop bandwidth can be obtained by dividing eq. 5.19 by 2π.

$$f_{BW} = \frac{I_{CP1}K_1R}{2\pi N} \tag{5.28}$$

The charge pump current in the fine tuning loop is set as 4 mA. The divider ratio is 64. The gain of the oscillator K_1, 100MHz/V, is kept low due to high detector gain, as was mentioned previously. Therefore, R is the tuning parameter for the loop bandwidth. The loop bandwidth was designed for 300 KHz. This has been done for the dynamic detection of capacitive change every 3 μs.

The charge pump architecture for the fine tuning loop is shown in Fig. 5.7. The pMOS transistor delivers the UP current and nMOS transistor delivers the DOWN current. This architecture is used in order to have a low noise charge pump. For a particular charge pump current moderately sized transistors are used with high gate-source voltage [154]. For the course tuning loop a traditional low-current charge pump is used with a large capacitor to block the noise.

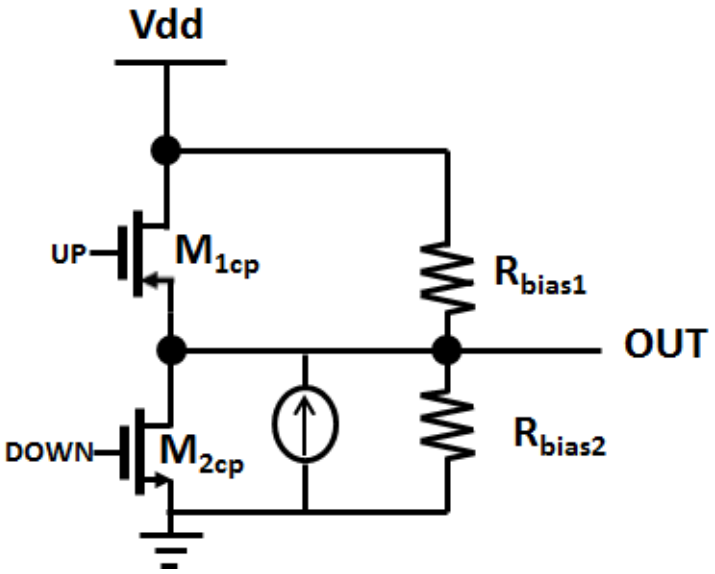

Figure 5.7 Charge pump architecture for fine tuning loop.

The voltage divider network comprising of the resistors R_{bias1} and R_{bias2} at the output of the charge pump stabilizes the DC output voltage at a desired value of Vdd x ($R_{bias2}/R_{bias1} + R_{bias2}$). At the same time the fine tuning loop gain of the oscillator is kept constant against PVT variations. The value of R_{bias1} and R_{bias2} is 1 KΩ.

The VCO sensitivity is described as the voltage shift caused by the frequency response due to a single particle on the sensor. This voltage shift should be higher than the standard deviation of the voltage caused by the noise. The second order PLL results in a flat voltage spectrum with decay depending on $1/f^2$ at high frequency. This voltage spectrum is low-pass filtered by a relatively slow operational amplifier shown in Fig. 5.5, implying the loop bandwidth should be small for a good resolution. As mentioned above, the loop bandwidth is designed for 300 KHz. The oscillator sensitivity in detection of capacitive pulses is discussed in the results section.

5.3 Results and discussion

The sensor system is fabricated in standard 0.13 µm SiGe:C BiCMOS process as explained in the previous chapter. The BEOL stack with the metallization was discussed in the previous chapters. The fabricated chip is shown in Fig. 5.8. The total area of the chip is 2.4 mm^2.

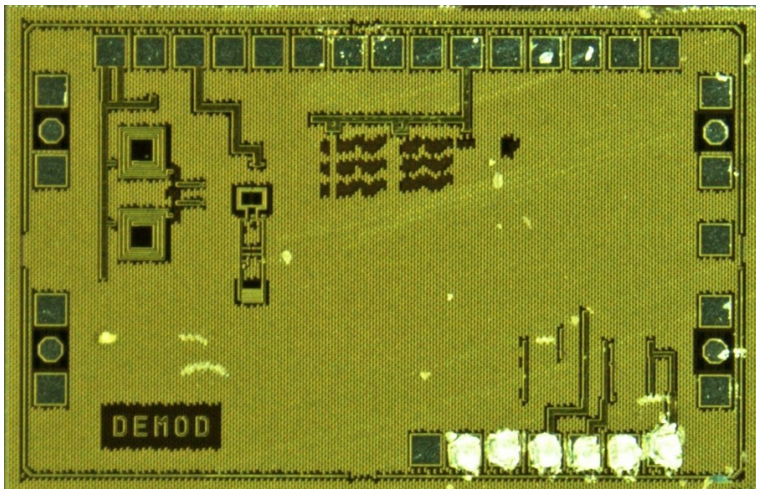

Figure 5.8 Chip photograph of the sensor and demodulator architecture.

For the electrical characterization of the chip, the chip was mounted on a FR4 board using dielectric glue. The operating frequency range of the sensor system is 12 GHz to 14.5 GHz. The test chip has an RF output from the sensor oscillator in order to characterize the sensor. Wire bonding technique is used to make the electrical connections from the chip to the FR4 board. The operating frequency range of the sensor makes wire bonding a feasible approach for electrical connections. The total package size of the system is 5 cm x 2 cm. As mentioned above, the sensing principle being based on high-frequency dielectric detection requires no additional reference electrodes for measurements. Therefore, no additional bulky test-benches are required for the measurement setup, restricting the overall size of the system to the package size of the chip. This small size of the chip therefore makes the chip lucrative for LOC application.

The fastest frequency modulation rate that the sensor system is capable of determining, defines the fluid pressure or velocity that can be approximately used with such a sensor system. This is in turn determined by the settling time of the PLL. The PLL settling time, the higher is the velocity of the fluid system that can be used. The value of the capacitor C_{coarse} defines the settling time of the PLL. Fig. 5.9 shows the simulated settling time of the PLL as a function of the value of C_{coarse}..

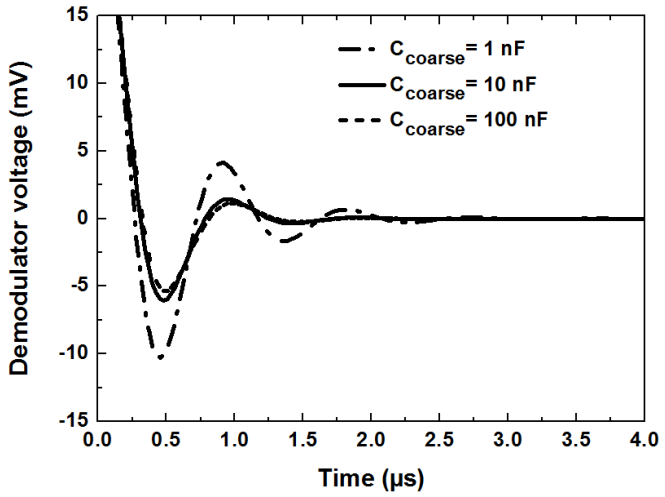

Figure 5.9 Simulated settling time of the PLL as a function of the coarse loop filter capacitance. The settling time obtained is 3 µs. Capacitance change every 3 µs can be accurately detected.

For higher value of C_{coarse} the PLL has a faster settling time and a value of 10 nF gives a settling time of approximately 3 µs. However, physically integrating of 10 nF capacitor is impossible on the chip due to huge area constraint. Therefore, the 10 nF capacitor can be implemented externally on the board where the chip is mounted. This gives the flexibility to adjust the settling time of the PLL and in turn the sensor system in accordance with the intended application. This makes the chip suited for a wide range of applications requiring different fluid velocities in the microfluidic system. In the present analysis, the settling time of the PLL shows the minimum required measurement time of the system could be as low as 3 µs to 5 µs. Therefore, extremely fast measurements can be performed as compared to the established sensor platforms.

Fig. 5.10 shows the simulated demodulator output voltage for a sinusoidal frequency modulation. The modulation period chosen is 100 µs and the modulation index is 0.0001 (100 parts per million). From the sensing aspect, these simulation conditions translate to capacitance change due to particle flow every 100 µs. Therefore, the capacitive modulation pulses discussed in Fig. 5.3 (b), will the period of 100 µs. This kind of period of capacitance change depicts extremely low solute or particle concentration in a solution. The modulation index relates to the change in

resonant frequency of the oscillator to the presence of a particle on top of the embedded IDC sensor. With the closed loop operating frequency of 14.3 GHz, the modulation index of 0.0001 translates to a change of 1.43 MHz. Therefore, the sensor shows high order of sensitivity and detection resolution along with very fast response time.

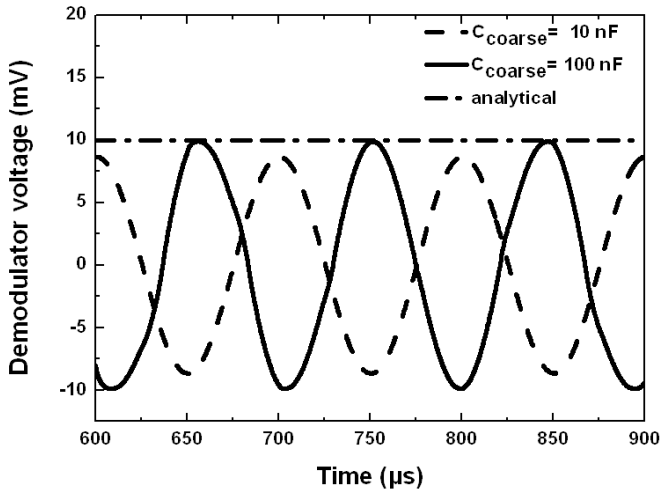

Figure 5.10 Simulated demodulator output for input modulating voltage of period 100 µs. The period of the voltage being much higher than the settling time of PLL, it is accurately followed by the demodulator.

As seen from the simulation results, the demodulator output voltage follows the modulating voltage. This can be attributed to the fact, that the modulation period is much slower compared to the PLL settling time and therefore, any modulation of the frequency due to capacitance change is accurately followed.

The electrical measurement of the chip shows that the overall DC current drawn by the chip from a 3.3 V supply is 80 mA. A measurement of the process variation was conducted to deduce the reproducibility of the chip. Several chips were measured from the same wafer and the output characteristics were not seen to vary more than 0.2%. The resonant oscillator circuit was characterized and measured to determine the operating frequency of the sensor. Fig. 5.10 shows the output spectrum of the closed loop resonant oscillator circuit. The tuning range of the PLL is from 12.6 GHz to 14.3 GHz as was measured by tuning the bias voltage of the on chip C_{coarse} varactor. The output power is -6.7 dBm and the reference spur level is below -62 dBm. From the output spectrum shown in Fig. 5.10, the noise level compared to the signal output is shown; this noise floor is low enough to allow the locking of the PLL. Additionally, high order low pass filter is employed for a smooth detector output at a given detector gain. As mentioned in the previous sections in order to determine the sensitivity of the demodulator independently of

fluidic system, a small sinusoidal signal V_{mod} was applied to the modulating capacitor. The output voltage of the demodulator is taken as mentioned in the block diagram of the demodulator architecture and is fed to an operational amplifier for further amplification. The modulation input of the VCO has a gain of 100 MHz/V at a DC level of 1.25 V. By adding a sinusoidal low-frequency modulation signal of 10 mV peak-to-peak amplitude to a DC voltage of 1.25 V the oscillator frequency changes by 1 MHz in open loop condition.

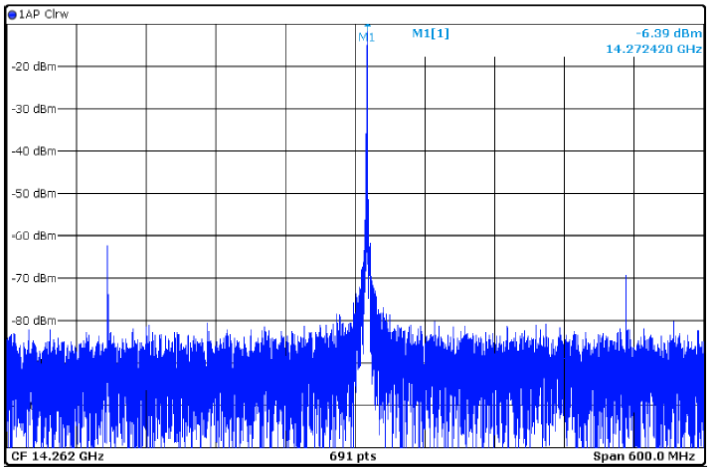

Figure 5.11 The output spectrum of the sensor oscillator. The operating frequency is 14.272 GHz.

This change of 1 MHz translates to a modulation index of 0.00007 or 70 parts per million. In closed-loop operation, the oscillator frequency is kept constant, while the fine-tuning voltage is modulated. The demodulation sensitivity is obtained by changing the modulation frequency and measuring the rms value of the demodulator output voltage.

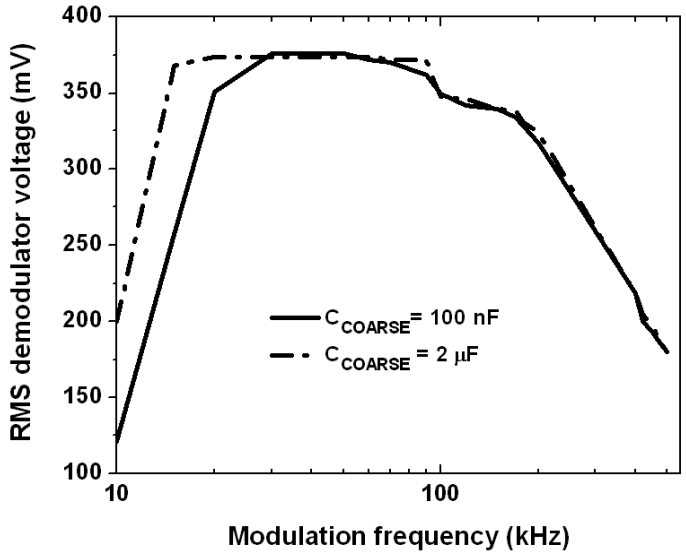

Figure 5.12 Demodulator output voltage as a function of the modulation period. The demodulator voltage follows the input period till 300 KHz (3.3 µs).

Fig. 5.12 shows the demodulator output as the function of the period of modulation. The applied DC voltage is 10 mV peak to peak. The PLL is unable to follow the signal above the loop bandwidth of 300 KHz (time period 3 µs). In such a case the demodulator output voltage is reduced. In terms of the sensing aspect, modulating frequency 300 kHz relates to a measurement speed of 3 µs. Therefore, following the fluidic integration, every 3 µs a capacitance change due to flow of particle on top of the senor can be accurately detected. This measurement time is sufficiently small when compared to the state-of-the-art particle sensing. The proposed architecture can, therefore, sufficiently increase the time efficiency of such microelectronics integrated fluidic systems. However, slower fluid flow can be detected using a larger value for the C_{coarse} capacitor. In order to detect changes of the order of milliseconds a higher coarse tuning filter capacitor C_{coarse} is required. The lower limit for the C_{coarse} value of 100 nF is 50 KHz corresponding to 20 µs. This lower limit can be further increased as seen in Fig. 5.12, where the C_{coarse} value of 2 µF extends the lower limit of measurement to 20 KHz. This accounts for a measurement speed where a change of capacitance up to every 50 µs can be detected. Therefore, based on the application and the fluid velocity required, appropriate C_{coarse} capacitor can be used on the board. This makes the overall sensor system suited for wide range of fluid velocities.

The sensitivity of the sensor obtained from the electrical characterization using the modulating capacitor, is of the order of 70 ppm. For the closed loop operation at 14.3 GHz, this resolution translates to the detection limit of 1 MHz. For the modulating capacitor used in this work, this renders a change of 60 aF for initial capacitance value of 18 fF. From the aspect of frequency shift with respect to permittivity ambient of the IDE, this ultra-low modulation index detection capability shows a change of 0.25 in the absolute permittivity value in the dielectric ambient of the IDC. With the measured sensitivity and resolution, the sensor is highly suited for sensing extremely low particle concentrations.

The capacitive detection technique is also independent of the polarity of the particles in the fluidic system. This is primarily due to the sensing principle being based on the dielectric contrast between the particles and the suspending medium. Therefore, the sensor system can be ideally used for charged and uncharged species. As mentioned previously, the measurement with the modulating capacitor is analogous to the capacitance modulation caused by the particle flow in a fluidic system. Therefore, the above measurements show that the established model is highly suitable for particle detection in fluidic systems. Another important aspect of LOC systems is the feasibility of the same outside laboratory conditions [156, 157], where the difficulty stems out due to external conditions, like temperature variations mechanical stress etc. The working of the established prototype sensor system in such conditions will be dependent on the packaging. However, the external condition will have negligible influence on the sensing concept due to on-chip stabilisation and configuration capabilities of the chip. In the

subsequent sections the capability of correlation technique to eliminate the external noise is also shown. Therefore, the sensor system can be ideally used outside laboratory conditions as well. The sensor enhances the measurement time and also possesses self-calibrating and reconfigurable features, which can be utilized for different applications based on different fluid flow rates. The stability of the sensor circuit is obtained by the voltage divider at the charge pump output. This keeps the oscillator gain and the detector gain constant with respect to PVT variations.

5.4 Dual demodulator architecture

In this section of the chapter dual demodulator architecture is proposed; the dual demodulator has two sensors that can be aligned on the same microfluidic channel. Such an architecture is used to counteract the problem of noise in the fluid based sensor system.

5.4.1 Elimination of noise by time-averaging

The significant effect of noise in the sensing system is the limitation in the accuracy of the particle counting process. A long-term measurement technique with time averaging capabilities can be a potential solution to the problem. In this case we use two demodulators on the same chip as described above. The corresponding chip is shown in Fig. 5.13.

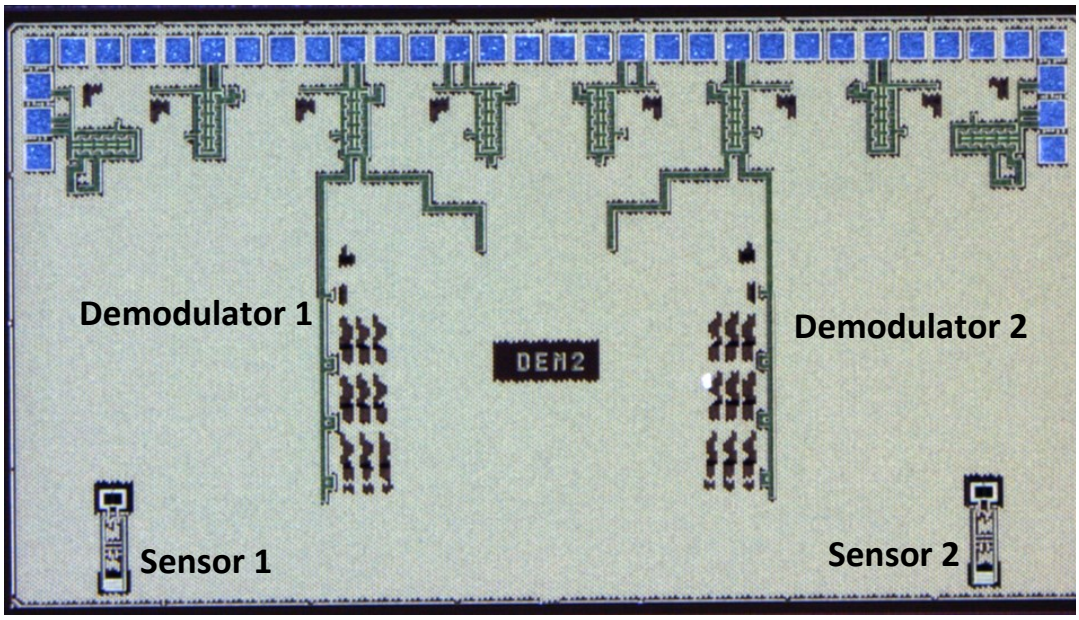

Figure 5.13 Chip photograph showing dual demodulator architecture.

The two demodulator architectures are decoupled with different power supplies supplying the demodulators. Such a system removes any correlated noise that could have otherwise affected the system if same power supply was used. The dual demodulator architecture is now modelled and the capability of eliminating noise from the system is depicted.

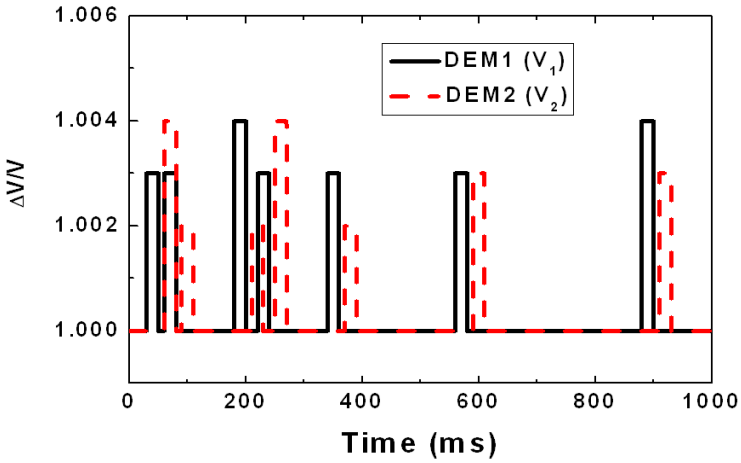

Figure 5.14 Pulse train emulating the signals from 2 VCOs which are delayed by time Δt.

For this modelling purpose, we consider two demodulator detectors with sensors located at different positions of a stream line in a fluidic channel. For simplicity, we assume that the momentary frequencies of the free-running sensor embedded oscillators represent a chain of rectangular pulses with random position. The corresponding demodulator outputs are shown in Fig. 5.14.

The demodulator output has the same waveform as the frequency output from the oscillators, since the PLL settling is fast compared to the frequency modulation. It can be calculated by multiplying the frequency change with the FM detector gain.

The cross-correlation between the two detector output voltages is defined by

$$C(t,\tau) = < V_2(t+\tau)V_1(t) > \tag{5.29}$$

where the brackets denote the stochastic average. In steady state, the stochastic average can be calculated by time averaging over a long period of time T_{max}.

$$C(\tau) = \frac{1}{T_{max}-\tau} \int_0^{T_{max}-\tau} V_2(t+\tau)V_1(t)dt \tag{5.30}$$

If the time is sampled with the step width T_s, we can define

$$t_n = nT_s\,, \quad n = 0,1,2,\ldots\ldots N \tag{5.31}$$

and

$$\tau_m = mT_s, \quad m = 0,1,2,\ldots\ldots M \tag{5.32}$$

The cross-correlation is then given by

$$C_m = \frac{1}{N-m}\sum_{n=m}^{N} V_n^{(2)} V_{n-m}^{(1)} \tag{5.33}$$

For the chain of pulses depicted in Fig. 5.14, the cross-correlation is given shown in Fig. 5.15. The peak maximum of the triangle gives the variance of the voltage, and the peak position gives the delay between the two detectors.

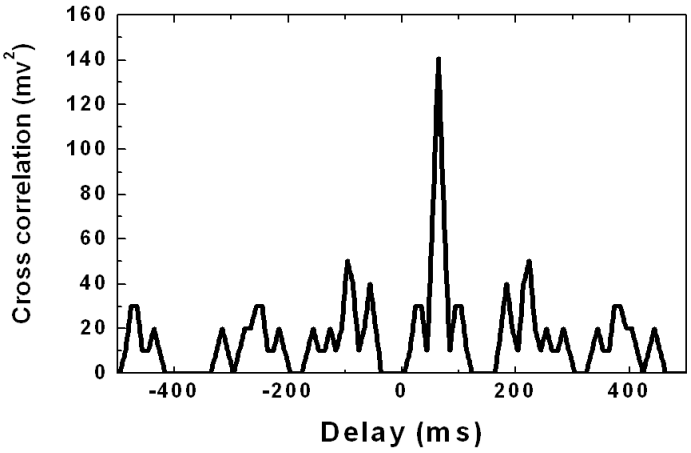

Figure 5.15 Correlation between the two demodulator voltage outputs.

The main advantage of the correlation method is the fact that non-correlated noise voltages v_1 and v_2 added to the ideal detector outputs V_1 and V_2 will be eliminated, provided that the number N of data points is sufficiently large. In order to illustrate the noise reduction capability, we added strong random noise to the demodulator output signals.

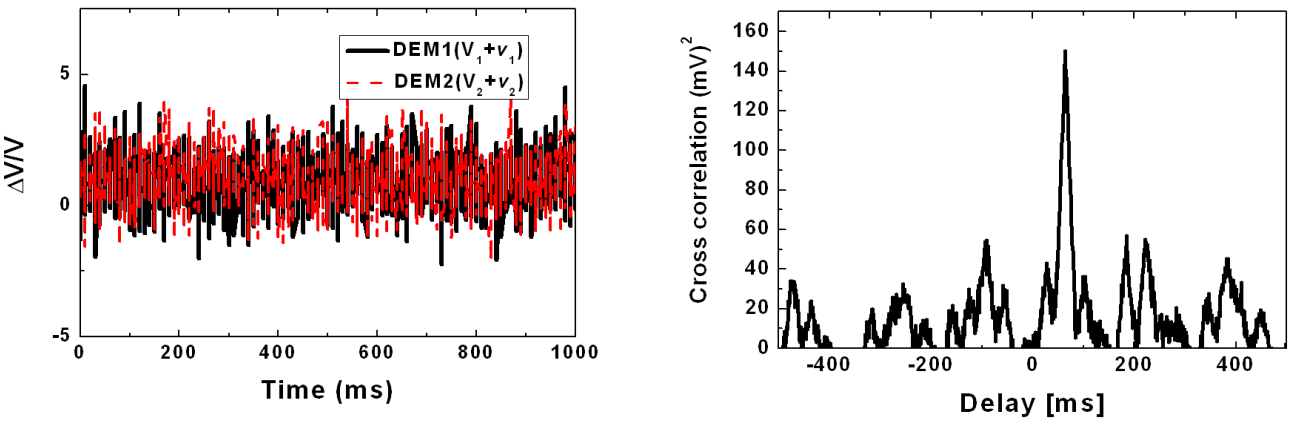

Figure 5.16 Pulse trains showing frequency pulses from two oscillators covered with random noise. Cross correlation between the pulses shows the delay time equal to the one obtained in Fig. 5.15.

A correlation between the two pulse sequences infested with random noise signals demonstrates the elimination of the non-correlated noise shown in Fig. 5.16. It is evident from Fig. 5.16, non-correlated noise voltages on the two detector outputs can be ideally eliminated by the principle of time averaging. Device noise, thermal noise and *1/f* noise accounts for this kind of non-correlated noise.

As mentioned above another type of noise in silicon chips arises from the power supply or termed as supply noise [158]. This type of noise may result in strongly correlated noise in the two demodulators, especially, if they are integrated on the same chip. Since correlated noise will not be eliminated by time averaging, noise coupling between the demodulators through supply or substrate should be minimized. This entails for separate biasing of the two demodulators and is discussed in [159]. Sufficient distance between noise aggressors and noise victims, and the use of guard bands around critical circuit blocks are of advantage as well. Moreover, electromagnetic coupling through close and parallel bond wires must be avoided.

Another type of environmental noise is temperature noise. This type of noise was discussed in the context of oscillator-based reactance sensors [160], where environmental noise was reduced by noise cancellation and filtering. Since temperature changes are correlated noise sources for the two sensor capacitances, our approach cannot eliminate this type of noise. However, if the temperature changes are much slower than the total measurement time, they have a small effect on the demodulator sensitivity. Moreover, bandgap references for each of the two demodulators can be used to stabilize the supply voltages with respect to temperature variations.

5.4.2 Particle concentration and flow-rate

In order to detect the concentration of particles and flow rate in the laminar flow system using the two demodulator architecture, the dynamics of the individual demodulator has to be optimized while $V_1(t)$ in Fig. 4 is the individual demodulator output signal. The two tuning loops of the demodulator comprising of C_{coarse} and C_{fine} have time constants τ_{coarse} and τ_{fine} respectively. τ_{coarse} determines the sensitivity of the detector system and has to be considerably large compared to the delay between the "frequency change" events at the two oscillators due to the flow of particle on top of the respective sensors.

$$\tau_{coarse} > \Delta t \tag{5.34}$$

Δt is the delay between the sensors. From the demodulator architecture shown in Fig. 4, and analysis of dual loop PLL [162] it is known that a frequency variation of the oscillator is restored by the coarse tuning loop and the time constant is given by,

$$\tau_{coarse} = \frac{C_{coarse}\Delta V_2}{I_{CP2}} \tag{5.35}$$

where ΔV_2 is the voltage change on the coarse tuning loop due to frequency modulation as shown in Fig. 4. I_{CP2} has been described above, is the charge pump current. The condition mentioned in equation (29) for highly sensitive architecture, requires a high value of τ_{coarse}; this can be achieved by lowering the I_{CP2} in conjunction with a high C_{coarse}. In the case where the τ_{coarse} is smaller than Δt, $V_2(t)$ in Fig. 4 can be taken as the output of the individual demodulator. Such a condition arises for extremely slow flow rate or very low solute concentration which causes the "frequency change" event at the two oscillators to be widely spaced. A similar mathematics done for V_2 (t), as was done for V_1 (t) would show a loss of sensitivity in such a situation. However, $V_2(t)$ can be used as an output by sacrificing the sensitivity as the delay is very large and the output voltage pulses are far apart from each other. In that case the C_{coarse} value should be small for fast settling of V_2 (t). Thus, a self-calibration for different flow rates is seen in the dual demodulator approach as well.

In order to obtain the concentration of particles in the suspension we assume that the frequency pulses obtained from the two sensors are proportional to the particle density. This assumption is valid for low to medium solute concentration in the suspension, which is typically the case in fluidic systems. As mentioned in a previous section the temperature and process variation have minimum influence on our demodulator architecture, which implies that the output voltage of the two demodulator sensor is only proportional to the frequency changes in the oscillator. Therefore, the concentration of particles in the solution can be obtained from the cross-correlation of the two output signals and can be given as,

$$n_{particle} = \alpha\sigma_v^2 \tag{5.36}$$

where σ_v is the magnitude of the correlation peak and α is a proportionality constant.

From the analysis it is seen that there is no theoretical limitation of particle concentration detection, as the correlation peak will grow with time and can be estimated. Therefore, any concentration of solute in a suspension can be estimated. However, if the measurement conditions (for example temperature) change during the measurement time, detection of the real concentration can be affected and such a condition can be avoided using bandgap references as mentioned above.

The delay time of the correlation peak can be used to obtain the flow rate of the particles. If the sensors are separated by a distance *s* and the peak of the correlation occurs at Δt, the flow rate can be written as,

$$v_{particle} = \frac{s}{\Delta t} \tag{5.37}$$

In order to detect particles with different dielectric characteristics the voltage pulses would be used. For particles with different dielectric permittivity the height of the output voltage pulse will be different for different particles as is shown in Fig. 5.14. In order to detect the concentration of different particles in the suspension the height of the voltage pulses should be analyzed. However, this requires time recording of the output pulses which in turn would require excessive data processing and increase the complexity and area of the chip.

5.5 Conclusion

We have presented a highly sensitive PLL demodulator architecture in conjunction with a capacitance based frequency shift sensor for detection of dynamic capacitance change. The sensor system can be employed towards particle counting in a flow assisted fluid system. A sensitivity of 70 ppm was experimentally measured using a modulating capacitor. This sensitivity allows a sensing capability of 1 MHz frequency shift for 14.3 GHz oscillator sensor. From the frequency shift sensor aspect this translates to the detection capability of 0.25 in the absolute permittivity value. Therefore, in the context of flow based sensors with very low concentration of particles in the suspension this technique offers extremely high sensitivity. The second significant property of the sensor is its self-calibration capability based on the fluid flow rate. Capacitance change as fast as every 3 μs can be accurately detected by the sensor system and has been shown. The fast measurement approach reduces the measurement time considerably. Owing to the high operating frequency of the sensor, low-frequency dispersion mechanisms can be avoided while utilizing the sensor for biological suspensions. On the other hand, the sensor has a very low-frequency (few KHz) output making the handling of the sensor highly simple. A configuration of two such detectors in a stream of particles in a microfluidic channel is proposed, where the system noise is suppressed by time averaging. After calibration, this method will provide particle density, mean velocity and fluid flow rate for a laminar flow in a microfluidic device.

CONCLUSION and OUTLOOK

In this thesis, "More Than Moore" strategy is employed to establish integrated CMOS high-frequency biosensors. From the aspect of the development of POC diagnostic systems or typical LOC devices, this single chip solution based on "More Than Moore" approach, provides the right platform for miniaturized "easy to handle" hand-held devices. The single chip solution not only eases the sensing operation by making it an "all-electrical" approach, but, with easier data acquisition capabilities and measurement techniques, reduces the size of the measurement test-bench and the overall area of the sensor system. The miniaturization of the overall system is one of the key advantages of the "all-electrical" single chip solution when compared to the state-of the art optical, electrochemical techniques. The limitations of optical or electrochemical sensors were outlined in the thesis and the clear advantage of single chip solution was presented by considering various biosensing applications. In one of the sections of the thesis, it was shown that the data output from the sensor system can be a simple DC voltage value, thus, elucidating why complex measurement system is not needed for this kind of sensors. Another important aspect of single chip solution is the high sensitivity of the sensor system which stems from the fact that the data acquisition circuit is very close to the sensor owing to the single chip solution. The cost of the overall sensor system is reduced considerably as well, due to the following aspects:

- ease of fabrication due to the know process technology
- the "all-electrical" sensing scheme requires no biomarkers
- due to extremely small sample volume, the cost of analyte is less

The other aspect of the thesis is the use of high-frequency permittivity detection as the sensing technique. The first immediate advantage of use of high-frequency technique is the miniaturization of the sensor. This was seen all through-out the thesis work where IDC was used as the sensor and the overall size of the sensor is of the order of few hundreds of micrometers. This miniaturized sensor size is of the order of biomaterials like biological cells. It also reduces the volume of the analyte sample needed for sensing. As mentioned above, reduction in the analyte volume reduces the cost of the overall sensor application. This was observed in the establishment of the immunosensor for creatinine. Solution volume as low as 2 µl was measured using the sensor systems. The other advantage of high-frequency dielectric measurement stems from the aspect of dielectric dispersion of biological suspensions. At lower frequencies biological suspensions show dispersion mechanisms based on the parameters of the solute present in the suspension and also based on the solution and sensor electrode interface. At higher frequencies these dispersion mechanisms are no longer dominant and thus the sensor data analyzing and processing become considerably easier. The unwanted surface chemistry of

electrode and solution interface or the other analyte parameter dependent dispersion mechanisms no longer play any role in the sensor data output. High-frequency biosensors based on permittivity detection also evades from the use of reference electrodes, which is commonly used for other electrical sensors like electrochemical sensors and low-frequency impedance sensors. This aids in further miniaturization of the overall sensor system. The high-frequency BiCMOS biosensors based on permittivity detection also provide the additional advantage of negligible incubation time for sensing. This is due to the capability of measuring extremely small changes in permittivity as depicted by the developed sensors.

The developed sensor system was applied for various applications like immunosensing, glucose sensing, detection of analyte concentrations in suspensions, etc. Standard BiCMOS technology was used for the fabrication of the sensor system. This chapter summarizes the technology platform along with the established applications of the biosensor platform.

Design and Integration

Standard BiCMOS technology (0.25 µm and 0.13 µm) of IHP was used for the fabrication of the biosensors. The topmost metal layers of BEOL metal stack (TM1 and TM2) were utilized for the design of the sensor. The top most metal layer ensures closest proximity of the sensor to the biomaterial. The biomaterials for e.g. protein molecules are immobilized on top of the passivation layer above the topmost metal layer. The polymer based microfluidic system is as well bonded on top of the TM2 metal layer. The top metal layers also provide high quality factor of the sensor due to high thickness of the metal layers. The quality factor of the sensor was shown to be a very significant parameter of the sensor design. The sensor being used as a resonator in conjunction with a pair of inductors, determined the overall quality factor of the resonator. Thus, the design of the active circuit (CMOS oscillator) driving the oscillations of the resonator is determined by the quality factor of the overall resonator, as the losses in the resonator is compensated by a negative resistance mechanism in the active devices (transistors). In case of the designed biosensor, the quality factor of the resonator is degraded by the loss factor of the biomaterial (for e.g. biological suspension). Therefore, design of the active circuit calls for special attention as compared to the standard communication circuits. The highest loss factor that can be incurred for a specific application had to be taken into account for the design of the active oscillator circuit. The influence of the biomaterials on the quality factor of other passive RF components (inductors) in the circuit results in the increase in area budget. However, owing to the single chip solution, the data acquisition circuits being on the same chip, the overall sensor system size is smaller when compared to the optical or hybrid amperometric techniques [55, 58, 64].

IDC structure was used as the sensor in the thesis. At the given frequency range of operation the designed IDCs were shown to be purely capacitive- structures. The IDCs were shown to obey the quasi-static approximations of the Maxwell equations. The sensing concept was based on the variation of the fringing electric field between the fingers of the IDC due to the presence of

materials of different values of permittivity on top of it. The intensity of the electric field of the IDC decreases exponentially in the normal direction of the IDC. The depth to which the electric field penetrates in the material under test (biomaterials) is determined by the geometry of the IDC. The capacitance density can also be tuned based on the geometry of the IDC. Thus, based on the application the IDC can be designed.

The influence of the passivation layer thickness was shown to play an important role in the sensitivity of the sensor system. As the field degrades exponentially in the perpendicular direction of the IDC, the thickness of the passivation layer was shown to influence the amount of electric field penetrating into the biomaterial on top of the passivation layer and in turn affecting the sensitivity of the system. The sensor was shown to be sensitive up to a passivation thickness of 10 μm.

Thus with careful consideration of the technology and other design aspects, single chip biosensors designed for various applications like immunosensing, glucose sensing etc., were shown.

Dielectric Immunosensor

One of the main applications of the biosensors developed in this thesis was to employ the sensors in immunosensing application for detection of creatinine. Creatinine concentration is one of the most frequently detected parameters in clinical diagnostics, as it is the index for renal glomerular infection. The concentration of creatinine in serum and urinary excretion is primarily unaffected by dietary changes such as intake of a creatinine-free diet. Therefore, undoubtedly it is one of the safest detected parameters.

In lieu with the target of the thesis to establish single chip biosensor solutions, one of the main goals while developing the immunosenor was to accomplish immobilization of creatinine molecules on the standard passivation layer (Si_3N_4) of CMOS/BiCMOS technology. This was achieved by a modified surface chemistry as described in chapter 3 of the thesis. The ability to immobilize creatinine molecules on the surface of Si_3N_4 ensured no additional post-processing step of the sensor chip and therefore, lays the foundation for next generation single chip immunosensors as opposed to the hybrid ones published in the literature [30, 31, 44, 40, 41].

Established competitive ELISA approach was used for detection of the creatinine concentration. Incubated anti-creatinine antibodies in different concentrations of creatinine solution were made to interact with the chip bound creatinine molecules. Different amount of antibodies binding to the chip bound creatinine molecules gave the measure of the creatinine concentration used in the incubation phase. The results obtained show that the concentration of creatinine can be detected in clinically relevant range of 0.88 μM to 88 μM and is comparable to amperometric or optical techniques used presently. On the other hand, a better dynamic range in case of electrical

measurements was observed in comparison to the optical technique with approximately equal sensitivity.

A frequency shift of 35 MHz was observed with every 10 fold increase in the concentration of creatinine used in the incubation phase. This sensitivity was measured to be considerably higher than the process and measurement variation of approximately 4 MHz. Thus, the high-frequency immunosensor established in this thesis work was shown to be quite robust and there was high repeatability of the measurement results. A lot of published literature show that creatinine enzyme immunoassays can specifically measure the concentration of creatinine in real samples like serum. Therefore, it can be stated that the established high-frequency sensor is capable of measuring the cretainine concentration in real samples as well. The other aspect of the immunosensor is the ability pf measuring concentration in the nano-molar range. Therefore, such an immunosensor can be adapted for other clinically relevant analytes as well.

Detection of Analyte Concentration

Detection of analyte concentration is a major area of research in biosensor applications. Determination of concentration of cells like white blood corpuscles or red blood corpuscles in serum or detection of living and dead cells in a suspension, determination of glucose concentration etc., are few major applications of detection of analyte concentration in a suspension. In this thesis as one of the applications of the high-frequency biosensor, detection of concentration of various anlyte in bio-suspension was focused on. One of the main goals in this part the thesis was to integrate microfluidic system with the BiCMOS sensor chip. Two possible approaches for the microfluidic integration were explored. One was to construct a non-conducting wall around the sensor. This approach was relatively straightforward and required no additional post-processing step. The second approach was based on the bonding of polymer (PDMS) based microfluidic systems with the sensor chip. The PDMS microfluidic system was fabricated using a soft lithography technique. For the bonding of the microfluidic system to the sensor chip an additional post-processing step of chemical mechanical polishing of the BiCMOS chip was conducted in order to meet the planarity requirements for the accurate bonding of the microfluidic system and the BiCMOS chip.

Various analyte concentrations in suspensions were detected using various sensor systems. The sensors operating at 6 GHz and 12 GHz were used as glucose concentrations. The sensitivity of the sensors when fabricated on TM1 and TM2 of the BiCMOS stack was compared. The sensor fabricated on TM1 metal layer (sensor operating at 6 GHz) demonstrated considerable sensitivity and could distinguish 10 % increase in the concentration of glucose in the suspension. This matches with simulation showing the influence of passivation layer on the sensitivity of the system. It should be mentioned here that the sensor on TM1 has two passivation layers (SiO_2 and Si_3N_4) between its surface and the glucose solution.

The 12 GHz sensor system was further used to demonstrate the capability of detection of concentration of particles in a suspension. Concentration of micro-beads suspended in a solution was detected using this sensor system. Therefore, such a sensor architecture can be applied to various cytometric applications. The theoretical basis of working of the sensor system in cytomteric application was explored and was shown that the average permittivity of the suspension is dependent on the orientation polarization of water molecules in the suspension. The presence of particles influences the orientation of water molecules based on Einstein Stoke's equation and therefore, causes a change in the overall permittivity based on their concentration. This matches with the theory proposed for high frequency sensors, where other dispersion mechanisms have negligible influence on the sensor output. The 12 GHz sensor system was also used to establish proof of principle for establishment of minimally invasive plaque sensors. The sensor was utilized to detect the concentration of fat and calcium in aqueous phase.

Another important aspect of the sensor system investigated in this part of the thesis was the capability of imaging of biomaterials based on the permittivity distribution. Two sensors operating at 7 GHz and 8 GHz were investigated for the imaging applications. The sensor systems were shown to be able to accurately image the spatial distribution of permittivity. In the work shown, a lateral resolution of the order of μm was shown. Such a sensor can be applied for near field imaging of cancerous tissues. Thus, high-frequency BiCMOS biosensors with versatile applications were demonstrated in this section of the thesis.

Towards Particle Counting

Single particle sensing and counting is another significant research avenue in the area of biosensors. To this aspect, in this thesis a highly sensitive capacitive sensor system was designed and electrically characterized, depicting the ability to measure capacitance change of the order of auto Farrads. Such small change in capacitance can be related to extremely low solute or particle concentration in suspensions or single particle. The sensor system is suited for dynamic fluid system. Ultra-high-speed measurement capability of the order of 3 μs was demonstrated with the sensor system.

A dual loop PLL demodulator architecture was used for the development of the high precision sensor system. The flow of particles on top if the sensor embedded in an oscillator was modeled as the oscillation frequency modulation of the oscillator. A self-calibrating feature was employed in the PLL architecture for detection of very small capacitive changes. A theoretical formulation of the working of the demodulator architecture was established. A modulating capacitor was incorporated in the design for electrical characterization of the sensor system. A change of 1 MHz at the operating frequency of 14.3 GHz was detected accurately. In terms of capacitance change this translates to a change of 60 aF at the starting capacitance of 18 fF. The key feature of

the sensor system is the DC output. This makes the sensor architecture extremely flexible and easy to handle.

Noise, which is a significant source of major problems in biosensors, was addressed in this section of the thesis. Dual demodulator architecture was proposed and the technique of cross-correlation was employed to remove the non-correlated noise form the system. The sensor system can be accurately used to count the particles and also extract the flow rate and overall concentration of the particles.

Outlook

The thesis shows the feasibility of establishing integrated CMOS/ BiCMOS biosensors suitable for a variety of applications, like immunosensors, glucose sensors, cytomteric sensors and more. This single chip solution is the first step towards producing cheap and easy to handle POC diagnostic devices. Most of the sensor systems shown in this thesis have high-frequency outputs. The next viable step is the complete system integration with digital output. The prior requirement in order to establish the complete sensor system is the conversion of the high-frequency output to DC output. One such sensor system with DC output was shown in chapter 5 of the thesis. However, the system was suited primarily for biosensors assisted with flow based fluidic systems. For more static applications, methods of conversion of high-frequency sensor signals to DC values need to be implemented. These methods could involve use of PLL applicable for static approaches, or implementation of frequency counters. Thus, conversion of the high-frequency sensor signals to DC output is the most primary and significant step for system integration. The next step towards system integration with digital outputs is the implementation of analog to digital converters (ADCs). With digital outputs the sensor systems will become more user-friendly and easy to handle. Therefore, gradual steps should be taken to establish a complete biosensor module from the established sensor architectures. Being a single chip solution, these sensor architectures provide the freedom to develop on chip digital circuitry for signal processing. The signal processing circuits being very close to the sensor system will also provide maximum sensitivity. Due to the close proximity no degradation of signal will take place unlike the hybrid integrated biosensors.

The next enhancement of the sensor systems is the development of parallel sensing schemes. To this aspect, sensor array was demonstrated in chapter 4 of the thesis work. The rational step towards establishing parallel sensing schemes is the enhancement of this array into more number of units or pixels. Standard microtitre plates can be take as reference examples for the establishment of this parallel sensing approach. However, parallel sensing scheme with multiple sensors can be a complex system to handle due to routing of a large number of high frequency signal paths. Considerable amount of research work has to be invested in order to develop the right strategy for parallel sensing. This kind of sensing approach would also require a suitable

automation of the sensor system in order to control the sensor operations, for e.g., with switches. The digital control of switches will require automated control using for e.g., a microcontroller. Therefore, automated parallel sensing schemes should be looked at to increase the throughput of such sensor architectures.

From the biological aspects more applications should be targeted at using the developed BiCMOS biosensors. Some significant applications like immunosensing, glucose sensing, and detection of concentration of particles in a suspension have already been addressed in this thesis. One such example of diversification of application of these sensor systems is the establishment of an "all-electrical" alternative for the established micro-titre plates used for the growth culture of cells in an aqueous environment. The sensor systems have already been shown to be able to detect small variations of concentration of particle s in a suspension. Establishment of such intelligent micro-titre plates for growth culture would be an extension of the concentration detection sensor. Other applications can involve diversification of the immunosensor for various proteins, specific glucose molecule sensor, etc. Establishing spectroscopy technique is another outlook to the work. If an overall sensor system is designed for the frequency range covering from MHz to GHz ranges, the same sensor chip can be used for understanding the low frequency attributes of biological samples as well as their concentration which can be detected better at high frequency.

All in all, in this thesis a new approach towards biosensors has been demonstrated with the establishment of complete BiCMOS integrated biosensor platform. This approach has the potential for establishing new POC devices for diverse applications and at the same time with extreme ease of handling and reduced cost.

BIBLIOGRAPHY

[1] C. D. Chin, V. Linder and S. K. Sia, "Lab-on-a-chip devices for global health: past studies and future opportunities", *Lab chip*, 2006, **7**, 41-47

[2] C. Wilmott and J. E. Arrowsmith, "Point-of-care testing", *Surgery,* 2010, **28**, 159-160

[3] E. Petryayeva and W. Russ Algar, "Toward point-of-care diagnostics with consumer electronic devices: the expanding role of nanoparticles", *RSC Advances,* 2015, **5**, 22256-22282

[4] C. D. Chin, V. Linder and S. K. Sia, "Commercialization of microfluidic point-of-care diagnostic devices", *Lab Chip*, 2012, **12**, 2118-2134

[5] J. S. Daniels and N. Pourmand, "Label-free impedance biosensors: opportunities and challenges", *Electroanalysis*, 2007, **19**, 1239-1257

[6] N. M. M. Pires, T. Dong, U. Hanke and N. Hoivik, "Recent developments in optical detection technologies in lab-on-a-chip devices for biosensing applications", *Sensors*, 2014, **14**, 15458-15479

[7] S. Lopez, "Pulse Oximeters: Fundamentals and Design", NXP, FreeScale Semiconductors Document

[8] M-I Mohammed and M. P. Y. Desmulliez, "Lab-on-a-chip based immunosensor principles and technologies for the detection of cardiac biomarkers: a review", *Lab Chip*, 2011, **11**, 569-595

[9] F. Rusling, C.V. Kumar, J. S. Gutkind and V. Patel, "Measurement of biomarker proteins for point-of-care early detection and monitoring of cancer", *Analyst*, 2010, **135**, 2496-2511

[10] A. M. Foudeh, T. F. Didar, T. Veres and M. Tabrizian, "Microfluidic designs and techniques using lab-on-a-chip devices for pathogen detection for point-of-care diagnostics", *Lab Chip*, 2012, **12**, 3249-3266

[11] N. Wongkaew, P. He, V. Kurth, W. Surareungchai and A. J. Baemner, "Multi-channel PMMA microfluidic biosensor with integrated IDUAs for electrochemical detection*", Anal. Bional. Chemistry*, 2013, **405**, 5965-5974

[12] M. Ferrari, "Cancer nanotechnology", *Nat. Rev. Cancer*, 2005, **5**, 161-171

[13] S. Pennathur and D. K. Fygenson, "Improving fluorescence detection in lab on chip devices", *Lab Chip*, 2008, **8**, 649-652

[14] L. M. Lee, X. Cui and C. Yang, "The application of on-chip optofluidic microscopy for imaging Giardia lamblia trophozoites and cysts", *Biomedical Microdevices*, 2009, **11**, 951-958

[15] N. Ramalingam, Z. Rui, H. B. Liu, C. C. Dai, R. Kaushik, B. M. Ratnaharika and H. Q. Gong, "Real-time PCR-based microfluidic array chip for simultaneous detection of multiple waterborne pathogens", *Sensors and Actuators B Chemical*, 2010, **145**, 543-552

[16] R. Ishimatsu, A. Naruse, R. Liu, K. Nakano, M. Yahiro, C. Adachi and T. Imato, "An organic thin film photodiode as a portable photodetector for the detection of alkylphenol polyethoxylates by a flow fluorescence-immunoassay on magnetic microbeads in a microchannel", *Talanta*, 2013, **117**, 139-145

[17] N. Yildirim, F. Long, C. Gao, M. He, H.C. Shi and A. Z. Gu, "Aptamer based optical biosensor for rapid and sensitive detection of 17 β-estradiol in water samples", *Environmental Science and Technology*, 2012, **46**, 3288-3294

[18] M. Wolf, D. Juncker, B. Michel, P. Hunziker and E. Delamarche, "Simultaneous detection of C-reactive protein and other cardiac markers in human plasma using micromosaic immunoassays and self-regulating microfluidic networks", *Biosensors and Bioelectronics*, 2004, **19**, 1193-1202

[19] J. Ziegler, M. Zimmermann, P. Hunziker and E. Delamarche, "High-performances immunoassays based on through stencil patterned antibodies and capillary systems" *Analytical Chemistry*, 2008, **80**, 1763-1769

[20] C. Joensson, M. Aronsson, G. Rundstroem, C. petterson, I. Medel-Hartvig, J. Bakker, E. Martinsson, B. Liedberg, B. MacCraith, O. Oehman and J. Melin, "Silane-dextran chemistry on lateral flow polymer chips for immunoassays", *Lab Chip*, 2008, **8**, 1191-1197

[21] X. L. Su and Y. Li, "Quantum dot biolabeling coupled with immunogenetic separation for detection of Escherichia coli" *Analytical chemistry*, 2004, **76**, 4806-4810

[22] M. Nichkova, D. Dosev, A. E. Davies, S. J. Gee, I. M. Kennedy and B. D. Hammock, "Quantum dots as reporters in multiplexed immunoassays for biomarkers of exposure to agrochemicals", *Analytical letters*, 2007, **40**, 1423-1433

[23] L. J. Chabonniere and N. Hildebrandt, "Lanthanide complexes and quantum dots: a bright wedding for resonance energy transfer" *European journal of Inorganic Chemistry*, 2008, 3241-3251

[24] R. C. Stringer, D. Hoehn and S. A. Grant, " Quantum dot based biosensor for detection of human cardiac troponin 1 using a liquid core waveguide" *IEEE Sensors Journal*, 2008, **8**, 295-300

[25] L. Gervais and E. Delmarche, "Toward one step point of care immunodiagnostics using capillary-driven microfluidics and PDMS substrates", *Lab Chip*, 2009, **9**, 3330-3337

[26] K. E. Sapsford, T. Pons, I. L. Medintz and H. Mattoussi, "Biosensing with luminescent semiconductor quantum dots", *Sensors*, 2006, **6**, 925-953

[27] K. Kerman, T. Endo, M. Tsukamoto, M. Chikae, Y. Takamura and E. Tamiya, "Quantum dot-based immunosenosr for the detection of prostate-specific antigen using fluorescence microscopy", *Talanta*, 2007, **71**, 1494-1499

[28] M. Zimmermann, P. Hunziker and E. Delmarche, "Autonomous capillary system for one step immunoassays", *Biomedical Microdevices*, 2009, **11**, 1-8

[29] A. Xiang, F. Wei, X. Lei, Y. Liu and Y. Guo, "A simple and rapid capillary chemiluminesce immunoassay for quantitatively detecting human serum HbsAg", *European Journal of Clinical Microbiology Infect. Dis*., 2013, **32**, 1557-1564

[30] I. H. Cho, E. H. Paek, Y. K. Kim, J. H. Kim and S. H. Paek, " Chemiluminometric enzyme-linked immunosorbent assays (ELISA)-on a chip biosensor based on cross-flow chromatography", *Analytical Chim. Acta*., 2009, **632**, 247-255

[31] H.Huang, X. L. Zheng, J. S. Zheng, J. Pan and Y. P. Pu, "Rapid analysis of alpha-fetoprotein by chemiluminescence microfluidic immunoassay system based on super-paramagnetic microbeads" *Biomedical Microdevices*, 2009, **11**, 213-216

[32] M. Yang, S. Sun, Y. Kostov and A. Rasooly, "An automated point-of-care system for immunodetection of taphylococcal enterotoxin B", *Analytical Biochemistry*, 2011, **416**, 74-81

[33] D. Caputo, G. de Cesare, L. S. Dolci, M. Mirasoli, A. Nascetti, A. Roda and R. Scipinotti, "Microfluidic chip with integrated a-Si.H photodiodes for chemiluminescence-based bioassays", *IEEE Sensors Journal*, 2013, **13**, 2595-2602

[34] M. Hao and Z. Ma, "An ultrasensitive chemiluminescence biosensor for carcinoembryonic antigen based on autocatalytic enlargement of immunogold nanoprobes", *Sensors*, 2012, **12**, 17320-17329

[35] M. Yang, Y Kostov, H. A. Bruck and A. Rasooly, "Carbon nanotubes with enhanced chemiluminescence immunoassay for CCD-based detection of staphylococcal enterotoxin B in food" *Analytical Chemistry*, 2008, **80**, 8532-8537

[36] F. Darain, P. Yager, K. L. Gan and S. C. Tjin, "On chip detection of myoglobin based on fluorescence", *Biosensors and Bioelectronics*, 2009, **24**, 1744-1750

[37] A. Bhattacharyya and C. M. Klapperich, "Design and testing of a disposable microfluidic chemiluminescent immunoassay for disease biomarkers in human serum samples", *Biomedical Microdevices*, 2007, **9**, 245-251

[38] D. M. Vykoukal, G. P. Stone, P. R. C. Gascoyne, E. U. Alt, J. Vykoukal, "Quantitative detection of bioassays with a low-cost image-sensor array for integrated microsystems", *Angew. Chem. Int. Ed.*, 2009, **121**, 7785-7790

[39] C. C. Lin, F. H. Ko, C. C. Chen, Y. S. Yang, F. C. Chang and C. S. Wu, "Miniaturized metal semiconductor metal photocurrent system for biomolecular sensing via chemiluminescence", *Electrophoresis*, 2009, **30**, 3189-3197

[40] J.R. Wojciechowski, L. C. Shiver-lake, M. Y. Yamaguchi, E. Fuereder, R. Pieler, M. Schamesberger, C. Winder, H. J. Prall, M. Sonnleitner and F. S. Ligler, "Prganic photodiodes for biosensor miniaturization", *Analytical Chemistry*, 2009, **81**, 3455-3461

[41] O. Krupin, H. Asiri, C. Wang, R. N. Tait and P. Berini, "Biosensing using straight long-range surface plasmon waveguides", *Optics Express*, 2013, **21**, 698-709

[42] A.M Foudeh, J. T. Daoud, S. P. Faucher, T. Veres and M. Tabrizian, "Sub-femtomole detection of of 16s rDNA from legionella pneumophila using surface plasmon resonance imaging", *Biosensors and Bioelectronics*, 2014, **52**, 129-135

[43] E. Ouellet, C. Lausted, T. Lin, C.W.T. Yang, L. Hood and E. T. Lagally, "Parallel microfluidic surface plasmon resonance imaging arrays", *Lab Chip*, 2010, **10**, 581-588

[44] S. Unser, I. Bruzas, J. He and L. Sagle, "Localized Surface plasmon resonance biosensing: Current challenges and approaches", *Sensors*, 2015, **15**, 15684-15716

[45] B. N. Feltis, B. A. Sexton, F. L. Glenn, M. J. Best, M. Wilkins and T. J. Davis, "A hand-held surface plasmon resonance biosensor for the detection of ricin and other biological agents", *Biosensors Bioelectronics*, 2008, **23**, 1131-1136

[46] T. M. Chinowsky, M. S. Grow, K. S. Johnston, K. Nelson, T. Edwards, E. Fu and P Yager, "Compact high performance surface plasmon resonance imaging systems", *Biosensors Bioelectronics*, 2007, **22**, 2208-2215

[47] T. M. Chinowsky, J. G. Quinn, D. U. Bartholomew, R. Kaiser and J. L. Elkind, " Performance of the spreeta 2000 integrated surface plasmon resonance affinity sensor", *Sensors and Actuators B: Chemical*, 2003, **91**, 266-274

[48] S. Wang, X. Zhao, I. Khimji, R. Akbas, W. Qiu, D. Edwards, D. W. Cramer, B. Ye and U. Demirci, "Integration of cell phone imaging with microchip ELISA to detect ovarian cancer HE4 biomarker in urine at the poibt-of-care", *Lab Chip*, 2011, **11**, 3411-3418

[49] J. C. Jokerst, J. A. Adkins, B. Bisha, M. M. Mentele, L. D. Goodridge and C. S. Henry, "development of a paper-based analytical device for calorimetric detection of selsect foodborne pathogens", *Analytical Chemistry*, 2012, **84**, 2900-2907

[50] A. Rasooly, H. A. Bruck and Y. Kostov, "An ELISA lab-on-a-chip (ELISA-LOC)", *Methods Molecular Biology*, 2013, **949**, 451-471

[51] F. Zhou, M. Wang, L. Yuan, Z. Cheng, Z. Wu and H. Chen,"Sensitive sandwich ELISA based on a gold nanoparticle layer for cancer detection", *Analyst*, 2012, **137**, 1779-1784

[52] F. Li, L. Jiang, J. Han, Q. Liu, Y. Dong, Y. Li and Q. Wei, "A label-free amperometric immunosensor based for the detection of carcinoembryonic antigen based on novel magnetic carbon and gold nanocomposites", *RSC Advances*, 2015, **5**, 19961-19969

[53] C. Chen, G. Xie, D. Yang, H. Xiao, Y. Fu, Y. Tan and S. Yao, " Recent advances in electrochemical glucose biosenosrs:a review", *RSC Advances*, 2013, **3**, 4473-4491

[54] J. Hajdukiewicz, S. Boland, P. Kavanagh, A. Nowicka, Z. Stojek and D. Leech, "Enzyme-amplified amperometric detection of DNA using redox mediating films on gold microelectrodes", *Electroanalysis*, 2009, **21**, 342-350

[55] A. Ramanaviciene and A. Ramanavicius, "Pulsed amperometric detection of DNA with an ssDNA/polypyrrole-modified electrode", *Analytical Bioanalytical Chemistry*, 2004, **379**, 287-293

[56] X. Zhu, K. Ino, Z. Lin, H. Shiku, G. Chen and T. Matsue, "Amperometric detection of DNA hybridization using multi-point, addressable electrochemical device", *Sensors and Actuators B: Chemical*, 2011, **160**, 923-928

[57] N.J. Forrow, G. S. Sanghera, S. J. Walters and J. L. Watkin, "Development of a commercial amperometric biosensor electrode for the ketone β-3-hydroxybutyrate", *Biosensors Bioelectronics*, 2005, **20**, 1617-1625

[58] J. Wang, "Electrochemical glucose biosensors", *Chemical Reviews*, 2008, **108**, 814-825

[59] S. Kang, A. Nieuwenhuis, K. Mathwig, D. Mampallil and S. G. Lemay, " Electrochemical single-molecule detection in aqueous solution using self-aligned nanogap transducers", 2013, *ACS Nano*, 2013, **7**, 10931-10937

[60] S. Ko, B. Kim, S. S. Jo, S. Y. Oh and J. K. Park "Electrochemical detection of cardiac troponin I using a microchip with the surface functionalized polydimethylsiloxane channel", *Biosensors Bioelectronics*, 2007, **23**, 51-59

[61] D. Purvis, O. Leonardova. D. Farmakovsky and V. Cherkasov, "An ultrasensitive and stable potentiometric immune sensor", *Biosensors Bioelectronics*, 2003, **18**, 1385-1390

[62] A.G. Gehring, D. L. Patterson and S. I. Tu, "Use of a light-addressable potentiometric sensor for the detection of Escherichia coli O157", *Analytical Biochemistry*, 1998, **258**, 293-298

[63] K. Chumbimuni-Torres, J. Wu, C. Clawson, M. Galik, A. Walter, G. Flechsig, E. Bakker, L. Zhang and J. Wang, "Amplified potentiometric transduction of DNA hybridization using ion-loaded liposomes", *Analyst*, 2010, **135**, 1618-1623

[64] E. Ogabiela and S. B. Adeloju, "A potentiometric phosphate biosensor based on entrapment of pyruvate oxidase in a polypyrrole film", *Analytical Methods*, 2014, **6,** 5290-5297

[65] J. G. Ayenimo and S. B. Adeloju, "Improved potentiometric glucose detection with ultra-thin polypyrrole-glucose oxidase films", *Analytical Methods*, 2014, **6**, 8996-9006

[66] S. Viswanathan, H. Radecka and J. Radecki, "Electrochemical biosensors for food analysis", *Monatsh. Chem.*, 2009, **140**, 891-899

[67] Z. Shi, Y. Tian, X. Wu, C. Li and L. Yu, "A one-piece lateral flow impedimetric test strip for label-free clenbuterol detection", *Analytical Methods*, 2015, **7**, 4957′4964

[68] A. H. Loo, A. Bonanni and M. Pumera, "Impedimetric thrombin aptasensor based on chemically modified graphenes", *Nanoscale*, 2012, **4**, 143-147

[69] X. Munoz-Berbel, N. Vigues, M. Cortina-Puig, R. Escude, C. Garcia-Aljaro, J. Mas and F. X. Munoz, "Impedimetric approach for monitoring bacterial cultures based on the changes in the magnitude of the interface capacitance", *Analytical Methods*, 2010, **2**, 1036-1042

[70] Abott Point of care, USA

[71] L. Rassaei, E. D. Goluch and S. G. Lemay, "Substrate dependent kinetics in tyrosinase-based biosensing: Amperometry vs Spectrophotometry", *Analytical and Bioanalytical Chemistry*, 2012, **493**, 1577-1584

[72] S. Goh, And R. J. Ram, "Impedance spectroscopy for in situ biomass measurements in microbioreactor", *14th International Conference on Miniaturized Systems for Chemistry and Life Science*, Netherlands, 2010.

[73] E. E. Kommenhoek et al, "Monitoring of yeast cell concentration using micromachined impedance sensor", *Sensors and Actuators B: Chemical*, 2006, **115**, 384-389

[74] A. Faenza, M. Bocchi, N. Pecorari, E. Franchi and R. Guerrieri, "Impedance measurement technique for high sensitivity cell detection in micro structures with non-uniform conductivity distribution", *Lab Chip*, 2012, **12**, 2046-2052

[75] Micronit microtechnologies, Electrochemical Impedance spectroscopy chips (EIS Chips)

[76] Gamry Instruments, Electrochemical Impedance spectroscopy

[77] M. Nikolic-Jaric, S. F. Romanuik, G. A. Ferrier, G. E. Bridges, M. Butler, K. Sunley, D. J. Thomson and M. R. Freeman, "Microwave frequency sensor for detection of biological cells in microfluidic channels", *Biomicrofluidics*, 2009, **3**, 1-15

[78] G. E. Moore, "Cramming more components onto integrated circuits", *Electronics*, **38**, 1965

[79] W. Arden, M. Brillouet, P. Cogez, M. Graef, B. Huizing and R. Mahnkopf, "More-Than-Moore": White Paper

[80] K. H. Lee, J. O. Lee, S. Choi, J. B. Yoon and G. H. Cho, "A CMOS label-free DNA sensor using electrostatic induction of molecular charges", *Biosensors Bioelectronics*, 2012, **31**, 343-348

[81] C. Stagni, C. Guiducci, L. Benini, B. Ricco, S. Carrara, B. Samori, C. Paulus, M. Schienle, M. Augustyniak and R. Thewes, " CMOS DNA sensor array with integrated A/D conversion based on label-free capacitance measurement", *IEEE Journal of Solid-State Circuits*, 2006, **41**, 2956-2964

[82] E. Anderson, J. Daniels, H. Yu, T. Lee and N. Pourmand, " A label-free CMOS DNA microarray based on charge sensing", *IEEE Instrumentation and Measurement Technology Conference*, Canada, 2008

[83] A. Hassibi and T. H. Lee, "A programmable 0.18 μm CMOS electrochemical sensor microarray for biomolecular detection", *IEEE Sensors Journal*, 2006, **6**, 1380-1388

[84] K. Lee, J. Nam, S. Choi, H. Lim, S. Shin and G. Cho, "A CMOS impedance cytometer for 3D flowing single-cell real time analysis with ΔΣ error correction" *IEEE, International Solid-State Circuits Conference Digest of Technical Papers (ISSCC)*, USA, 2012, 304-306

[85] Y. Adiguzel and H. Kulah, "CMOS cell sensors for point-of-care diagnostics", *Sensors*, 2012, **12**, 10042-10066

[86] E. Ghafar-Zadeh and M. Sawan, "CMOS based capacitive detection lab-on-chip: design and experimental results", *IEEE Custom Integrated Circuits Conference (CICC)*, USA, 2007

[87] S.S. Stuchly, C. E. Bassey, "Microwave coplanar sensors for dielectric measurements", *Measurement Science technology*, 1998, **9**, 1324-1329

[88] A. I. Gubin, AA. Barannik, N. T. Cherpak, S. Vitusevich, A. Offenhaeusser and N. Klein, "Whispering-gallery mode resonator technique for charactrization of small volumes of biochemical liquids in microfluidic channel", *IEEE European Microwave Conference Proceedings*, UK, 2011, 615-618

[89] D. J. Rowe, A. Porch, D. A. Barrow, C. J. Allender, "Microfluidic device for compositional analysis of solvent systems at microwave frequencies", *Sensors and Actuators B: Chemical*, 2012, **169**, 213-221

[90] J.C. Booth, J. Mateu, M. Janezic, J. Baker-Jarvis and J. A. Beall, "Broadband permittivity measurements of liquid and biological samples using microfluidic channels", *IEEE/MTT-S, International Microwave Symposium*, USA, 2006, 1750-1753

[91] K. Grenier and D. Dubuc, "Integrated broadband microwave and microfluidic sensor dedicated to bioengineering*", IEEE trans. on Microwave Theory and Techniques*, 2009, **57**, 3247-3253

[92] K. Grenier, D. Dubuc, T. Chen, F. Artis, T. Chretiennot, M. Poupot and J-J. Fournie, "Recent advances in microwave-based dielectric spectroscopy at the cellular level for cancer investigation", *IEEE Trans. on Microwave Theory and Techniques,* 2013, 61, 2023-2030

[93] M. Nikolic-Jaric, S. F. Romanuik, G. A. Ferrier, G. E. Bridges, M. Butler, K. Sunley, D. J. Thomson and M. R. Freeman, "Microwave frequency sensor for detection of biological cells in microfluidic channels", *Biomicrofluidics*, 2009, **3**, 1-15

[94] Y. Yang, H. Zhang, J. Zhu, G. Wang, T.-R. Tzeng, X. Xuan, K. Huang and P. Wang, "Distinguishing the viability of a single yeast cell with an ultra-sensitive radio frequency sensor", *Lab Chip*, 2010, **10**, 553-555

[95] J. Chien, M. Anwar, E. Yeh, L. P. Lee and A. M. Niknejad, "A 6.5/17.5 GHz dual-channel interferometer-based capacitive sensor in 65 nm CMOS for high-speed flow cytometry", *IEEE,/MTT-S International Microwave Symposium*, USA, 2014

[96] H. Wang, C. Sideris and A. Hajimiri, "A frequency-shift based CMOS magnetic biosensor with spatially uniform sensor transducer gain", *IEEE Custom Integrated Circuits Conference (CICC)*, USA, 2010

[97] A. Manz, "Miniaturized total chemical-analysis systems: a novel concept for chemical sensing", *Sensors and Actuators B: Chemical*, 1990, **1**, 244-248

[98] M. Kaynak, M. Wietstruck, C. Kaynak, S. Marschmeyer, P. Kulse, K. Schulz, H. Silz, A. Krueger, R. Barth, K. Schmalz, G. Gastrock and B. Tillack, "BiCMOS integrated microfluidic platform for bio-MEMS applications", *IEEE/MTT-S, International Microwave Symposium*, USA, 2014

[99] C. B. Kayanak, M. Kaynak, M. Wietstruck, St. Marschmeyer, P. Kulse, K. Schulz, H. Silz, a. Krüger, R. Barth, K. Schmalz and B. Tillack, "Modeling and characterization of BiCMOS embedded microfluidic platform for biosensing applications", *Silicon Monolithic Integrated Circuits in RF Systems (SIRF – Biowireless 14)*, USA, 2014

[100] S. K. Sia and G. M. Whitesides, "Microfluidic devices fabricated in poly (dimethylsiloxane) for biological studies", *Electrophoresis*, 2003, **24**, 3563-3576

[101] G.M. Whitesides "Overview the origins and the future of microfluidics", *Nature*, 2006, **442**, 368-373

[102] B. Eversmann, M. Jenkner, F. Hofmann, C. Paulus, R. Brederlow, B. Holzapfl, P. Fromherz, M. Merz, M. Brenner, M. Schreiter, R. Gabl, K. Plehnert, M. Steinhauser, G. Eckstein, D. Schmitt-landsiedel and R. Thewes," A 128 x 128 CMOS biosensor array for extracellular recording of neural activity", *IEEE Journal of Solid-State Circuits*, 2003, **38**, 2306-2317

[103] L. Lin, L. Xiaowen and A-J. Mason, "Die-level photolithography and etchless parylene packaging process for on-CMOS electrochemical biosensors", *IEEE International Symposium on Circuits and Systems (ISCAS)*, 2012, Korea

[104] B. Heinemann, H. Ruecker, R. Barth, J. Drews, O. Fursenko, T. Grabolla, R. Kurps, St. Marschmeyer, A. Scheit, D. Schmidt, A. Trusch, D. Wolansky and Y. Yamamoto, " SiGe p-n-p HBTs with 265 GHz f_{max}, 175 GHz f_t and 3.65-ps gate delay", *IEEE Electron Device Letters*, 2014, **35**, 814

[105] LM. Silva, AM. Salgado and MA. Coelho, "Development of an amperometric biosensor for phenol detection", *Environmental Technology*, 2011, **32**, 493-497

[106] T. H. Lee, "The design of CMOS radio-frequency integrated circuits", 2nd Edition, Cambridge University press, 2003

[107] C. Kittel, "Introduction to solid state physics", 8th Edition, 2004

[108] H. P Schwan, "Electrical properties of tissue and cell suspensions", *Advances in Biological and Medical Physics*, 1957

[109] R. Pethig and D. B. Kell, "The passive electrical properties of biological systems: their significance in physiology, biophysics and biotechnology", *Phys. Med. Biology*, 1987, **32**, 933-970

[110] B. Razavi, "RF Microelectronics", 2nd Edition, Prentice Hall Communication, 2011

[111] C. N. Chang, Y. C. Wong, and C. H. Chen, "Full-wave analysis of coplanar waveguides by variational conformal mapping technique", IEEE Trans. Microwave Theory and Techniques, 1990, **38**, 1339-1344

[112] G R. Garg, "Analytical and Computational Methods in Electromagnetics", Artech House

[111] K. Sundara-Rajan, A. V. Mamishev and M. Zahn, "Fringing electric and magnetic field sensors", *Encyclopedia of Sensors*, 2006, 1-12

[112] G. D. Alley, "Interdigital capacitors and their application to lumped-element microwave integrated circuits", *IEEE Transactions Microwave Theory and Techniques*, 1970, **18**, 1028-1033

[113] JS. Wei, "Distributed capacitance of planar electrodes in optic and acoustic surface wave devices", *IEEE Journal of Quantum Electronics*, 1977, **13**, 152-158

[114] R. Igreja and C. J. Dias, "Analytical evaluation of the interdigital electrodes capacitance for a multilayered structure", *Sensors and Actuators A*: Physical, 2004, **112**, 291-301

[115] A. Warsinke, "Point-of-care testing of proteins", *Analytical Bioanalytical Chemistry*, 2009, **5** 1393-1405

[116] S. Feng, R. Caire, B. Cortazar, M. Turan, A. Wong and A. Oczan, " Immunochromatographic diagnostic test analysis using google glass", *ACS Nano*, 2014, **8**, 3069-3079

[117] P. Sithigorngul, S. Rukpratanporn, N. Pecharaburanin, P. Suksawat, S. Longyant, P. Chaivisuthangkura and W. A. Sithigorngul, "A simple and rapid immunochromatographic test strip for detection of pathogenic isolates of Vibrio harveyi", *Journal of Microbiological Methods*, 2007, **71**, 256-264

[118] T. Peng, W. Yang, W. Lai, Y. Xiong, H. Wei and J. Zhang, "Improvement of the stability of immunochromatographic assay for the quantitative detection of clenbuterol in swine urine", *Analytical Methods*, 2014, **6**, 7394-7398

[119] F. F. Bier and S. Schumacher, "Integration in bioanalyis: technologies for Point-of-Care testing", *Adv. Biochem. Eng. Biotechnol*. 2013, **133**, 1-14

[120] F. Ricci, G. Adornetto and G. Palleschi, "A review of experimental aspects of electrochemical immunosensors", *Electrochimica Acta*, 2012, **84**, 74-83

[121] A. Warsinke, "Electrochemical biochips for protein analysis", *Adv. Biochem. Engin/Biotechnol*., 2008, **109**, 155-193

[122] G.Gauglitz, "Direct optical detection in bioanalysis: an update", *Analytical Bionalaytical Chemistry*, 2010, **398**, 2363-2372

[123] Y. Wan, Y. Su, X. Zhu, G. Liu and C. Fan, "Development of electrochemical immunosenosrs towards point of care diagnostics", *Biosensors Bioelectronics*, 2013, **47**, 1-11

[124] V. Mani, B. Chikkaveeraiah, V. Patel, J. S. Gutkind and J. F. Rusling, "Ultrasensitive immunosensor for cancer biomarker proteins using gold nanoparticle film electrodes and multienzyme-particle amplification", *ACS Nano*, 2009, **3**, 585-594

[125] C. Gabriel, S. Gabriel and E. Corthout, "The dielectric properties if biological tissues: Literature survey", *Physical Medical Biology*, 1996, **41**, 2231-2249

[126] T. Hanai, N. Koizumi and A. Irimajiri, "A method for determining the dielectric constant and the conductivity of membrane-bounded particles of biological relevance", *Biophys. Struct. Mech*., 1975, **1**, 285-294

[127] D. Johnson, in *Clinical Chemistry* (Ed. E. H. Taylor), Wiley, 1989, 55-82

[128] M. Z. Jaffe, "Uber den Niederschlag, welchen pikrinsäure in normalem Harn erzeugt und über eine neue Reaction des Kreatinins", *Zeitschrift für Physiologische Chemie,* 10 (1886)

[129] P. Fossati, L. Prencipe and G. Berti, "Enzymic creatinine assay: A new calorimetric method based on hydrogen peroxide measurement" *Clin. Chem.*, 1983, **29**, 1494-1496

[130] A. Benkert, F. Scheller, W. Schoessler, C. Hentschel, B. Micheel, O. Behrsing, G. Scharte, W. Stoecklein and A. Warsinke, "Development of a creatinine ELISA and an amperometric antibody-based creatinine sensor with a detection limit in the nanomolar range", *Analytical Chemistry*, 2000, **72**, 916-921

[131] L. Li, C. Li, Z. Zhang and E. Alexov, "On the dielectric constant of proteins: smooth dielectric function for macromolecular modeling and its implementation in Delphi", Journal of Chem. Theor. Comput., 2013, **9**, 2126-2136

[132] P. Kukic, D. Farrell, L. P. MacIntosh, B. Garcia-Moreno, E. K. S. Jensen, Z. Toleikis, K. Teilum and J. E. Nielsen, "Protein dielectric constants determined from NMR chemical shift perturbations" J. Am. Chem. Soc., 2013, **135**(45), 16968–16976.

[133] C. Spegel, A. Heiskanen, L. H. D. Skjolding and J. Emneus, "Chip based electroanalytical systems for cell analysis", *Electroanalysis*, 2008, **20**, 680-702

[134] A. Han and A. B. Frazier, "Ion channel characterization using single cell impedance spectroscopy", *Lab Chip*, 2006, **6**, 1412-1414

[135] K.-H. Han, A. Han and A. B. Frazier, "Microsystems for isolation and electrophysiological analysis of breast cancer cells from blood", *Biosensors Bioelectronics*, 2006, **21**, 1907-1914

[136] K. Cheung, S. Gawad and P. Renaud, "Impedance spectroscopy flow cytometry on chip label-free cell differentiation" *Cytometry, Part A*, 2005, **65**, 124-132

[137] D. D. Carlo and L. P. Lee, "Dynamic single-cell analysis for quantitative biology" *Analytical Chemistry*, 2006, **78**, 7918-7925

[138] M. Lisker, A. Trusch, A. Krueger, M. Fraschke, P. Kulse, St. Marschmeyer, J. Schmidt, Ch. Meliani, B. Tillack, T. Kraemer, N. Weimann, I. Ostermay, O. Krueger, T. Jensen, T. Al-Sawaf, V. Krozer and W. Heinrich, " Combining SiGe BiCMOS and InP processing in an on-top chip integration approach", *ECS Transactions*, 2014, **64**, 177-194

[139] C. McDonald and G. M. Whitesides, "Polydimethylsiloxane as a material for fabricating microfluidic devices", *Accounts of Chemical Research*, 2002, **35**, 491-499

[140] M. D. Belrhiti, S. Bri, A. Nakheli, M. Haddad and A. Mamouni, "Dielectric constant determination of liquid using regular waveguide structure combined with EM simulation", *Journal of Mater. Environ. Sci*., 2012, **3**, 575-584

[141] W. Kuang and S. O. Nelson, "Dielectric relaxation characterization of fresh fruits and vegetables from 3 to 20 GHz", *Journal of Microwave power and electromagnetic energy*, 1997, **32**, 114-122

[142] V. V. Meriakri, E. E. Chigrai, D. Kim, I. P. Nikitin, L. I. Pangonis, M. P. Parkhomenko and J. H. Won, "Dielectric properties of glucose solutions in the milimitre-wave range and control of glucose content in blood", *IOP Measurement Science and Technology*, 2006, **18**, 1-6

[143] T. H. Basey-Fisher, S. M. Hanham, S. A. Maier, M. M. Stevens, N. M. Alford and N. Klein, "Microwave relaxation analysis of dissolved proteins: towards free solution biosensing", Applied Physics Letters, 2011, **99**, 233703

[144] M. Y. Koledintseva, R. E. DuBroff and R. W. Schwartz, "A Maxwell-Garnett model for dielectric mixtures containing conducting particles at optical frequency", *Progress in Electromagnetics Research, Pier*, 2006, **63**, 223-242

[145] K. K. Kaerkkaeinen, A. H. Sihvola and K. I. Nikoskinen, "Effective permittivity of mixtures: Numerical validation by the FDTD method", *IEEE transactions on Geoscience and Remote Sensing*, 2000, **38**, 1303-1308

[146] P. L. Weissberg, "Atherogenesis: Current Understanding of the Causes of Atheroma," *Heart,* 2000, **83**, 247-252

[147] R. Ross, "The Pathogenesis of Atherosclerosis: A Perspective for the 1990s". *Nature*, 1993, **362**, 801-809

[148] B. N. Potkin, et al., "Coronary Artery Imaging with Intravascular High-frequency Ultrasound", *Circulation*, 1990, **81**, 1575-1585

[150] D. Huang, et al., "Optical Coherence Tomography," *Science*, 1991, **254**, 1178-1180[

[151] N. Haandbaek, O. With, S. C. Buergel, F. Heer and A. Hierlemann, "Microfluidic sensor using resonance frequency modulation for characterization of single cells", *17th International Conference on Miniaturized Systems for Chemistry and Life Science*, Germany, 2013

[152] H. Lee, Y. Liu, R. M. Westervelt and D. Ham, "IC/microfluidic hybrid system for magnetic manipulation of biological cells", *IEEE Journal of Solid State Circuits*, 2006, **41**, 1471-1480

[153] K. Hu, S. A. Osmany, J. C. Scheytt and F. Herzel, "An integrated 10 GHz low-noise phased lock loop with improved PVT tolerance", *Analog Integrated Circuits and Signal Processing*, 2011, **67**, 319-330

[154] F. Herzel, S.A. Osmany and J. C. Scheytt, "Analytical phase noise modeling and charge pump optimization for fractional-PLLs", *IEEE Transactions on Circuits and Systems I, Regular papers*, 2010, **57**, 1914-1924

[155] F. Herzel, G. Fischer and H. Gustat, "An integrated CMOS RF Synthesizer for 802.11a Wireless LAN", *IEEE Journal of Solid-State Circuits*, 2003, **38**(10), 1767-1770

[156] G. Konvalina and H. Haick, "Sensors for breath testing: from nanomaterials to comprehensive disease detection", *Acc. Chem. Res.*, 2014, **47**, 66-76

[157] H. Haick, Y. Broza, P. Mochalski, V. Ruzsanyi and A. Amann, "Assessment origin and implementation of breath volatile cancer markers", *Chem. Soc. Rev.* 2014, **43**, 1423-1449

[158] F. Herzel and B. Razavi, "A study of oscillator jitter due to supply and substrate noise", *IEEE Transactions on Circuits and Systems II: Analog Digital Signal Processing*, 1999, **46**, 56-62

[159] S.A. Osmany, F. Herzel, J. C. Scheytt, "Analysis and minimization of substrate spurs in fractional-N frequency synthesizers", *Analog Integrated Circuits and Signal Processing*, 2013, **74**, 545-556

[160] H. Wang, C. C. Weng and A. Hajimiri, "Phase noise and fundamental sensitivity of oscillator-based reactance sensors", *IEEE Transactions on Microwave Theory and Techniques*, 2013, **61**, 2215-2229

LIST of RELATED PUBLICATIONS

Conference Proceedings

[1] S. Guha et al, "Integrated high-frequency sensors in catheters for minimally invasive plaque characterization", European Microelectronics and Packaging Conference and Exhibition, September 2015, Friedrichshafen, Germany

[2] S. Guha et al., "12 GHz CMOS MEMS lab-on-chip system for detection of concentration of suspended particles in bio-suspensions", Biodevices, January 2015, Lisbon, Portugal

[3] S. Guha et al., "An 8 GHz CMOS near field bio-sensor array for imaging spatial permittivity distribution", IEEE-MTT-S International Microwave Symposium, May 2014, Tampa, USA

[4] S. Guha et al., "CMOS lab on chip device for dielectric characterization of cell suspensions based on a 6 GHz Oscillator", IEEE European Microwave Conference, September 2013, Nuremberg, Germany

[5] (Invited) S. Guha et al., "High frequency biomedical sensors integrated with polymer microfluidic systems", Biomedical Workshops, IEEE European Microwave Conference, September 2013, Nuremberg, Germany

[6] S. Guha et al, "CMOS based sensor for dielectric spectroscopy of biological cell suspensions", International Conference on Electrical Bioelectrical Impedance (ICEBI), May 2013, Heiligensatdt, Germany

[7] S. Guha et al, "CMOS MEMS microfluidic systems for cytometry at 5 GHz", International Conference on Microfluidic Handling Systems (MFHS), October 2012, Enschede, Netherlands

[8] F.I. Jamal, S. Guha and C. Meliani, "A SiGe BiCMOS dielectric sensor utilizing an open-ended microstrip line in a 28 GHz Colpitt's Oscillator", IEEE European Microwave Conference,September 2014, Rome, Italy

[9] S. Vehring, S. Guha, F. I. Jamal and C. Meliani, "Permittivity sensor based on 60 GHz patch antenna", German Microwave Conference (GEMIC), April 2015, Nuremberg, Germany

[10] F. I. Jamal, S. Guha, S. Vehring, D. Kissinger and C. Meliani, "K-Band BiCMOS based near field biomedical dielectric sensor for detection of fat and calcium in blood", IEEE European Microwave Conference, September 2015, Paris, France

[11] C. Meliani, S. Guha, F. I. Jamal, M. Eissa and S. Vehring, "Integrated mm-wave near-field sensor concepts for biomaterial characterization", European Microwave Week, September 2015, Paris, France

[12] F. I. Jamal, S. Guha, M.H. Eissa, J. Boerngaber, D. Kissinger and J. Wessel, "Comparison of Microstrip Stub Resonators for Dielectric Sensing in Low-Power K-band VCO", IEEE Topical Conference, Biowireless, Radio Wireless Week, January 2016, Austin, Texas, USA.

[13] F.I. Jamal, S. Guha, M.H. Eissa, Ch. Meliani, D. Kissinger, J. Wessel "A 24 GHz Dielectric Sensor Based on Distributed Architecture", Proc. German Microwave Conference (GeMiC), 2016, 173

[14] M.H. Eissa, F.I. Jamal, S. Guha, Ch. Meliani, D. Kissinger, J. Wessel "Low-Power Planar Complex Dielectric Sensor with DC Readout Circuit in a BiCMOS Technology", IEEE MTT-S International Microwave Symposium (IMS), 2016, San Francisco, USA

[15] F.I. Jamal, S. Guha, M.H. Eissa, Ch. Meliani, H.J. Ng, D. Kissinger, J. Wessel "A Fully Integrated Low-Power K-Band Chem-Bio-Sensor with On-Chip DC Read-out in SiGe BiCMOS Technology", European Microwave Conference (EuMC) 2016, London, UK

[16] D. Wagner, F.I. Jamal, S. Guha, Ch. Wenger, J. Wessel, D. Kissinger, D. Ernst, K. Pitschmann, B. Schmidt, M. Detert, "Packaging of a BiCMOS Sensor on a Catheter Tip for the Characterisation of Atherosclerotic Plaque", 6th Electronics System-Integration Technology Conference (ESTC), 2016, Grenoble, France

Journal Articles

[1] S. Guha et al, "Label free sensing of creatinine using a 6 GHz CMOS near-field dielectric immunosensor", *Analyst*, 2015, **140**, 3019-3027

[2] S. Guha et al., "Self-calibrating highly sensitive dynamic capacitance sensor towards rapid sensing and counting of particles in laminar flow systems", *Analyst*, 2015, **140**, 3262-3272

[3] S. Guha et al, "CMOS based sensor for dielectric spectroscopy of biological cell suspension", IOP *Journal of Physics*, 2013, **434**

[4] F.I. Jamal, S. Guha, M.H. Eissa, J. Borngräber, Ch. Meliani, H.J. Ng, D. Kissinger, J. Wessel, "Low-Power Miniature K-Band Sensors for Dielectric Characterization of Bio-Materials", IEEE Transactions on Microwave Theory and Technique, 2017, **65** (3), 1012-1023

Patents Filed

[1] "Inhomogene Übertragungsleitung zur positionsaufgelösten Permittivitätsbestimmung", IHP.413.PCT-Anmeldung, am 29.01.206, AZ: PCT/EP2016/051887 (European Patent)

[2] "Schaltbarer Messträger zur positionsaufgelösten Permittivitätsbestimmun"
IHP.408.14, DE-Patentanmeldung am 02.02.2015, AZ: 10 2015 201 771.0 (German Patent)

LIST of FIGURES

LIST of TABLES

LIST of ABBREVIATIONS

IHP Microelectronic – Innovations for High Performance Microelectronics, Leibniz institute for innovative Microelectronics

SiGe: Silicon Germanium

MOSFET – Metal oxide semiconductor field effect transitor

POC – Point of Care

LOC – Lab on chip

DNA – Deoxy ribonucleic acid

CCD – Charge coupled device

ELISA – Enzyme linked immunosorbent assay

SPR – Surface plasmon resonance

CMOS – Complementary metal oxide semiconductor

BiCMOS – Bipolar Complementary metal oxide semiconductor

MEMS – Micro-electro-mechanical system

BEOL – Back end of line

RF – Radio frequency

IDC – Interdigitated capacitor

PDMS – Polydimethysiloxane

HBT – Heterojunction bipolar transistor

MIM – Metal insulator metal

TM – Top metal

FEOL – Front end of line

SRF – Self resonating frequency

MUT – Material under test

MOS – Metal oxide semiconductor

POCT- Point of care testing

Pd – Penetration depth

SEM – Scanning electron microscopy

FIB – Focused ion beam

Crea-BSA – Creatinine bovine serum albumin

PBS – Phosphate buffer solution

ADS – Agilent design system

CMP – Chemical mechanical polishing

CVD – Chemical vapor deposition

RIE – Reactive ion etching

PMMA – Polymethylmethacrylate

IVUS – Intra vascular ultrasound

OCT – Optical coherence tomography

PPM – Parts per million

PLL – Phase locked loop

VCO – Voltage controlled oscillator

PVT – Process voltage temperature

CP – Charge pump

FM – Frequency modulation

PFD – Phase frequency detector